# Master thesis

Covalent Coupling of Fluorescent pH Indicators in a Polymeric Matrix

Martin Strobl

Institute of Analytical Chemistry and Food Chemistry
University of Technology, Graz



Supervisor: Univ.-Prof. Dipl.-Chem. Dr.rer.nat. Ingo Klimant

Graz, 2013

*„More light“*

Last words of Johann Wolfgang von Goethe

**Abstract**

Determination of pH is one of the most performed analytical measurement in a wide range of sciences, including chemistry, biochemistry, biotechnology, marine science and many other applications. The measurement of pH is of great importance because most chemical reactions are dependent on it in some way. Usually a chemical reaction can only take place within a specific range of pH.

Traditionally, well-established electrochemical methods have been used for pH analysis providing accurate results within a relatively short time. However, luminescence pH sensors are insensitive against electromagnetic interferences and facilitate real-time monitoring. They are more easily miniaturized and provide higher sensitivity within their dynamic range.

Unfortunately, most pH sensors presented in literature are based on short-wave excitable indicators which are especially undesired in biological applications. In contrast, $BF_2$-chelated tetraarylazadipyrromethane (aza-BODIPY) dyes offers absorption/emission profiles in the near-infared (NIR) region providing many advantages: lower auto-fluorescence and scattering background, deep penetration of (biological) probes by using NIR light, and economically priced excitation light source. Additionally, aza-BODIPY based indicator dyes possess outstanding photo-stability.

In this thesis a synthetic strategy towards the covalent immobilization of $BF_2$-chelated tetraarylazadipyrromethane based pH indicators in a poly(acryloylmorpholine) matrix is developed. The strategy relies on the preparation of a co-polymerizable indicator dye employing EDC/NHS coupling and its subsequent photo-co-polymerization. The covalently linked pH indicator is prevented from leaching which enhances the performance of the produced pH sensor with respect to sensor stability and shelf life. Furthermore, photophysical properties of the developed sensor are examined and compared with a pH sensor exhibiting only physically entrapped indicator dyes. Finally, ionic strength dependence and dynamic response of the pH sensor has been investigated.

**Kurzfassung**

Diese Arbeit beschäftigt sich mit der Entwicklung von kovalent immobilisierten aza-borondipyrromethan basierenden Indikatorfarbstoffen in eine Poly(acryloylmorpholin)matrix. Die Strategie beruht auf die Synthese eines polymerisierbaren Indikatorfarbstoffs mittels EDC/NHS-Kupplung und darauffolgender Photo-co-polymerisation. Der synthetisierte pH-Sensor ist geschützt vor eventuellen Auswaschungsprozessen was eine wesentliche Verbesserung hinsichtlich Signalstabilität und Haltbarkeit zur Folge hat.

Des Weiteren werden die photo-physikalischen Eigenschaften des synthetisierten pH-Sensors untersucht und mit jenem Sensor verglichen dessen Indikatorfarbstoffe lediglich physikalisch in die Polymermatrix eingebettet wurden.

**Statutory Declaration**

I declare that I have authored this thesis independently, that I have not used other than the declared sources / resources, and that I have explicitly marked all material which has been quoted either literally or by content from the used sources.

Date Signature

**Acknowledgement**

This master thesis is the final part of an exciting studying time full of experiences that positively shaped my life. At this point, I would like to thank those people for their help throughout these years and especially during the work of this thesis.

Special thanks go to Head of Institute Univ.-Prof. Dipl.-Chem. Dr.rer.nat. Ingo Klimant for the useful comments, remarks and engagement through the learning process of this thesis. I would like to thank Sergey Borisov for introducing me to the topic as well for the support on the way. Further thanks go to Tijana, who constantly and essentially helped me how to develop and set up smart experiments and always took time to support me in scientific writing. I would like to thank the whole working group for creating such a comfortable and friendly working atmosphere

The most gratitude is to my family for the financial support and motivation in all the years.

**Contents**

## 1. Theoretical Backgrounds

### 1.1 Luminescence[1a]

Luminescence (lat. *lumen* = light) is a process of emission of photons from an electronically excited species. It was first introduced by the physicist Eilhardt Wiedeman and describes 'all those phenomena of light which are not solely conditioned by the rise in temperature'. Hence luminescence implies *cold light* which is opposed to incandescence (*hot light*).

Molecules exhibiting luminescence can be of very different kinds including a wide range of organic compounds (e.g. fluorescein, rhodamines), inorganic species (ions, crystals, glasses) and organometallic complexes.

According to the mode of excitation various types of luminescence can be distinguished. Table **1** gives an overview of important luminescence types.

**Table 1: Important luminescence phenomena according to the mode of excitation.**

| Mode of excitation | Type of luminescence |
|---|---|
| **Absorption of light (Photons)** | **Photoluminescence (Fluorescence, Phosphorescence)** |
| Electroluminescence | Electric field |
| Chemical process (e.g. oxidation) | Chemoluminescence |
| X-rays, α-rays or other ionizing radiation | Radioluminescence |

### 1.2 Absorption[1b]

Upon absorption of photons, electrons are promoted from a ground state (GS) to an unoccupied, energetically higher lying excited state (ES). The energy gap between those two states corresponds to the energy of photons absorbed.

$$E_{ES} - E_{GS} = h\nu \qquad \text{Equation 1}$$

| | | | |
|---|---|---|---|
| $E_{ES}$ | Energy of excited state | ν | frequency of the absorbed photon ($s^{-1}$) |
| $E_{GS}$ | Energy of ground state | h | Planck's constant ($6{,}62*10^{-34}$ Js) |

Other types of light-matter interactions can dramatically affect absorption and subsequent luminescence such as reflection, scattering, diffraction or refraction.

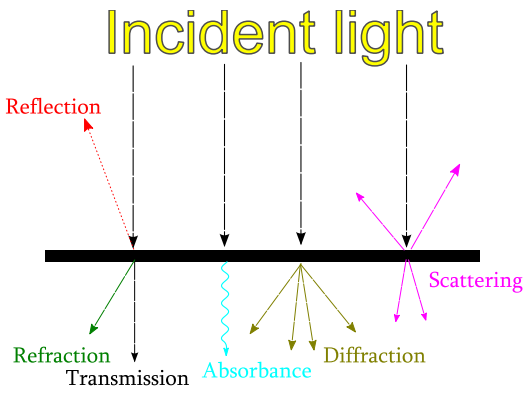


**Figure 1: A schematic illustration of interfering interactions when light meets matter.**

Generally, absorption of light promotes an electron from the highest occupied to the lowest unoccupied molecular orbital (HOMO → LUMO). The energy required for electron transition (Eq. **1**) depends on the molecular orbitals involved and is usually increasing in the following order:

$$n \longrightarrow \pi^* < \pi \longrightarrow \pi^* < n \longrightarrow \sigma^* < \sigma \longrightarrow \sigma^*$$

$\pi \longrightarrow \pi^*$ and $n \longrightarrow \pi^*$ transitions are often localized in the visible region and therefore of high relevancy for spectroscopic applications. For $\pi \longrightarrow \pi^*$ transitions, the presence of unsaturated groups (multiple double bonds, aromatic rings) is needed. Functional groups (C=O, C-OH, $C\text{-}NH_2$) additionally possess non-bonding electrons located on heteroatoms such as oxygen and nitrogen. The corresponding MOs are called n orbitals. $\sigma \longrightarrow \sigma^*$ transitions depend on high energies in the deep UV and will not be considered here.

Electron transitions are allowed if the spin multiplicity remains unchanged and is related to the following equation:

$$M = 2\,|S| + 1 \qquad \text{Equation 2}$$

*M* Spin multiplicity of an electronic state

*S* Sum of electron spins populating that state

Consequently, singlet-singlet transitions (S→S-transitions) and triplet-triplet transitions (T→T-transitions) are allowed, whereas S→T-transitions and T→S-transitions are quantum-mechanically forbidden.

**Beer-Lambert law**

In most cases, absorbance of a sample follows the Beer-Lambert Law.

$$A(\lambda) = log\frac{I_0}{I}\varepsilon(\lambda)dc$$ Equation 3

| | |
|---|---|
| *A* | Absorption |
| $I_0$ | Intensity of light entering the sample |
| *I* | Light intensity after passing through the sample |
| $\varepsilon(\lambda)$ | Molar absorption coefficient of the dye at a certain wavelength λ ($M^{-1}cm^{-1}$) |
| *c* | dye concentration (M) |
| *d* | optical path length of the sample |

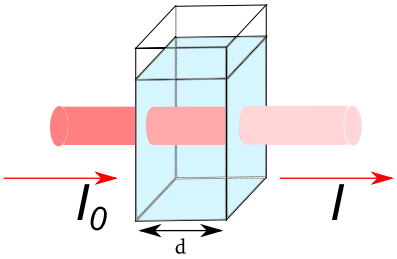


**Figure 2: Graphic demonstration of Beer-Lambert Law**

The molar absorption coefficient ε(λ) indicates how strongly a molecule absorbs light at a certain wavelength (λ)

### 1.3 The Frank-Condon-Principle[1c]

According to the Born-Oppenheimer approximation, electronic transitions take place much faster than movements of nuclei due to the small mass of electrons. The time needed for promotion of an electron to a higher lying unoccupied molecular orbital is about $10^{-15}$ s. In comparison with the characteristic time for molecular vibrations ($10^{-10}$-$10^{-12}$s), a time too long for significant displacement of nuclei. Consequently, nucleic movements such as molecular vibrations do not play a role in electronic processes.

Theoretically, the distance between nuclei in the ES will be equal to the one in the GS. Due to weaker binding between two atoms in the ES, the minimum of the morse potential is located at larger bond length.

Thus, excited electrons will most likely be transferred to higher lying vibrational levels of the excited state. However, electronic excitation is quickly followed by a process of non-radiative vibrational relaxation to the lowest vibrational level of the corresponding electronic state.

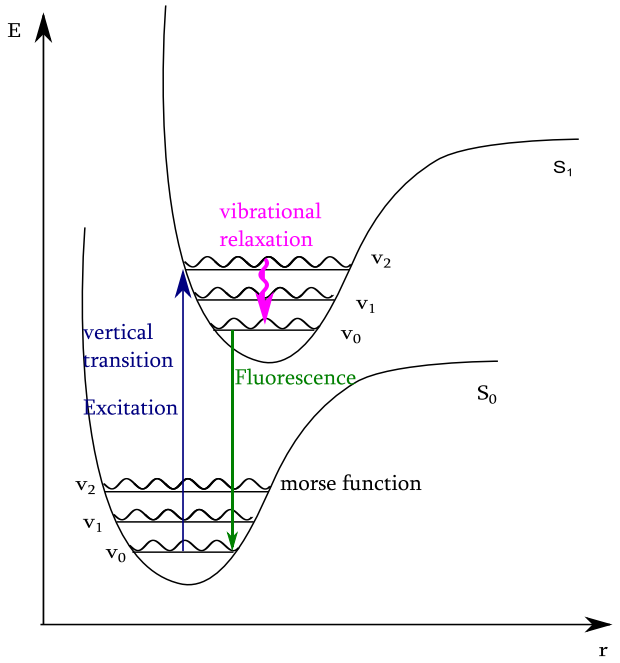


**Figure 3: Illustration of the Frank-Condon Principle. The morse potential of the excited state is located at larger bond length due to weaker binding between atoms. Consequently, excited electrons are most likely placed into higher lying vibrational levels of the ES.**

## 1.4 Perrin-Jablonski diagram[1d]

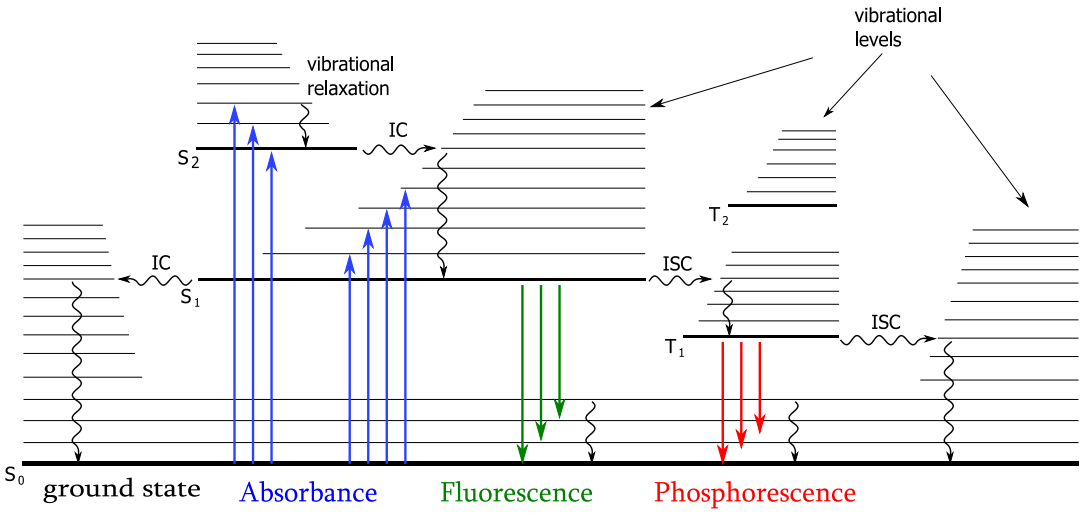


**Figure 4: A Jablonski diagram illustrating de-excitation pathways upon absorption**

The Perrin-Jablonsky diagram demonstrates radiative and non-radiative de-excitation processes between electronic states upon absorption: Internal conversion, fluorescence,

intersystem crossing, phosphorescence and delayed fluorescence. The singlet electronic states are denoted $S_0$ (fundamental electronic state), $S_1$, $S_2$,... and the triplet states, $T_1$, $T_2$,... Vibrational levels are associated with each electronic state.

### 1.4.1 Internal conversion

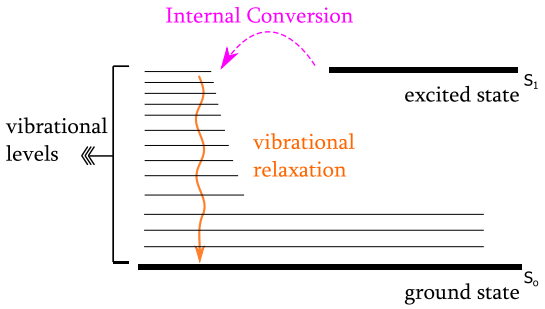


**Figure 5: Illustration of Internal Conversion (IC) and subsequent vibrational relaxation towards the final lower-lying electronic state.**

Internal conversion IC is a non-radiative transition from an excited state to vibrational levels of a lower lying electronic state of same spin multiplicity. IC is usually followed by vibrational relaxation to the corresponding vibrational ground state. The excess of energy can be transferred by collisions of the excited molecules with the surrounding solvent molecules or over the vibrations and rotations of the excited molecules itself. IC can also occur between $S_1$ and $S_0$ but is less likely due to much larger energy gap between them. Therefore, other deactivation processes like emission of photons (fluorescence) and intersystem crossing (ISC) can compete with IC. Internal conversion occurs within $10^{-11}$s -$10^{-9}$s and is ten times slower than subsequent vibrational relaxation.

### 1.4.2 Intersystem crossing

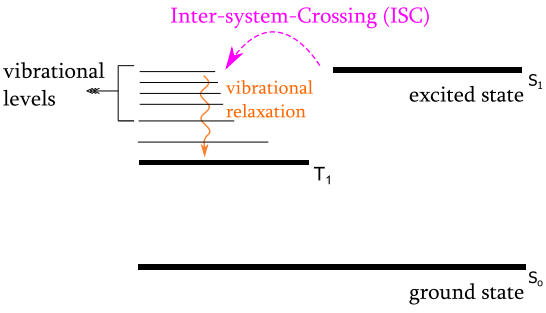


**Figure 6: Illustration of Intersystem Crossing (ISC)**

Intersystem crossing (ISC) is a transition between two isoenergetic vibrational levels but of different spin multiplicity. The process is commonly followed by vibrational relaxation towards the vibrational ground state. ISC occurs at a time-scale of $10^{-10}$ -$10^{-11}$s which is

slower compared with IC. Theoretically, this transition is quantum-mechanically spin-forbidden due to its change in spin multiplicity. However, in rare cases spin-orbit coupling can be large enough to provide probability for ISC. For example the presence of heavy atoms (e.g. Br, Pb) increases spin-orbit coupling and thus favours crossing. It should be noted that all deactivation processes $T_1 \rightarrow S_0$ are spin-forbidden as well and in respect of Hund's law reverse ISC to $S_1$ is improbable due to the lower lying energy level of $T_1$. Consequently, once intersystem crossing has occurred, the lifetime of $T_1$ can be around $10^{-6}$ – 1 s.

### 1.4.3 Fluorescence

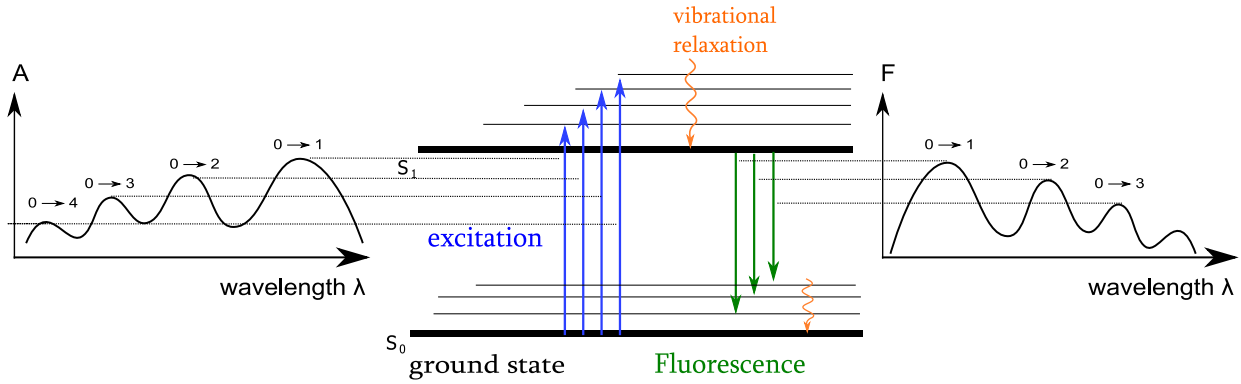


**Figure 7: Fluorescence illustrated in a Jablonski diagram. Peaks in absorption and emission spectra can originate from several vibrational transitions**

Fluorescence is a process of emission of photons between two singlet states, usually $S_1 \rightarrow S_0$. Theoretically, 0-0 transitions of absorption and fluorescence are located at the same wavelength. Due to energy losses caused by vibrational relaxation, emission spectra are in general red-shifted (located at higher wavelength, Stoke's rule). This shift of wavelength between absorption and fluorescence spectrum is called Stokes shift (see Fig. **9**). Absorption and emission spectra partially overlap under laboratory conditions which are in incoherency in respect of the principle of energy conservation. This can be explained that at room temperature a small portion of molecules is located in vibrational levels higher than the ground state (Boltzmann law). However, Stoke's rule usually disappears by working at low temperatures.

Fluorescence takes place from $S_1$ and therefore its characteristics are not influenced by the excitation wavelength, but are temperature dependent. Decay time of fluorescence is usually found within $10^{-10}$-$10^{-7}$s.

### 1.4.4 Phosphorescence

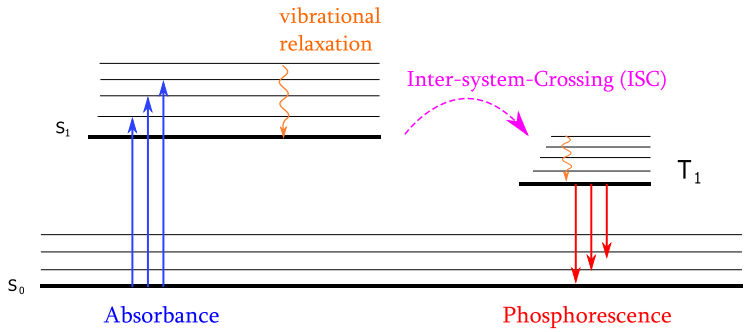


**Figure 8: Phosphorescence visualized in a Jablonsky diagram**

Phosphorescence is a radiative deactivation of an excited triplet-state $T_1$ towards a singlet ground state $S_0$ and its precondition is ISC. This process is spin-forbidden and rather slow ($10^{-6}$-1s) and thus seldom. However, phosphorescence can be generated by using organometallic heavy-metal complexes to enable effective spin-orbit coupling. ISC and IC compete with phosphorescence and are predominant at high temperatures and in solution. Consequently, using a rigid medium and operating at low temperatures favours phosphorescence. The phosphorescence spectra are located at wavelengths higher than fluorescence spectra because the energy level of $T_1$ is lower than that of $S_1$.

### 1.4.5 Delayed Fluorescence

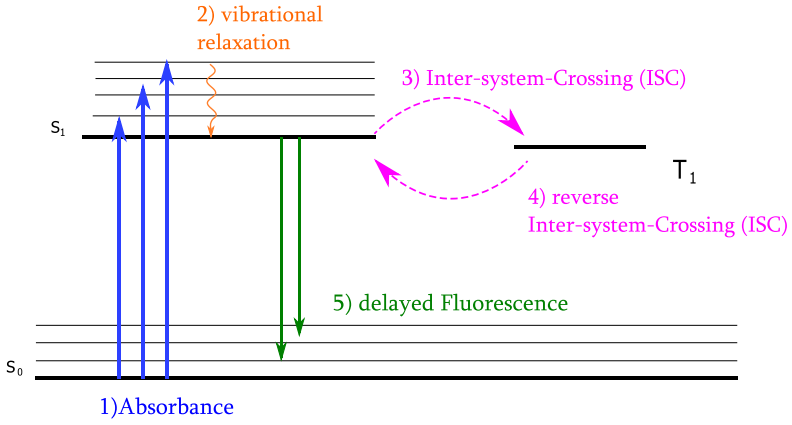


**Figure 9: A Jablonski diagram illustrating delayed fluorescence**

When the energy gap between $S_1$ and $T_1$ is small and the lifetime of $T_1$ is long enough reverse ISC ($T_1 \rightarrow S_1$) can occur. The resulting emission spectrum is identical to its fluorescence spectrum but with much longer decay time constant.

Two cases of delayed fluorescence can be distinguished: E- type and P-type.

Delayed fluorescence of E-type (first observed in eosin) is thermally activated. Consequently, the higher the temperature, the higher is its efficiency. Aromatic hydrocarbons normally do not show this process due to the large energy gap between $S_1$ and $T_1$ but in fullerenes E-type fluorescence can be very efficient.

For P-type delayed fluorescence concentrated solution is necessary. Then collisions between molecules in $T_1$ states can provide enough energy for turning back to the $S_1$ state. P-type delayed fluorescence was first observed with pyrene.

### 1.5 Lifetime[1e]

Radiative relaxation processes are determined by characteristic lifetimes.

After a short pulse of light promotes a certain fraction of molecules A to the excited state $S_1$ subsequent de-excitation processes do not occur immediately. A molecule typically remains a certain time in the excited state ($S_1$, $T_1$,...) before undergoing radiative or non-radiative transitions. The rate of disappearance of excited molecules is described by using simple first-order kinetics:

$$-\frac{d[A^*]}{dt} = k[A^*] \qquad \text{Equation 4}$$

*[A*]* Concentration of excited species A

Here k indicates the deactivation rate for all possible deactivation processes, which is further specified by:

$$k = \Sigma(k_{deactivation}) = k_{radiative} + k_{non-radiative} \qquad \text{Equation 5}$$

Integration of differential equation from t = 0 to t and $[A^*]_0$ to [A*] results in:

$$[A^*] = [A^*] * e^{-kt} \qquad \text{Equation 6}$$

Inversion of first-order rate constant k [$s^{-1}$] yields $\tau$ which indicates the lifetime of the excited state.

$$\tau = 1/k \qquad \text{Equation 7}$$

Insertion of equation **7** into equation **6** yields:

$$[A^*] = [A^*] * e^{-t/r}$$ Equation 8

Equation **8** implies that fluorescence intensity decreases exponentially, once no more excitation takes place (Fig. **11**).

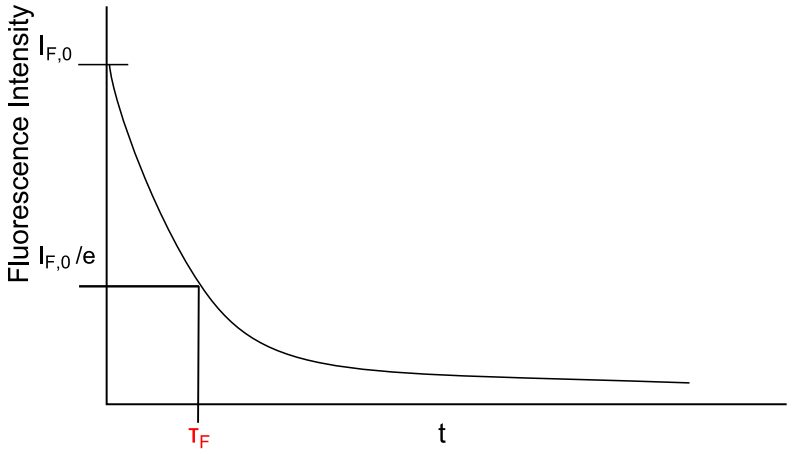


**Figure 10:**

**Exponential decay of fluorescence intensity $I_F$. $\tau_F$ indicates the time where about 63% of the excited molecules have fallen back to its ground state**

Setting t =τ:

$$\frac{[A^*]}{[A_0^*]} = e^{-1} \approx 0.368$$ Equation 9

Considering equation above, the lifetime τ can be interpreted as the duration where 63% of the excited molecules have relaxed to the ground state.

Lifetimes τ for excited $S_1$ states are generally in the range of $10^{-11}$-$10^{-7}$s whereas excited $T_1$ states show much longer lifetimes and range from $10^{-6}$ – $10^{0}$s

### 1.6 Fluorescence Intensity[1f]

The fluorescence intensity $i_F$ is characterized as the number of photons (mol, or einsteins) emitted per unit time(s) and per unit volume of solution.

$$A^* \rightarrow A + \text{photon}$$

$i_F$ is proportional to the current concentration of molecules still excited. The rate constant for radiative de-excitation $k_r$ is the proportionality factor.

$$i_F(t) = k_r\,[A^*]$$ Equation 10

In any fluorescence measurement, the obtained quantity is proportional to $i_F$ and the proportionality factor is depending on instrumental setup. Thus, it should always be considered that the numerical value of $I_f$ ('measured fluorescence') is recorded on an arbitrary scale (a.u.), depending on experimental conditions.

### 1.7 Quantum yields[1g]

The quantum yield $\Phi_F$ indicates the fraction of ES-molecules that fall back to the ground state (GS), accompanied by emission of photons and is formulated as follows:

$$\Phi = \frac{k_{radiative}}{k_{radiative} + k_{non-radiative}} = k_r \tau \qquad \text{Equation 11}$$

Additionally, $\Phi_F$ can also be described as the ratio of the amount of photons emitted during fluorescence and the number of photons absorbed by previous excitation.

### 1.8 Intermolecular Deactivation Processes (Quenching)[1h]

The previous chapter was limited to intrinsic de-excitation in excited molecules. Now intermolecular de-excitation phenomena in which an excited fluorophor F* interacts with another molecule Q will be considered. This process is collectively referred to as "Quenching".

Quenching leads to a decrease of fluorescence intensity, fluorescence quantum yield and/or decay time. It is a bimolecular process in which a variety of possible fluorescence quenching mechanisms can be involved: Transfer of energy, electrons or protons, excimer or exciplex formation, collision with a heavy atom (e.g. halogenids) or paramagnetic species (e.g. $O_2$, NO).

It should be noted that also intramolecular excited-state processes have an impact on fluorescence characteristics: intramolecular charge transfer, internal rotation, intramolecular proton transfer. However, discussion of these phenomena is beyond the scope of this thesis.

When fluorescence quenching is in competition with intrinsic de-excitation several cases can be distinguished:

Case A) The concentration to the quencher [Q] is in large excess. Thus, there is a probability that F* and Q are close to one another that interaction can occur within time of excitation. In

the case of static quenching the probability of finding Q within the encounter distance with F* is less than 1. If this possibility is equal to 1, [Q] can be considered constant. This is a typical case of a 'reaction' of pseudo-first order where [Q] has no influence on the kinetics of de-excitation processes. This can be usually observed in PPT (Photoinduced Proton Transfer) in aqueous solutions where the quencher acts as solvent.

Case B) [Q] is not in large excess. Interaction of F* and Q is not possible during the ES-lifetime (e.g. lifetime is too short, too viscous medium). However, in the case for long-range energy transfer quenching occurs if the interaction is significant at distances longer than the encounter distance.

Case C) [Q] is not in large excess but approach of F* with Q is possible during the excited-state lifetime. This type of quenching is called dynamic quenching and it is always diffusion-controlled. If the concentration of Q is high static quenching can additionally occur

### 1.8.1 Dynamic Quenching

In dynamic quenching the experimental quenching rate constant $k_Q$ is assumed to be time-independent. Dynamic quenching results in reduced fluorescence intensity and, moreover, in decreased decay time which is described by:

$$\frac{\tau_O}{\tau} = 1 + k_Q \tau_O [Q] \qquad \text{Equation 12}$$

$\tau_o$ Luminescence decay time in the absence of the quencher [s]

$\tau$ luminescence decay time at variable quencher concentration [s]

$k_Q$ Quenching rate constant [$M^{-1}s^{-1}$]

[Q] Quencher concentration

Stern-Volmer-constant $K_{SV}$ is given by multiplying $k_Q$ with $\tau_0$ and introducing $K_{SV}$ into equation **12** leads to the Stern-Volmer relation.

$$\frac{\phi_O}{\phi} = \frac{\tau_O}{\tau} = \frac{I_0}{I} = 1 + K_{SV}[Q] \qquad \text{Equation 13}$$

$I_0$ Luminescence intensity in the absence of the quencher

$I$ Luminescence intensity at a variable quencher concentration

$\Phi_0$ Luminescence quantum yield in the absence of the quencher

$\Phi$ Luminescence quantum yield at a variable quencher concentration

$K_{SV}$ Stern-Volmer constant

In general, plotting $I_0/I$ against [Q] yields a simple linear dependence. Stern-Volmer constant can be received from its slope

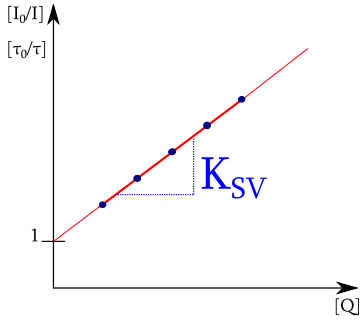


**Figure 11: Stern-Volmer plot illustrating dynamic quenching**

### 1.8.2 Static Quenching

In contrast to dynamic quenching, static quenching is not depending on molecular transport from Q to F* within the excited state lifetime. Static quenching is often induced by the formation of a non-fluorescent complex in the ground state. Characteristically, the ratio $\tau_0/\tau$ remains unchanged over [Q] whereas $I_0/I$ vs. [Q] plots are of the same shape as Stern-Volmer plots.

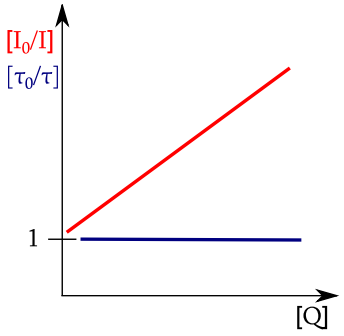


**Figure 12: Stern-Volmer plot in the case of static quenching**

In very viscous media the quencher molecule cannot collide with an excited fluorophor within its lifetime. Thus, a model called 'sphere of effective quenching' has been proposed. It implies that quenching only occurs if Q is located inside an encounter sphere of F* (Fig. **14**).

In static quenching only the quantity of excitable fluorophores is reduced while decay time of the excited state remains unchanged.

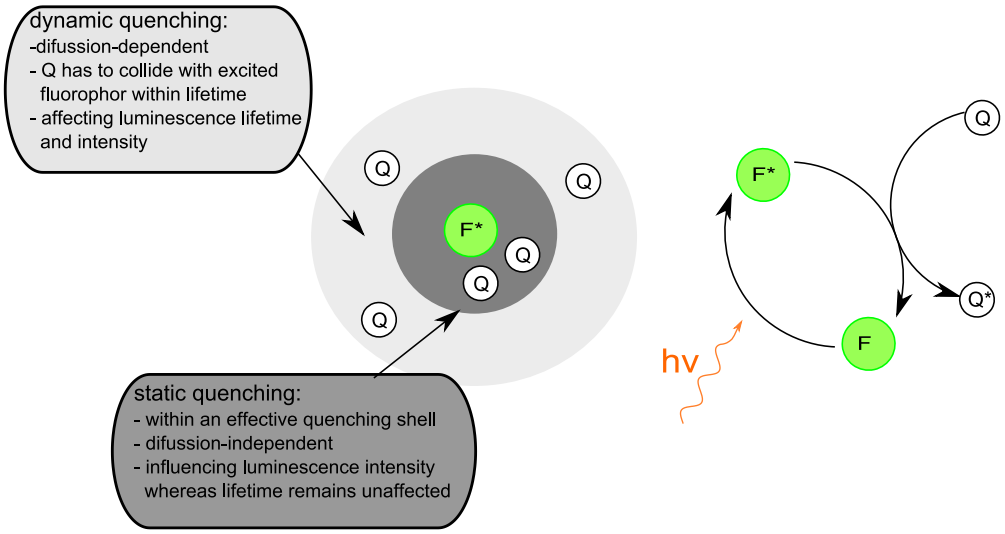


**Figure 13: Simplified scheme illustrating the difference of dynamic and static quenching. Static quenching refers to a situation of F and Q being in close distance to one another (effective quenching shell).**[2]

### 1.8.3 Simultaneous Static and Dynamic Quenching

When [Q] is constantly increasing static and dynamic quenching can act simultaneously. This is especially the case when the quencher is tending to form complexing agents which do not emit photons. This leads to a deviation of linearity of the Stern-Volmer plot at high [Q].

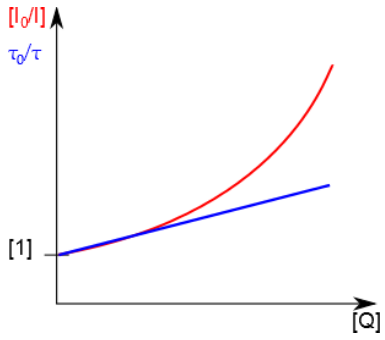


**Figure 14: Stern-Volmer plot illustrating simultaneous static and dynamic quenching**

### 1.8.4 Photoinduced Electron Transfer (PET)[1i,3]

PET is an important mechanism for fluorescence quenching. It has been extensively studied due to their major role in photosynthesis and photovoltaic devices. Compared with other quenching processes (ISC, electron exchange) PET is more predictable. The possibility of occurring electron transfer can be easily obtained from redox potentials of the fluorophor and quencher.

The excited fluorophor can be either the electron donor D or acceptor A although it is more common that the excited species acts as electron donor. Excited molecules can actually be both more strongly oxidizing and reducing agents than the same molecules in the GS. Figure **16** shows an energy diagram for PET assuming that molecules are already in contact.

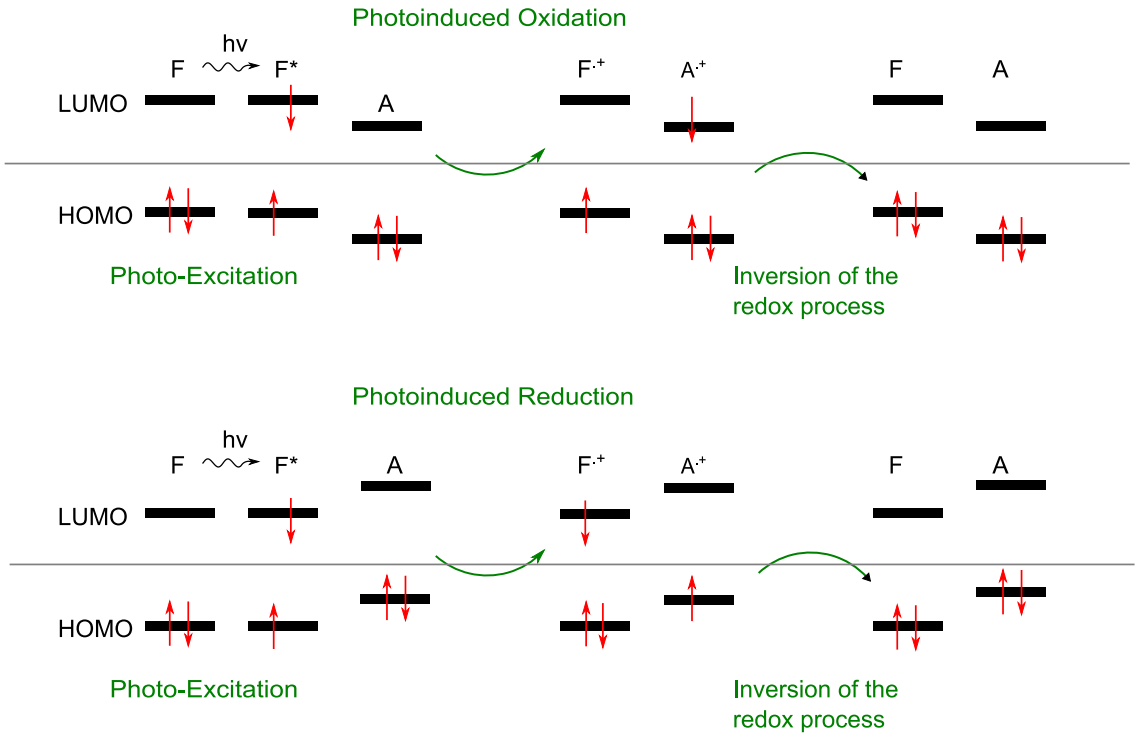


**Figure 15: Simplified scheme of PET mechanism and the inversion of the redox process. PET causes formation of radicals and change in spin multiplicity of the species.**

Upon excitation, F transfers an electron to the acceptor yielding a charge-transfer complex $[F_p^+A_p^-]$ (Fig. **17**). This species is usually quenched and returns back to the ground state without emission of photons. It has to be noted that in this process the total energy of the charge-transfer complex is decreased. It takes less energy for removing an electron from $S_1$

than from the $S_0$ state. Considering an electron accepting quencher the energy released on binding the electron is larger if the electron returns to the $S_0$ state than to the $S_1$ state.

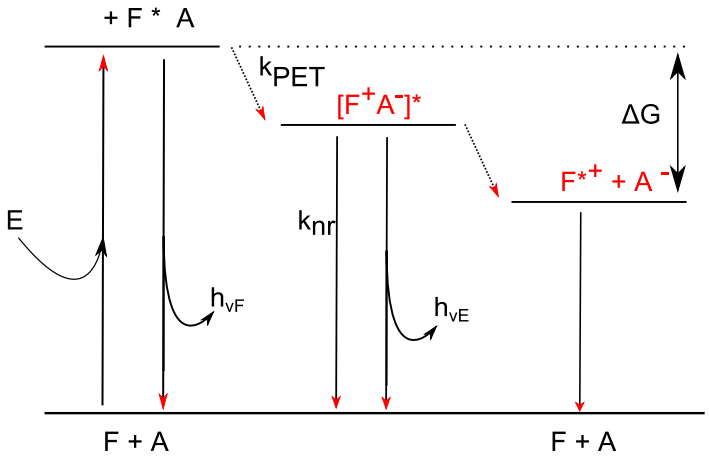


**Figure 16: Energy diagram for PET. The ES-molecule acts as electron donor. The charge-transfer complex $[F_p^+A_p^-]$ is non-fluorescent.**

No complex formation would be generated due to the energetically unfavourable ground state of both F and A. This process only results in fluorescence quenching. In the case that the original GS is never recovered PET can be considered as a photo-degradation process.

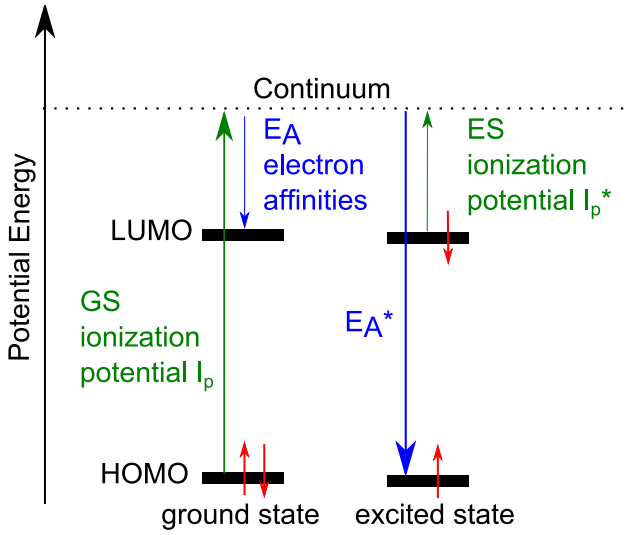


**Figure 17: Illustration of ionization potentials and electronic affinities in the GS and the ES. This simplified model indicates that ES-molecules receive both more strongly oxidizing and reducing properties than the same GS-molecules. Ionization potential of the ES-species is lowered and consequently, it is more easily oxidized. On the other hand, electron affinity of the excited molecule is increased and thus, more easily reduced.**

**Excimer formation**

When an excited molecule and an identical unexcited molecule collide with each other excimers (the term is created by assembling the words **exc**ited d**imer**) can be formed.

$$M^* + M \rightleftarrows (MM)^*$$

In this quenching process a new fluorophore is created and its fluorescence is not necessarily weaker than the one of the original fluorophore. Excimers can be considered as extended fluorophores which mostly results in a bathochromic shift in the emission spectra in respect with its fluorescent origin. Furthermore, excimer bands are structureless and do not show vibronic levels in contrast to the monomer. Excimer formation is diffusion-controlled. Thus, the higher the concentration of the fluorophore, the higher is the ability of excimer generation. Consequently, fluorescence intensity does not show a linear response in respect with increasing fluorophore concentration, especially at high values. Many aromatic hydrocarbons can form excimers (e.g. naphthalene, pyrene).

**Exciplex formation**

Exciplexes (**Exci**ted com**plex**) are complexes in the excited state. They differ from excimers by the fact that they are generated by collision with a dissimilar unexcited molecule.

$$D^* + A \rightleftarrows (DA)^* \qquad\qquad A^* + D \rightleftarrows (DA)^*$$

Exciplex formation is diffusion-controlled as well. Thus, detection of species will be accomplished at high concentration to ensure sufficient number of collisions during the excited-state lifetime. Besides concentration, temperature and viscosity should also be considered as important parameters influencing exciplex generation.

### 1.8.5 Photoinduced Proton Transfer[1j]

Based on PET excited state molecules can not only be electrochemically modified. Also the acidic and basic properties of an excited fluorophore upon excitation can change.

In this section only reactions where acids and bases are stronger in the excited state than in the ground state will be considered because this behaviour my cause a photo induced proton transfer (PPT). As a consequence, the p$K_a$ value of a proton donor group (e.g. OH substituent

of an aromatic ring) can be dramatically decreased compared to the $pK_a$ in the ground state. On the other hand, the $pK_a$ of a proton acceptor group in an excited fluorophore is enhanced in comparison with its unexcited origin. The reaction takes place in aqueous solution and water molecules can either act as proton acceptor or donor and are in close contact with an acid or base. Thus, photoinduced proton transfer is not diffusion-controlled.

The possibility of PPT depends on the lifetime of the excited species and the rates of proton transfer and other competitive de-excitation processes. Most extensively investigated cases are proton ejection in the ES where the proton donor is an acid and the proton acceptor is a water molecule represented in figure **19**.

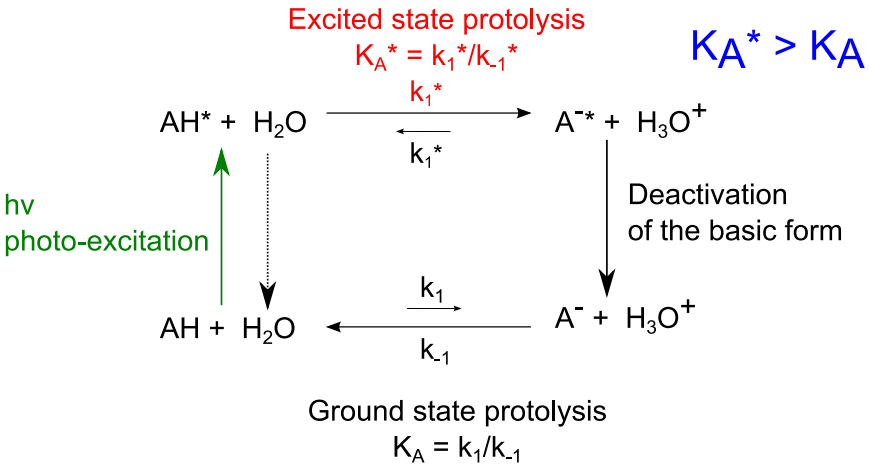


**Figure 18: Scheme of Photoinduced Proton Transfer (PPT) including activation, facilitated deprotonation of the acidic dye and its subsequent deactivation. K and K* represent the protolysis equilibrium values in the GS and ES*. This illustration indicates that $K_A^* > K_A$ upon excitation.**

The excited state $pK_a$ can be estimated by the Förster cycle that considers all four species shown in figure **20**.

$$pK_A^* - pK_A = C(\vartheta_{A^-} - \vartheta_{AH}) \qquad \text{Equation 14}$$

| | |
|---|---|
| $pK_A^* - pK_A$ | Difference between $pK_A$ values in the ES (*) and the GS |
| C | Constant of proportionality |
| $\vartheta_{A^-} - \vartheta_{AH}$ | Difference of frequency between basic and acid species |

According to equation **14** the excited $pK_a$ is lowered if the emission band of the basic form is bathochromically shifted compared with the acidic species. Consequently, the AH* is a

stronger acid than AH. The wavenumbers $\vartheta_{A^-} - \vartheta_{AH}$ corresponds to the 0-0 transition and its determination may be complicated. It is usually estimated to the average of frequencies observed in the absorption and the emission maximum.

Although the förster cycle is quite simple in use and thus extensively adopted, it is problematic when two absorption bands overlap or the electronic levels change during excited-state lifetime. Furthermore, the förster cycle can be hardly used when the excited acidic and basic forms are of different orbital origins.

### 1.8.6 Excitation Energy transfer (EET)[1k]

EET is a process where only energy is transferred from an excited molecule (D*) to an acceptor (A). It is called homotransfer when both donor and acceptor are chemically the same species. If D and A are not identical it is referred to as heterotransfer. EET can occur radiatively and non-radiatively.

**Radiative energy transfer**

$$D^* \rightarrow D + h\nu$$

$$h\nu + A \rightarrow A^* \text{ or } h\nu + D \rightarrow D^*$$

Radiative energy transfer is the emission of photons by a molecule D and subsequent absorption of these photons by a molecule A (or D). Its precondition is that the distance between D and A is larger than the wavelength of light emitted by molecule D. Interaction between the two molecules is not required. Radiative transfer causes a decrease in fluorescence intensity in the spectral overlap. This spectral phenomenon is called inner filter effect and is often accompanied with distortion of the emission spectra. This effect is unwanted in analytical application and can be effectively avoided by working with low dye concentrations and operating in a non-absorbing environment.

**Non-radiative energy transfer**

For non-radiative energy transfer interaction between a donor and an acceptor molecule is needed. It can also appear if the emission spectra of the donor and acceptor are overlapping each other. Equally to radiative ET, the extent of energy transfer correlates with the degree of overlap. Then some vibronic transitions in the donor and the corresponding transitions of the acceptor are practically of same energy and can couple with each other (i.e. are in resonance).

Thus, the term RET (resonance energy transfer) is often used. Fluorescence spectra are not changed in shape by RET but its intensity is decreased.

Two resonance energy transfer mechanisms have been established: Förster's and Dexter's mechanism.

FRET (Förster resonance energy transfer) is based on coulombic, dipole-dipole interactions and is effective over a distance up to 10 nm. In this case, the donor's electron is returning from the LUMO to the HOMO, while the electron of an acceptor is transferred from HOMO to the LUMO.

The FRET rate constant is given by:

$$k_T = \frac{1}{\tau_{D,0}} \left(\frac{R_0}{r}\right)^6 \qquad \text{Equation 15}$$

$k_T$ FRET rate constant ($s^{-1}$)

$\tau_{D,0}$ ES lifetime of the donor in absence of FRET (s)

$R_0$ Förster critical radius (nm)

r distance between donor and acceptor

This equation indicates that the efficiency of FRET is strongly changing at distances close to Förster critical radius ($R_0$). In contrast, Dexter's mechanism occurs at distances ≤ 1nm and is caused by intermolecular orbital overlap. However, Förster's mechanism is favoured even at small distances (if involved electronic transitions are not forbidden).

### 1.9 Optical chemical sensors (Optrodes)

Optical chemical sensors have received a great deal of attention from both academia and industry. They have found a wide application range in fields such as biomedical research,[4,5] marine biology[6,7], biotechnology[8,9], biological and toxicological screening[10],[11] and food packaging.[12] They are adequate in monitoring a variety of important species and parameters such as oxygen, ions and pH.

In principle, optical chemosensors obtain information about the analyte by binding between the analyte and a fully synthetic receptor over interaction with electromagnetic radiation. An optical sensor is based on two functional units: A recognition element (i.e. receptor), where specific interaction and identification of the analyte takes place; a transducer element that converts the recognition process into a measurable optical signal and a detector where change

of optical properties are converted into a readout unit.[13] Requirements for an analytical tool are usually reproducibility, linearity, dynamic range and sensitivity.

Optical sensors should additionally:

- show high luminescence brightness
- possess outstanding chemical and mechanical stability
- obtain high photostability
- be versatile in its scope (e.g. varying spectral properties or tuning dynamic range).
- be selective to the analyte of interest

Furthermore, sensors used in an (industrial) application are requested to be cheap, small, easy to use and robust.

Luminescence analytical tools are of great concern due to its high sensitivity and selectivity. It possesses high versatility, including intensity and decay time measurements, temporal and spatial resolution[14,15] of fluorescent techniques, kinetic studies,[16] and it enables also observation at various wavelengths. In brief, a huge amount of information can be achieved over electromagnetic radiation.

## 1.10 pH Indicator Dyes[11]

Traditionally, electrochemical methods have been utilized for pH analysis using an electrode. In most cases the glass electrodes provide accurate results in short time. Indeed, glass electrodes are well-established but optical pH sensors are more easily miniaturized and more robust against electromagnetic interferences. Fluorescent pH indicators also provide much better sensitivity within their dynamic range. Another benefit is the possibility of remote sensing by using fiber sensors.

Nevertheless, a significant drawback is the cross-sensitivity to ionic strength especially in low region.[17] The definition of pH implies that its value derives from activity of protons [$H^+$] and not concentration. However, pH measurements are dependent on concentration and not activity. Both are related over the Henderson-Hasselbalch equation:

$$pH = pK_A + log\frac{[A^-]}{[HA]} + log\frac{f_{A^-}}{f_{HA}} \qquad \text{Equation 16}$$

In very dilute solutions the activity coefficients $f_A$ and $f_B$ converge close to 1.

It should be made clear that $K_a$ is an 'apparent' constant which can be modified by a variety of factors such as ionic strength, specific interaction of indicator and environmental medium and micro-heterogeneous media (e.g. immobilisation layer)[18].

The high sensitivity of pH indicators is limited to a certain pH range, approximately ±1.5 units of $pK_a$ and refers to its application field:

For instance, in biotechnological systems pH-values around 6.5 are desired whereas physiological application (7.4) or marine systems (7.5-8.5) requires a higher pH range. However, $pK_a$ value of an indicator can be adjusted by introducing either electron-donating or electron-withdrawing groups. Furthermore, pKa is also influenced by immobilisation or entrapment of the indicator into a matrix.

Depending on its de-excitation mechanism (PPT, PET) several types of indicators can be classified:

### 1.10.1 Class A) pH-Indicators that show PPT (Photoinduced Proton Transfer)

Most PPT-based fluorophores principally show an increased acidity (lower $pK_a$) in the ES (excited state) than in GS (ground state). Consequentially, the excited fluorophore undergoes quick deprotonation, which results in an unchanged fluorescence spectrum of the basic form compared with its excitation spectrum. Nonetheless, a weak emission may result by geminate recombination of the acidic species. In other words only excitation spectra show pH dependency whereas emission spectra almost remain unchanged. Representatives of PPT are shown below:

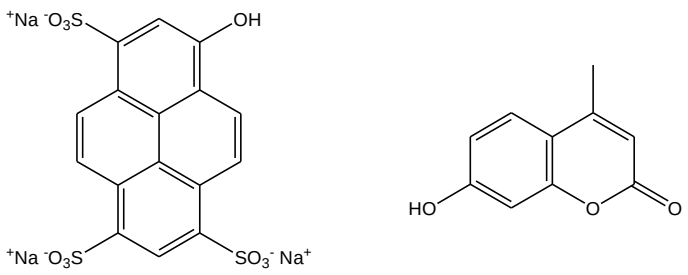


**Figure 19: Structures of widely used pH indicators that undergo Photoinduced Proton Transfer (PPT): HPTS (1-hydroxypyrene-3,6,8-trisulfonic acid trisodium salt, left) and 4-methyl-7-hydroxycoumarin (right).**

Pyranine and its derivates offer a pKa around 7 which is of great concern in intracellular measurements. They provide good photostability and have been used for pH sensing in a

variety of materials. Disadvantageous features are low excitation wavelength and its high sensitivity to ionic strength.[19,20] 4-methyl-7-hydroxycoumarin have found application in intracellular pH sensing.[21,22]

### 1.10.2 Class B) pH-Indicators that undergo PET (photoinduced electron transfer)

PET exhibiting pH-Indicators are usually modified by attaching an amine moiety to the dye. Fluorescence quenching is caused by photoinduced electron transfer from an amino group (receptor for $H^+$) to the aromatic backbone of the dye. Upon protonation of the amine electron transfer is blocked which results in an enhancement of fluorescence. This mechanism provides potentially higher sensitivity in respect with PPT.

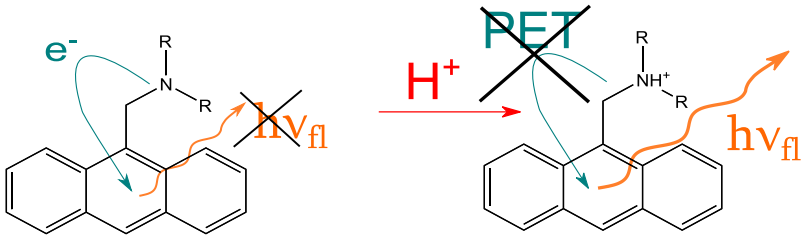


**Figure 20: Simplified Scheme of PET mechanism. Fluorescence intensity is decreased to zero (the indicator is "switched off") under basic conditions. Upon protonation, electron transfer is inhibited and thus enables fluorescence emission ("switched on").**

The following figure show some PET indicator dyes based on anthracene (left) and perylene (right) derivatives.[23, 24]

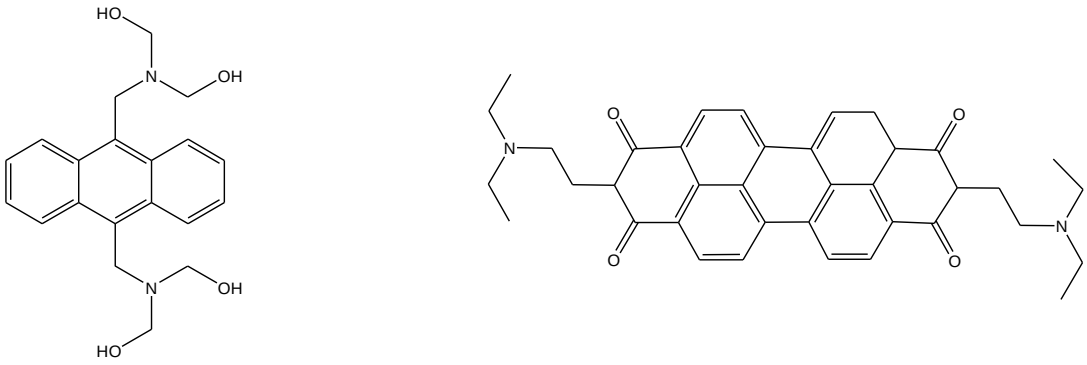


**Figure 21: Structures of PET based pH indicators exhibiting an amine moiety**

### 1.10.3 Class C) Fluorophores that exhibit neither PET nor PPT.

In this case the fluorescence spectra vs. pH should be similar compared with absorption spectra. This means that decreasing of pH results in downsizing of the basic form in both, absorption and emission band and a concomitant increase of the acidic form. Examples are eosin Y, fluorescein and its derivatives as well as SNARF and SNAFL.

Fluorescein dyes are one of the most investigated pH indicators. They are used in a variety of applications due to its extraordinary widespread pH response from 1 to 8 which can be explained by the occurrence of several transitions (neutral, monoanion, dianion form, Fig. **24**)

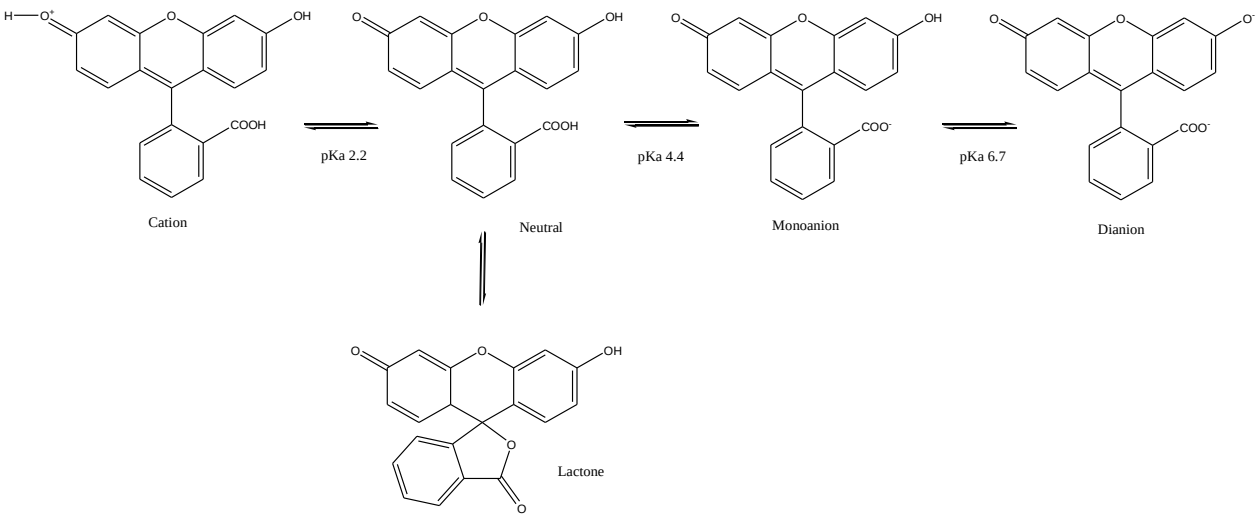


**Figure 22: Fluorescein undergoing several protolysis and lactonization equilibria**[17]

## 1.11 $BF_2$-Chelated Tetraarylazadipyrromethene Dyes

The previous discussed fluorescent pH indicators HPTS (8-hydroxypyrene-1,3,6-trisulfonic acid), 8- hydroxycoumarin, SNARF (seminaphthorhodafluors), carboxy-fluorescein and its derivatives are widely used even though they exhibit a variety of drawbacks. Carboxy-fluorescein, for instance, shows only moderate photostability and the same holds for its derivate 2', 7'-dihexylfluorescein (commonly used in marine systems).[17] In the case of HPTS, the $pK_a$ value is highly influenced by ionic strength and coumarins are only excitable in the near ultraviolet region (from 300 – 400 nm).

In some applications including cellular biology (determination of intracellular pH) it is necessary to apply red or near-infrared emissive fluorophores to fulfil a variety of

requirements: Due to the low absorption in the NIR region background signal and biomolecule's autofluorescence are significantly decreased. Additionally, NIR light enables deep penetration of the biological media and its excitation light source is economically priced. Nonetheless, the number of pH indicators having such desired spectral properties is limited.

SNARF indicators, for example, are prominent representatives of NIR chromophores but they show low photostability and exhibit moderate brightness.[25] The same drawbacks are held for cyanine dyes.[26]

In contrast, $BF_2$-chelated tetraarylazadipyrromethane dyes (aza-BODIPYs) possess excellent photo-physical properties and are accessible to structural modification (Fig. **23**). These indicator dyes show sharp bands in absorption and emission spectra and have high molar absorption coefficients (typically range from 40000 to 110000 $M^{-1}cm^{-1}$). They are usually resistant towards aggregation in solution and have excellent solubility properties in most common organic solvents (excluding water). [27]

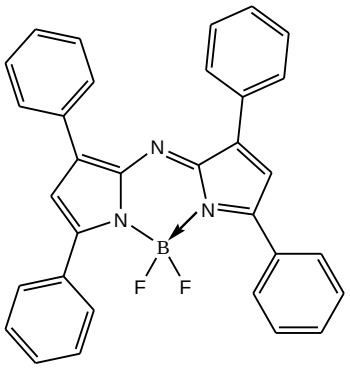


**Figure 23: $BF_2$-chelated tetraarylazadipyrromethane dye**

Two synthetic routes to prepare azadipyrromethene dyes are known.
One way of yielding unsymmetrical tetraarylazadipyrromethane is achieved by condensation of 2, 4-diaryl-5-nitroso-pyrroles with 2, 4-diarylpyrroles.[28]

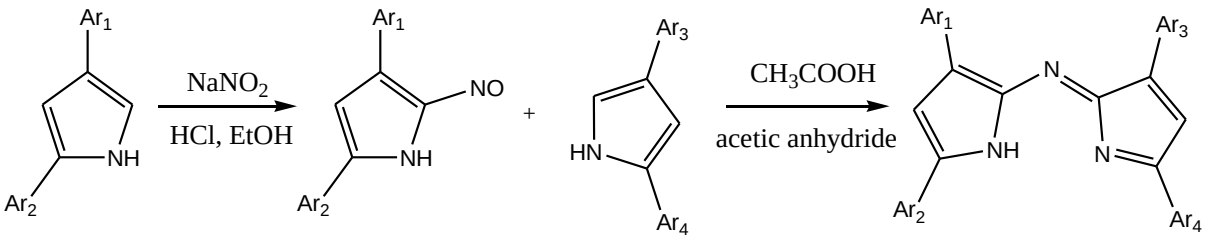


**Figure 24: Synthetic route of unsymmetrical tetraarylazadipyrromethane via condensation of 2, 4-diaryl-5-nitroso-pyrroles**

This strategy allows introduction of different aryl substituents with diverse functional groups. Unfortunately, final condensation is limited, especially if more than one aryl group is modified with a functional group.[28] Thus, this strategy may be unfavourable for preparation of functionalized pH indicator.

In the second method, diarylketones of chalcones are reacted with ammonium acetate at elevated temperatures.[29]

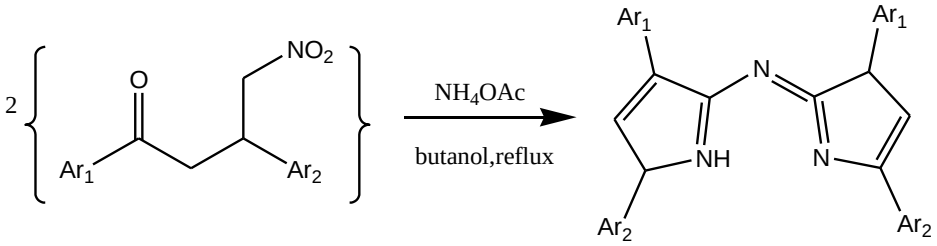


**Figure 25: Synthesis of symmetrical tetraarylazadipyrromethene.**

Tetraarylazadipyrromethane dyes (Fig. **24** and **25**) show virtually no fluorescence, possibly due to its non-planar molecule structure. Upon complexation of the dye with boron trifluoride the molecule is forced in a rigid structure which enables fluorescence (Fig. **26**). Additionally, the obtained p$K_a$ value is decreased to approximately 1 unit which can be explained by partially lowered π-conjugation between the pH sensitive phenolate and the aromatic backbone of the dye. Additionally, the electron-pulling power of the $BF_2$ group may also influence the pH sensitive properties. [30]

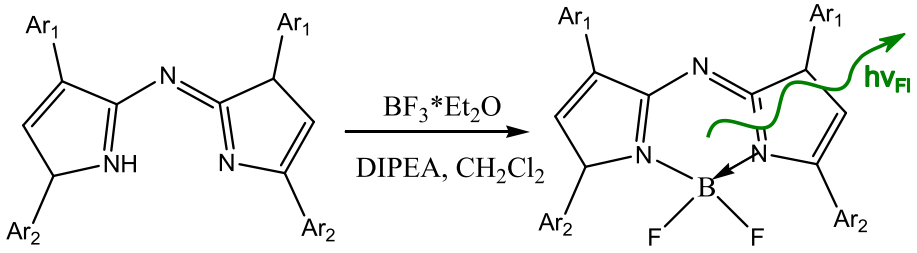


**Figure 26: Chelation of the azadipyrromethene dye with boron trifluoride enables fluorescence emission.**

$BF_2$-chelated tetraarylazadipyrromethane dyes are highly accessible for structural modification. Several aza-BODIPY dyes functionalized with amino- or hydroxyl substituents were reported by O'Shea and co-workers.[31,32,33,34,35] Thus, Jokic and co-workers have synthesized a series of new aza-BODIPYs.[30] Depending on introducing either electron-

donating or –withdrawing groups $pK_a$ values can be tuned from 7 to 11. Thus, these new pH indicators are suitable in a diverse range of analytical applications, especially in marine systems and for measurements at physiological pH.

However, sensors prepared with these aza-BODIPY dyes are based on physical entrapment. Although leaching was not critical its prevention is highly desirable, since it enhances the performance of the sensor with respect to long term stability and shelf life of the sensor.

### 1.12 Immobilisation

In the simplest case, immobilisation of a pH indicator is achieved by non-covalent entrapment of the dye in a rigid polymeric support. However, the indicator's mobility is thereby not suppressed which can cause a variety of problems such as leaching or dye aggregation within the matrix which can introduce quenching processes. Both cases result in alteration of the optical response and thus obtained measurement data may be imprecise or inaccurate.

In contrast, covalent linking of pH indicators to a polymeric network can prevent the dye from leaching and suppress its aggregation and migration within the polymer. Additionally, the concept of covalent coupling can fulfil a series of criteria relevant for practical applications:

a) It ensures signal stability and keeps signal drift at a minimum

b) Due to the increased stability time-consuming calibration of the sensor is not obligatory.

c) Shelf-life stability is enhanced and thus provides long-term application.

d) Covalent immobilisation prevents the pollution of the sample with the sensing compound which is of great concern, especially in food and medical applications.

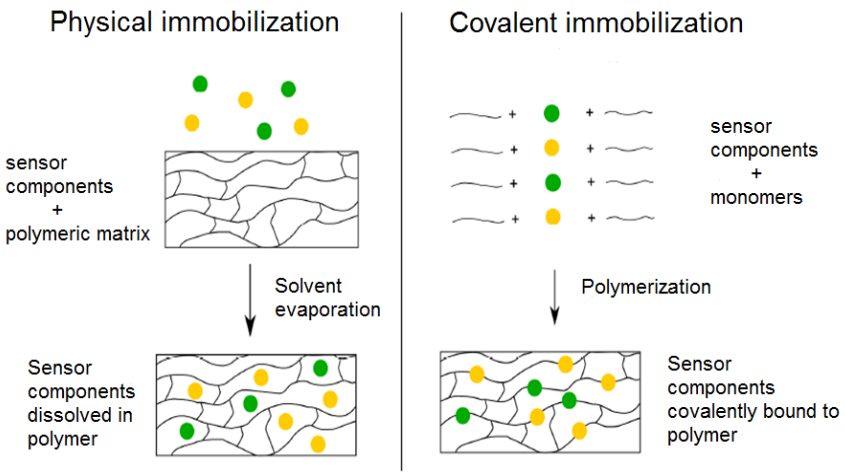


**Figure 27: Scientific approach for immobilization of indicator dyes: physical entrapment (left) and covalent linking (right).**

A favourable method for covalent immobilisation of a pH-indicator is based on functionalizing the dye with a monomeric residue that enables co-polymerisation of the indicator dye in a polymeric support. For that kind of ligation strategy some important criteria should be considered:

(i) The generated chemical bond should exhibit long-term stability in the sample (e.g. no hydrolysis) and the ligation strategy should be compatible with the functionalities of pH indicator and matrix. (ii) The linkage should not influence the sensor readout technique and photo-oxidation or photo-reduction should be kept at a minimum. (iii) Some practical considerations such as quantitative yield, by-product formation and reaction conditions should not be disregarded.

## 1.13 Immobilisation techniques

### 1.13.1 Lipophilization

A simple way to prevent pH-indicators from leaching is adding a lipophilic moiety to the dye. Due to the enhanced hydrophobicity it is possible to embed the indicator in lipophilic blocks of a polymer matrix. However, lipophilization may favour dye aggregation which can cause self quenching processes.

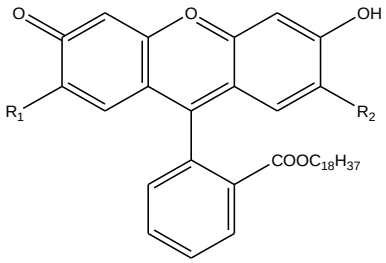


**Figure 28: Fluorescein which is lipophilized by esterfication of the carboxy group with an alkyl chain. This hydrophobic fluorescein derivative can be easily embedded in a polymeric matrix and thus is protected from leaching events.[17]**

### 1.13.2 Suzuki coupling

Suzuki cross-coupling is a palladium catalysed reaction which provides efficient and versatile ways for C-C-bond formation. This reaction is extensively used throughout organic chemistry and has found application in natural product synthesis.[36,37]

Suzuki coupling typically employs a Palladium catalyst, a base and an organyl halide which acts as a nucleophilic reagent. Its catalytic cycle is composed of three distinct steps: oxidative addition, transmetallation and reductive elimination.

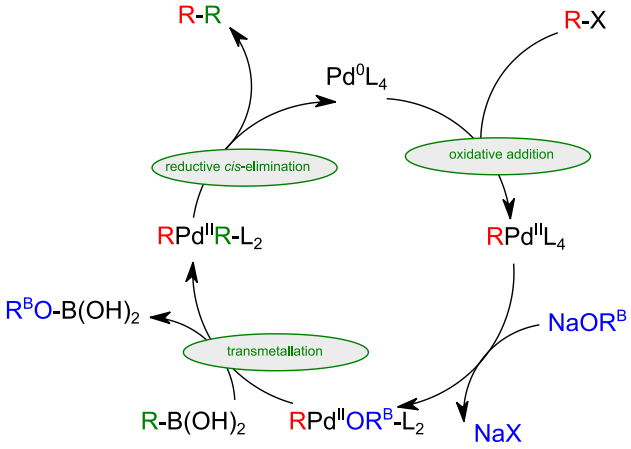


**Figure 29: Catalytic cycle of the Suzuki reaction**

This transition metal catalysed coupling reaction is highly desired due to their outstanding stability even in aqueous solution, limited side reactions, and low toxicity. It exhibits high functional-group tolerance, region- and stereospecifity and offers one-pot syntheses.

Hutter et al.[2] presented a covalent immobilization approach for an oxygen sensor system employing Suzuki coupling. The method relies on the introduction of a halogenide into the porphyrin structure. Subsequent functionalization with a polymerizable group opens the possibility of polymerisation resulting in a covalently linked oxygen sensor.

### 1.13.3 Click chemistry[38,39]

Click chemistry is typically characterized by simple reactions conditions, high yields, wide scopes, a high degree of modularity and readily available starting educts. A wide variety of different reactions are regarded to as "click chemistry" (Figure **27**). The MIC-Ligation is based on the addition of a thiol across a maleimido-moiety. The thiol-en-ligation is an addition of a thiol across a terminal olefin initiated by radicals. The widely used huisgen-azide-alkyne-coupling is a [3+2] cycloaddition of a terminal alkyne group and an azide.

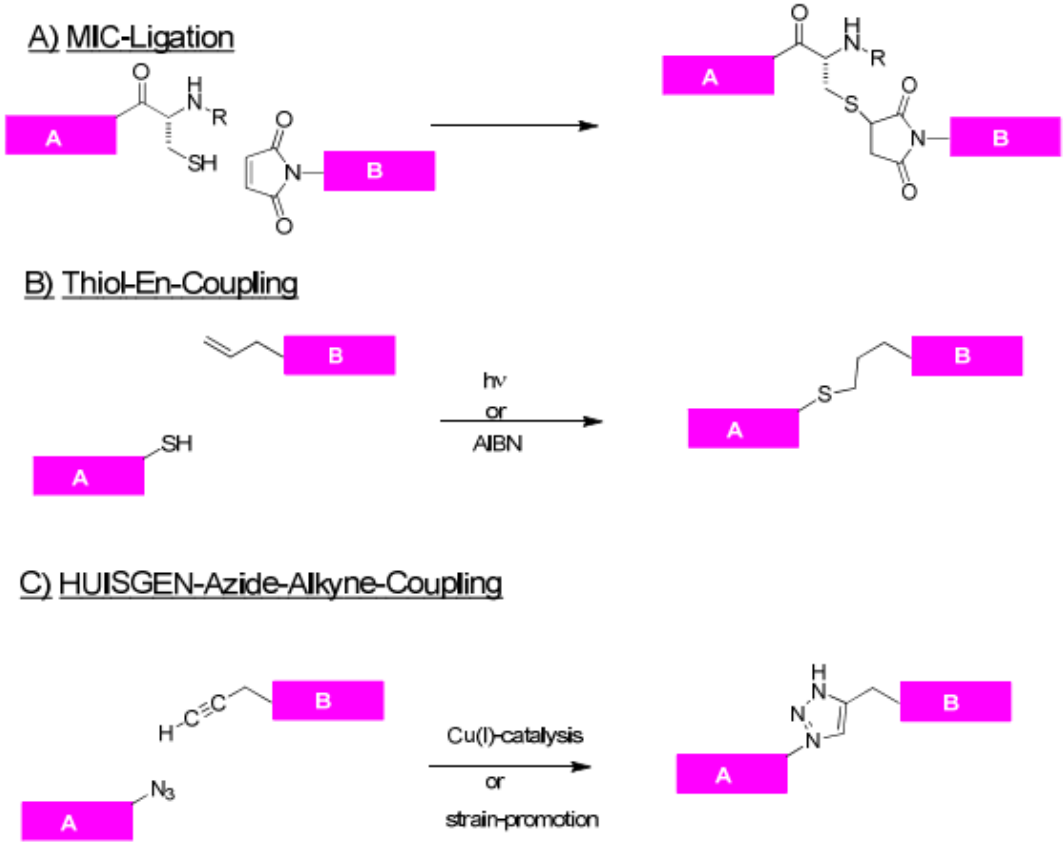


**Figure 30: An overview of representative ligation strategies classified as click chemistry reactions: A) MIC ligation. B) Thiol-En-ligation C) Huisgen-azide-alkyne coupling**

### 1.13.4 Bioconjugate crosslinking via EDC/NHS coupling [40]

Bioconjugation is a powerful tool for covalent coupling of indicators to a wide variety of polymer matrices. It provides a large number of well-established techniques which are characterized by high reproducibility, inexpensive chemicals and mild reaction conditions. These conjugation-techniques rely on functional groups occurring in proteins such as amines, carboxylic acids or thiol-residues.

**EDC/NHS coupling**

EDC ((1-ethyl-3-(3-dimethylaminopropyl) carbodiimide hydrochloride) is a well known coupling agent for use in bioconjugation which exhibits outstanding properties. The advantages of EDC are enhanced solubility (organic solvents and aqueous solution) and its urea by-product can be easily removed by aqueous extraction compared with its precursor DCC (*N*, *N'*-Dicyclohexylcarbodiimid).

EDC activates a carboxylic acid group by forming an O-acylisourea intermediate which can react with an amine to form an amide bond. However, this intermediate is highly unstable and can readily undergo hydrolysis. The efficiency of EDC coupling can be significantly increased by addition of NHS (N-Hydroxysuccimid) which stabilizes the intermediate by converting it into an NHS-ester.

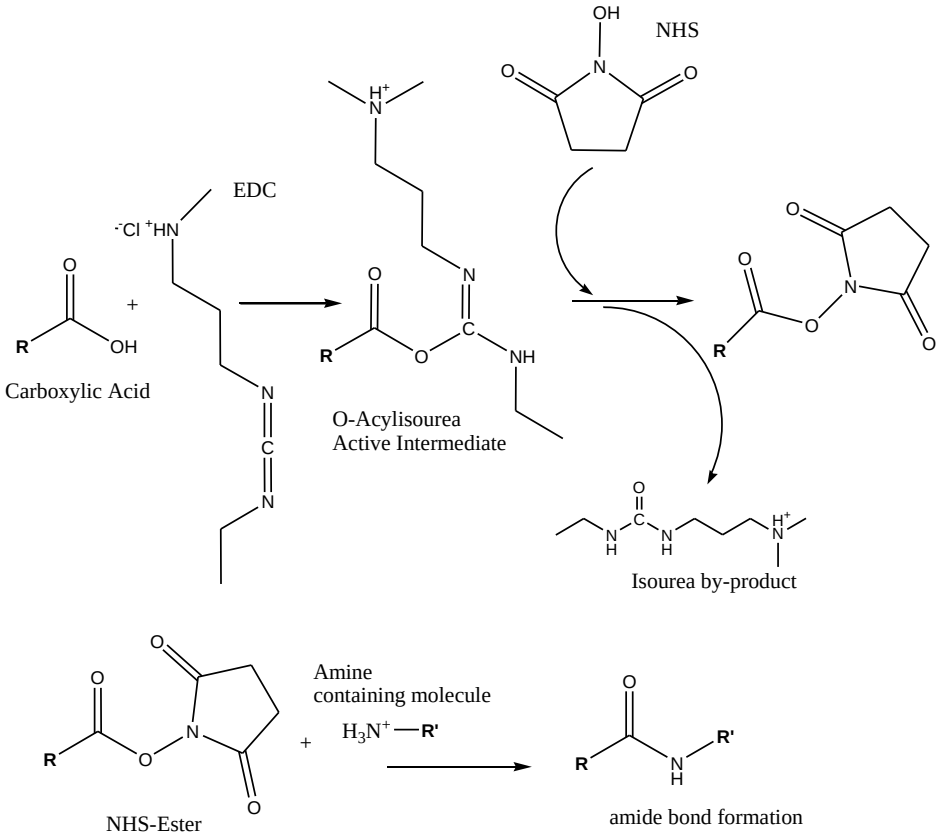


**Figure 31: A reaction scheme for EDC/NHS-coupling.**

## 2. Experimental Section

### 2.1 Methods

Absorption measurements were performed on a Cary 50 UV-VIS spectrophotometer from Varian, Palo Alto, United States (www.varianinc.com) at a medium scan rate using baseline correction and an adequate blank sample. pH sensors were placed in a home-made stainless steel flow-through cell, and absorption was monitored while buffers (with different pH and ionic strength) were passed through it.

The pH of the buffer solution was adjusted with a pH meter using a glass electrode (InoLab pH/ion, WTW GmbH & Co. KG, www.wtw.com). The pH meter was calibrated at 25°C with standard buffers of pH 7.01 and pH 4.01 (WTW GmbH & Co. KG, www.wtw.com). Ionic strength (IS = 20, 160 or 510 mM) of the buffers was adjusted by using sodium chloride as the background electrolyte.

Fluorescence spectra in solutions were recorded on a Hitachi-F-7000 spectrofluorometer (www.hitachi.com) and corrected for detector response. Fluorescence measurements for the pH sensor were performed on a Fluorolog (Horiba J. Y., www.horiba.com).

Relative quantum yields were determined by using tera-tert-butyl-29H,31H-phtalocyanine as a standard ($\phi = 0.44$ ) in THF according to Demas and Crosby.[41, 42]

NMR spectra were recorded on a 300 MHz instrument (Bruker; coupling constants *J* will be stated in Hz) in DMSO-$d_6$ or $CDCL_3$ with TMS (tetramethylsilane) as a standard.

Electron impact (EI, 70 eV) mass spectra were recorded on a Waters GCT Premier equipped with direct insertion (DI). MALDI-TOF mass spectra were monitored on a Micromass TofSpec 2E. The spectra were taken in reflectron mode at an accelerating voltage of +20kV.

## 2.2 Dye Synthesis

### 2.2.1 4-((E)-3-phenylacryloyl) benzoic acid

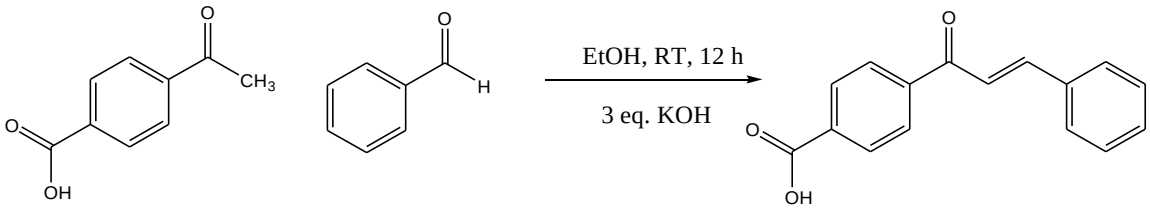


**Figure 32: Reaction scheme for the synthesis of 4-((E)-3-phenylacryloyl)benzoic acid**

4-Acetylbenzoic acid (1 eq, 5.00 g, 30 mmol), benzaldehyde (1 eq, 1.2 ml, 30 mmol) were dissolved in ethanol (250 ml) and an aqueous solution of NaOH (5.12 g, 90 mmol) was added. The reaction was stirred at room temperature for 12 hours. Then the solution was acidified with 1 M hydrochloric acid and the resulting precipitate was isolated by filtration and washed with water to give the product without any purification, as a yellow solid. (3.65 g, 73.0 %)

### 2.2.2 4-(4-nitro-3-phenylbutanoyl) benzoic acid (1a)

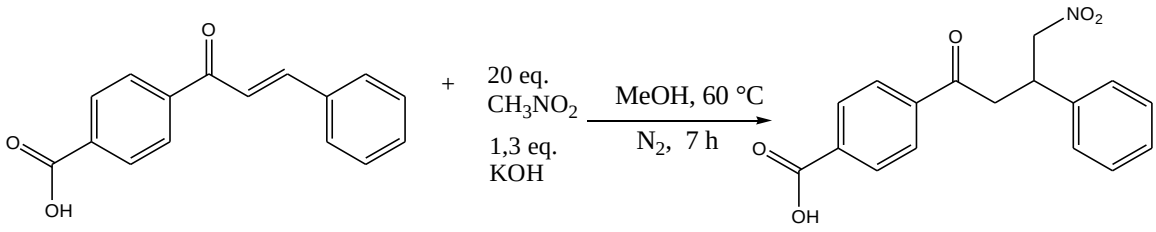


**Figure 33: Synthesis of 4-(4-nitro-3-phenylbutanoyl) benzoic acid**

**1a** (1 eq, 3.65 g, 15 mmol) was dissolved in methanol (250 ml), nitromethane (20 eq, 15.64 ml, 300 mmol) and KOH (1.3 eq, 1.06 g, 19.5 mmol) were added, and the reaction was heated under reflux for 7 hours under inert atmosphere of $N_2$. After cooling to room temperature, the solvent was removed in vacuum, and the obtained yellow solid was acidified with 1 M hydrochloric acid and partitioned between ethyl acetate (100ml) and $H_2O$ (100 ml). The organic layer was separated, dried over sodium sulphate, and evaporated under reduced pressure. The obtained product was used for further synthesis without purification. (2.47 g, 67.6 %)

### 2.2.3 1-(-4-Hydroxyphenyl)-4-nitro-3-phenylbutan-1-one (1b)

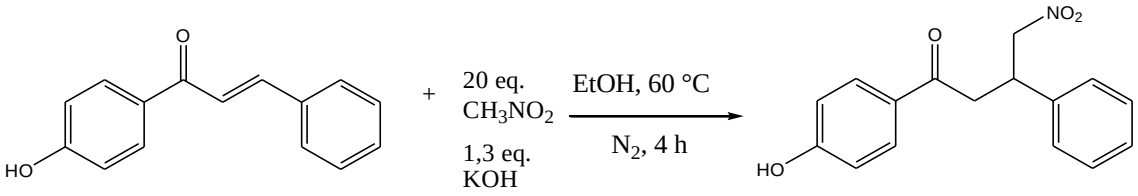


**Figure 34: Reaction scheme for the synthesis of 1-(-4-Hydroxyphenyl)-4-nitro-3-phenylbutan-1-one**

A solution of 1-(4-hydroxyphenyl)-3-phenylpropenone (1 eq, 2 g, 8.9 mmol), nitromethane (20 eq, 9.63 ml, 178 mmol) and KOH (1.3 eq, 0.6 g, 10.7 mmol) in EtOH (10 ml) was heated at 60 °C under reflux for 4 h under inert atmosphere of $N_2$. After cooling to room temperature, the solvent was removed in vacuum, and the oily residue obtained was acidified with 1 M hydrochloric acid and partitioned between ethyl acetate (50 ml) and $H_2O$ (50 ml). The organic layer was separated, dried over sodium sulphate, and evaporated under reduced pressure. The obtained product was used for further synthesis without purification (2.06 g, 80 %)

### 2.2.4 4-(2-((5-(4-hydroxyphenyl)-3-phenyl-1H-pyrrol-2-yl)imino)-3-phenyl-2H- pyrrol 5-yl)benzoic acid (1c)

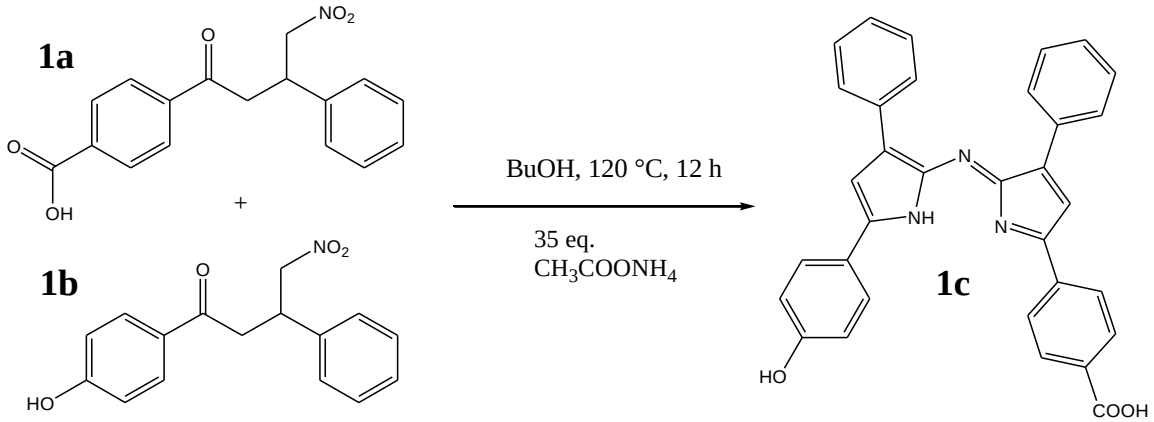


**Figure 35: Reaction scheme for the synthesis of 4-(2-((5-(4-hydroxyphenyl)-3-phenyl-1H-pyrrol-2-yl)imino)-3-phenyl-2H-pyrrol-5-yl)benzoic acid**

Compound **1a** (1 eq, 2 g, 7 mmol), compound **1b** ( 1 eq, 2.19 g, 7 mmol) and ammonium acetate (35 eq, 15.22 g, 245 mmol) were dissolved in butanol (100 ml) and heated under

reflux at a temperature of 120 °C for 12 h while stirring. After the reaction was cooled down to room temperature the solvent was removed in vacuum. The obtained solid was washed with water three times. Then the raw product was redissolved in tetrahydrofuran and was dried onto silica gel to facilitate column chromatography. The solid dried onto silica gel was placed atop a chromatography column packed with silica gel in dichloromethane.

Red, orange and yellow fractions and the symmetrical by-product were eluted with 2% THF/$CH_2Cl_2$. The final product was obtained by gradually increasing the polarity from 10-18% THF/$CH_2Cl_2$. The second symmetrical by-product remains on the column. Absorption spectra were recorded and thin-layer chromatography was performed using TLC-plates (15% THF/$CH_2Cl_2$) to identify fractions containing the product. The fractions were unified and the solvent evaporated. The final product was recrystallised from hexane/tetrahydrofuran mixture and dried in the oven at 60 °C. For the calculation, the theoretical yield of the asymmetrical product is set as 100%. (300 mg, 12%)

$^1$H NMR (300 MHz, DMSO-*d6*) δ: 8.19-8.06 (m, 8H); 7.99-7.96 (d, J = 8.3 Hz, 2H); 7.87 (s 1H), 7.51-7.33 (m, 7H); 7.08-7.05 (d, J= 8.6 Hz, 2H)

Electron impact direct insertion time-of-flight (EI-DI-TOF) *m/z* [$MH^+$] found 510.184, calc 510.1818.

### 2.2.5 4-(2-((5-(4-hydroxyphenyl)-3-phenyl-1H-pyrrol-2-yl)imino)-3-phenyl-2H-pyrrol-5-yl)-N-(3-methacrylamidopropyl)benzamide (1d)

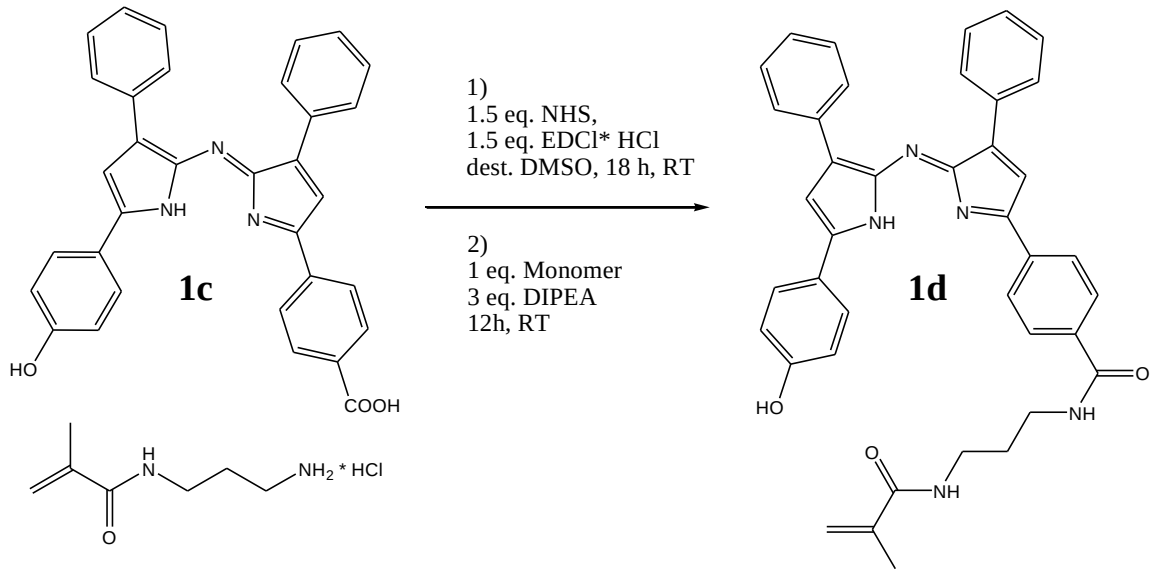


**Figure 36: Reaction scheme for the synthesis of 4-(2-((5-(4-hydroxyphenyl)-3-phenyl-1H-pyrrol-2-yl) imino)-3-phenyl-2H-pyrrol-5-yl)-N-(3-methacrylamidopropyl)benzamide**

Compound **1c** (1 eq, 300 mg, 0.59 mmol) was dissolved in dry DMSO (25 ml). N-hydroxysuccinimide (1.5 eq, 102 mg, 0,88 mmol) and 1-(3-Dimethylaminopropyl)-3-ethylcarboiimide hydrochloride (1.5 eq, 169 mg, 0.88 mmol) were added and the reaction was stirred at room temperature for 18 h under constant TLC monitoring (2% MeOH/$CH_2Cl_2$). After compound **1c** was fully converted N-(3-aminopropy) methacrylamide hydrochloride (1 eq, 105 mg, 0.59 mmol) and *N*,*N*-diisopropylethylamine (3 eq, 308 µl, 1.78 mmol) were added and the reaction mixture was stirred at RT for 12 h.

The raw product was precipitated by adding saturated aqueous NaCl solution. Upon centrifugation of the suspension and removal of the solvent, the precipitate was redissolved in $CH_2Cl_2$, washed with $H_2O$ three times (3x100 ml) and dried over $Na_2SO_4$. Then the solution was dried onto silica gel to facilitate column chromatography. The solid dried onto silica gel was placed atop a chromatography column packed with silica gel in dichloromethane. After removing unreacted NHS ester (1.5% MeOH/$CH_2Cl_2$) the final product was obtained by eluting with 2% MeOH/$CH_2Cl_2$. The factions containing the product (TLC: 3% MeOH/$CH_2Cl_2$) were combined and the solvent was removed by using rotary evaporator. In order to remove grease and other impurities the product was recrystallised from hexane/tetrahydrofuran yielding a blue solid (168 mg, 45%)

$^1$H NMR (300 MHz, DMSO-*d6*) δ: 8.63-8.6 (t, J = 5.7Hz, 1H); 8.19-7.97 (m, 10 H); 7.86 (s, 1H); 7.53-7.33 (m, 7H); 7.07-7.04 (d, J = 8.6Hz); 5.68 (s, 1H); 5.34 (s, 1H); 3.25-3.18 (m, 2H); 1.88 (s, 3H); 1.79-1.69 (m, 2H)

MALDI-TOF *m/z* found 634.2836, calculated 634.2818.

### 2.2.6 (Z)-4-(5-((5-(4-((3-methacrylamidopropyl)carbamoyl)phenyl)-3-phenyl-2H-pyrrol-2-ylidene)amino)-4-phenyl-1H-pyrrol-2-yl)phenyl acetate (1e)

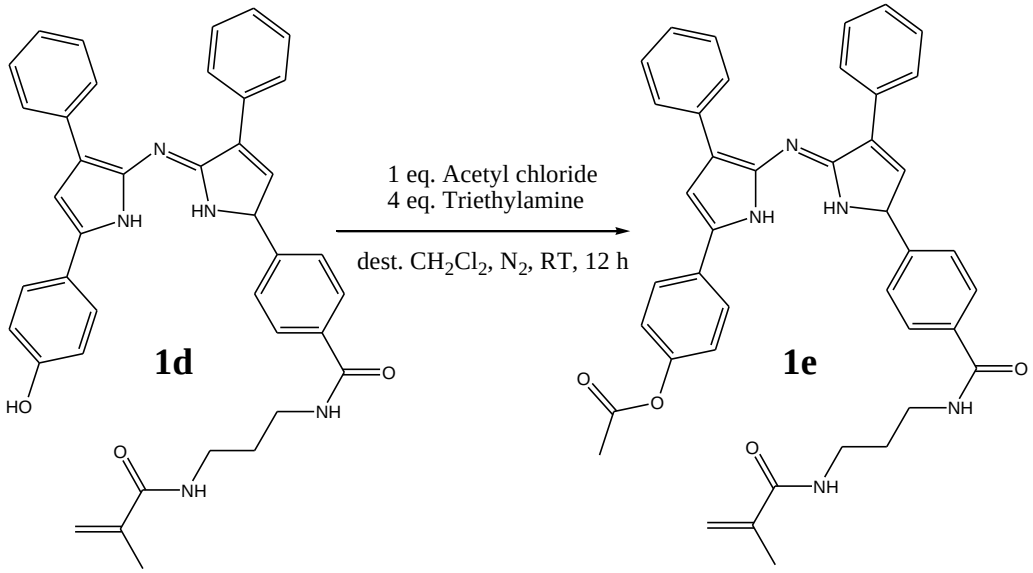


**Figure 37: (Z)-4-(5-((5-(4-((3-methacrylamidopropyl)carbamoyl)phenyl)-3-phenyl-2H-pyrrol-2-ylidene)amino)-4-phenyl-1H-pyrrol-2-yl)phenyl acetate**

Compound **1d** (1 eq, 160 mg, 0.25 mmol) was dissolved in dry $CH_2Cl_2$. After adding triethylamine (4 eq, 140 µl, 1 mmol), acetyl chloride (1 eq, 18 µl, 0.25 mmol) was slowly dropped into the solution. Acidic fumes were removed by constant flushing the reaction mixture under constant $N_2$ stream.

The solution was placed atop a chromatography column which was packed with dichloromethane. The final product was obtained by eluting with 1% MeOH/$CH_2Cl_2$. Upon separating the product, further purification was achieved by crystallization from hexane/tetrahydrofuran to give the final product as red metallic solid (81 mg, 48%).

$^1$H NMR (300 MHz, $CDCl_3$) δ: 8.65-8.61 (t, J = 5.8Hz, 1H); 8.25-8.22 (d, J = 8.5Hz, 2H); 8.1-7.96 (m, 9H); 7.79-7.68 (m, 9H); 7.79 (s, 1H); 7.68 (s, 1H); 7.51-7.38 (m, 8H); 5.68 (s, 1H); 5.34 (s, 1H); 3.24-3.18 (m, 2H); 2.35 (s, 3H); 1.88 (s, 3H); 1.79-1.69 (m, 2H)

MALDI-TOF *m/z* found 676.295 calculated 676.292.

### 2.2.7 $BF_2$ Chelate of 1e (1)

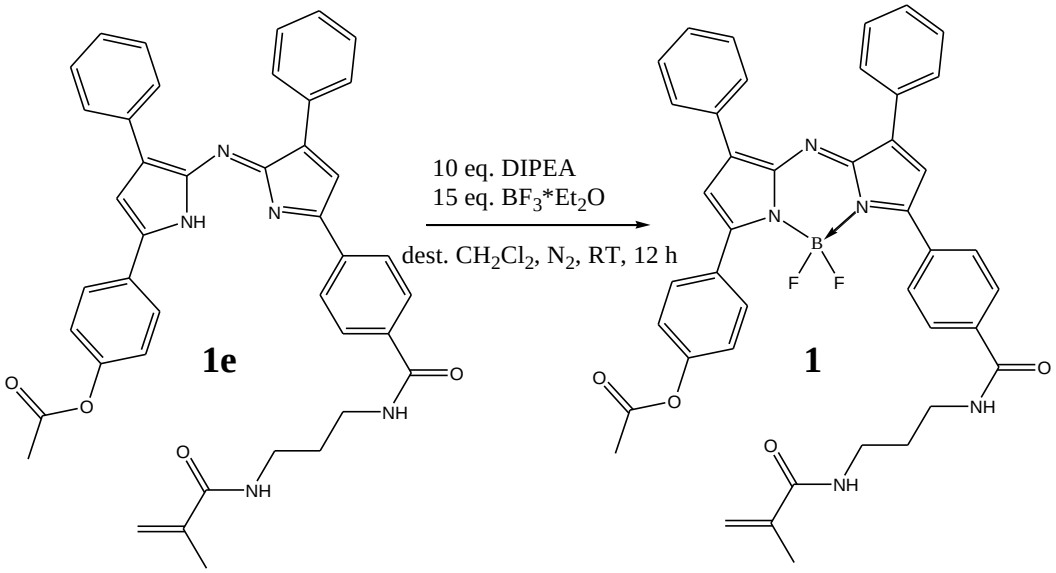


**Figure 38: Reaction scheme of $BF_2$ chelate of 1e**

After compound **1e** (1 eq, 80 mg, 0.12 mmol) was dissolved in dry $CH_2Cl_2$ (300 ml) *N*,*N*-diisopropylethylamine (DIPEA, 10 eq, 196 µl, 1.2 mmol) was added and stirred at room temperature for 45 minutes. Then, boron trifluoride diethyl etherate (15 eq, 220 µl, 1.8 mmol) was added and the reaction solution was stirred under $N_2$ for 24 h. The green solution was washed with $H_2O$ three times (3x200 ml) and dried over $Na_2SO_4$. The boron-free compound **1e** was removed by treating with $MgSO_4$ and the crude product was purified by column chromatography on silica-gel eluting with 2% MeOH/$CH_2Cl_2$. Further purification was achieved by recrystallisation of the product from tetrahydrofuran/ hexane mixture. (80 mg, 50%)

$^1$H NMR (300 MHz, $CDCl_3$) δ: 8.13-8.05 (m, 8H); 7.98-7.95 (d, J = 8.4Hz, 2H); 7.5-7.46 (m, 6H); 7.3-7.23 (m, 2H); 7.05 (s, 2H); 6.63-6.59 (t, J = 5.9Hz, 1H); 5.82 (s, 1H); 5.38 (s, 1H); 3.56-3.5 (q, J = 6.2Hz), 2H); 3.48-3.42 (q, J = 6.2Hz); 2.34 (s, 3H); 2.02 (s, 3H).

MALDI-TOF *m/z* found 723.2831, calculated 723.2836.

### 2.2.8 $BF_2$-chelate of 1d (2)

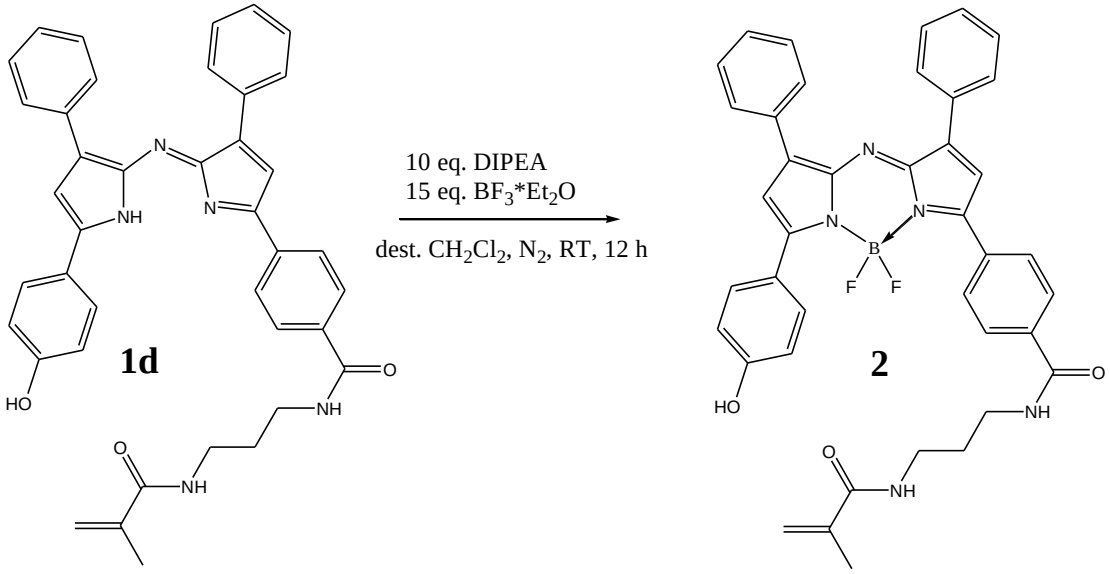


**Figure 39: Reaction scheme of $BF_2$ Chelate of 1d**

Compound **1d** (1 eq, 100 mg, 0.16 mmol) was dissolved in dry $CH_2Cl_2$ (350 ml). *N*,*N*-diisopropylethylamine (10 equiv, 261 µl, 1.6 mmol) was added and the reaction mixture was stirred for 45 min. Then, boron trifluoride diethyl etherate (15 eq, 294 µl, 2.4 mmol) was slowly added to the solution and stirred under inert atmosphere ($N_2$) at room temperature over night. During the course of the reaction, the $BF_2$-chelate partly precipitated from the reaction mixture. The solution was washed with $H_2O$ three times (3x200 ml) and dried over $Na_2SO_4$. After removing $CH_2Cl_2$ and redissolving in a small amount of tetrahydrofuran, boron-free compound **1d** was removed by treating with $MgSO_4$. The crude product was purified by column chromatography on silica-gel eluting with 2% MeOH/$CH_2Cl_2$. Further purification was achieved by dissolving the product with tetrahydrofuran and subsequent precipitating with hexane. (45 mg, 41%)

$^1$H NMR (300 MHz, DMSO-$d_6$) δ: 8.63 (t, J = 5.5Hz, 1H); 8.26-8.11 (m, 8H); 7.96 (d, J = 8.5Hz, 3H); 7.88 (s, 1H); 7.59-7.43 (m, 7H); 6.94 (d, J = 8.9Hz, 2H); 5.67 (s, 1H); 5.34 (s, 1H); 3.24-3.17 (m, 4H); 1.87 (s, 3H); 1.77-1.68 (m, 2H).

MALDI-TOF *m/z* found 682.2808, calculated 682.2731.

### 2.2.9 $BF_2$-chelate of 4-((5Z)-5-(3,5-diphenyl-2H-pyrrol-2-ylideneamino)-4-phenyl-1H pyrrol-2-yl)phenyl acetate (4)

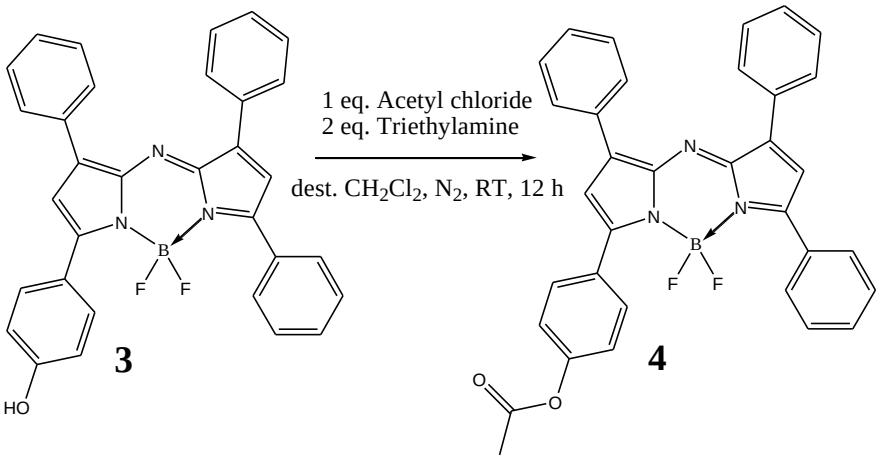


**Figure 40: Reaction scheme of $BF_2$-chelate of 4**

Compound **3** was synthesized according to procedure by Jokic et al.[30] After dissolving dye **3** (1 eq, 20 mg, 0.039 mmol) in dry $CH_2Cl_2$, triethylamine (2 eq, 11 µl, 0.078 mmol) was added and then acetyl chloride (1 eq, 3 µl, 0.039 mmol) was slowly dropped into the solution. The reaction was stirred at room temperature for 12 h. Acidic fumes were removed by constant flushing the reaction mixture under $N_2$ stream. Purification by column chromatography on silica gel eluting with $CH_2Cl_2$ and recrystallisation from hexane/tetrahydrofuran gave the final product as red metallic crystals (18 mg, 85%).

$^1$H NMR (300 MHz, $CDCl_3$) 8.1-8.06 (m, 8H); 7.51-7.44 (m, 9H); 7.22 (s, 1H); 7.05-7.02 (d, J = 8.2Hz, 2H); 2.33 (s, 3H)

MALDI-TOF *m/z* found 555.1931, calculated 555.1935

### 2.2.10 Preparation of a pH sensor

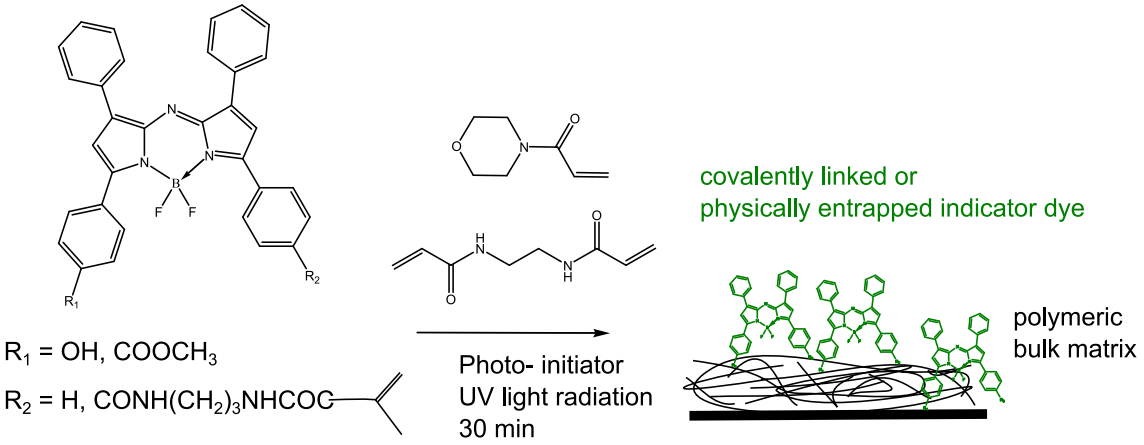


**Figure 41: Preparation of pH sensors using acryloylmorpholine as bulk matrix and ethylenbisacrylamide as cross-linker. Photo-copolymerisation was initiated by 2-hydroxy-4'-(2-hydroxyethoxy)-2-methylpropiophenone and UV light radiation.**

A dust-free glass slide was functionalized with polymerizable groups by coating it with a solution of methacryloxypropylmethyldichlorosilane (0.02 ml) in dry tetrahydrofuran (1ml). After the slide was dried for 10 min under a constant $N_2$ stream, unreacted silane was removed with acetone and the slide was dried at 60°C for 15 min. Then, the functionalized slide was covered with a monomer mixture containing 1-acryloylmorpholine (67.7 mg, 62 µl), cross-linker ethylenebisacrylamide (3.36 mg, 4 mol%), initiator 2-hydroxy-4'-(2-hydroxyethoxy)-2-methylpropiophenone (0.06 mg, 0.05 mol%) and dye **1** (0.36 mg, 0.1 mol%) under $N_2$. After 10 min the monomer solution was distributed over the slide by putting a non-functionalized slide on top. The obtained layer should be evenly spread over the slide without exhibiting any bubbles or hairlines. After the two glass slides were fixed with a tape, polymerization was started by illumination with a UV light source (366nm) under argon. After 30 minutes the polymerization was finished yielding a rigid polymer matrix with covalently coupled pH indicator.

**Table 2: Composition of monomer mixtures used for photo-co-polymerisation**

| pH sensor | dye 0.5 mg | acryloylmorpholine [mg] | ethylenebisacrylamide [mg] | photo-initiator [mg] |
|---|---|---|---|---|
| **A** | **1** | 93.44 | 4.65 | 0.081 |
| **B** | **2** | 99.20 | 4.93 | 0.082 |
| **C** | **4** | 132.14 | 6.57 | 0.109 |

## 3. Results and discussion

The aim of this work is the development of a synthetic strategy towards the covalent immobilization of $BF_2$-chelated tetraarylazadipyrromethane based pH indicators in a poly(acryloylmorpholine) matrix.

The scientific strategy to obtain polymeric material with covalently bound pH indicator was to co-polymerize the monomer matrix with a modified indicator containing a polymerizable group. This is achieved by functionalization of the indicator with carboxyl reactive group in order to attach methacrylate polymerizable groups. Subsequent photo-co-polymerization into a cross-linked polymer layer which in turn is covalently linked onto a glass substrate yields a pH sensor with covalently linked pH indicators.

### 3.1 Synthetic considerations

One synthetic route of yielding unsymmetrical tetraarylazadipyrromethane is achieved by condensation of 2, 4-diaryl-5-nitroso-pyrroles with 2, 4-diarylpyrroles.

Figure **41** gives an overview of preliminary experiments based on unsymmetrical synthesis of tetraarylazadipyrromethane according to Hall et al.[28] Hydroxyl-pyrrole could only be obtained in very low yield (15%) and subsequent conversion in its nitroso-pyrrole derivative failed under these indicated reaction conditions. Furthermore, condensation of hydroxyl-pyrrole and non-substituted nitroso-pyrrole did not obtain the desired unsymmetrical tetraarylazadipyrromethane in sufficient yield. These preliminary experiments indicated that this synthetic strategy is unfavourable for the synthesis of a functionalized aza-BODIPY dye. Hall et al.[28] synthesized unsymmetrical tetraarylazadipyrromethene dyes carrying only electron-donating subsituents on its aryl rings (*p*-$MeOC_6H_4$, *p*-$Et_2NCH_2C_6H_4$, *p*-$Me_2NC_6H_5$, etc.). It is very likely that the electron-pulling power of the hydroxyl group inhibits insertion of a nitroso-group into a pyrrole ring. Moreover, condensation of hydroxyl-pyrrole and even a non-substituted pyrrole results in a high amount of by-products which might be caused by the electron-withdrawing effect of the hydroxyl group. It is assumed that these phenomena also occur in carboxyl carrying aryl rings.

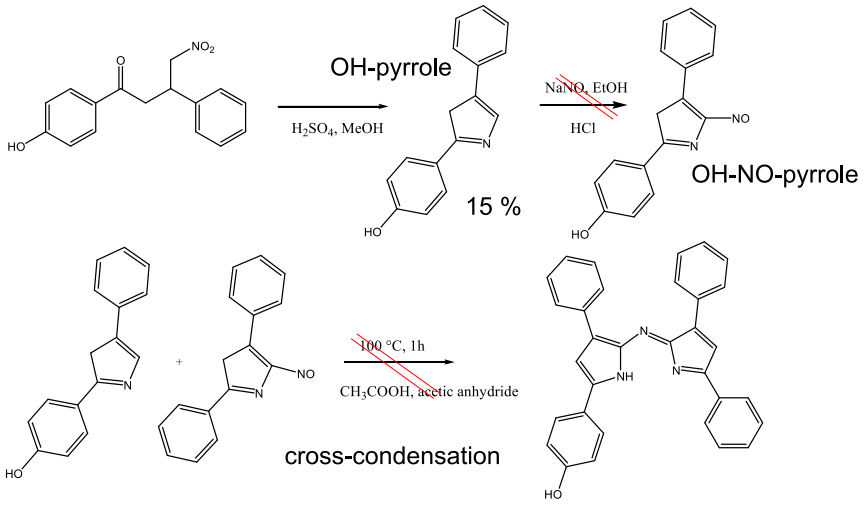


**Figure 42: Preliminary experiments based on unsymmetrical synthesis of tetraarylazadipyrromethane according to Hall et al.[28]**

Hence, another synthetic method where diarylnitroketones of chalcones were reacted with ammonium acetate at elevated temperature was assessed (shown in Figure **43)**.[30] Despite the fact that this synthesis results in a mixture of two symmetrical aza-BODIPYs and the aimed unsymmetrical dye, this approach is more feasible for several reasons: (i) The conversion of the nitromethane adducts into pyrrols and 5-nitrosopyrrrols is not required (less reaction steps); (ii) Thus, time-consuming purification and isolation of these intermediates is not necessary, (iii) The two symmetrical by-products can be easily removed by column-chromatography.

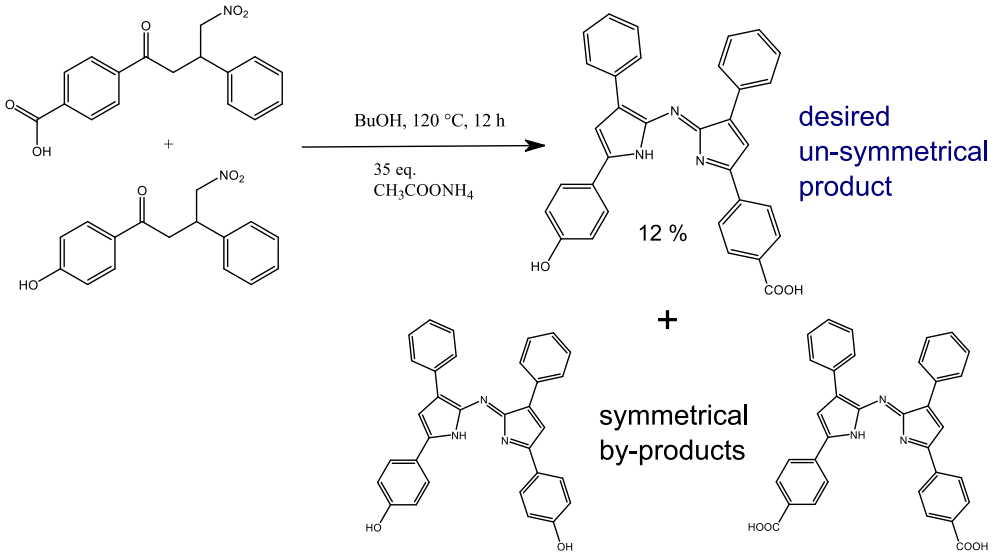


**Figure 43: Another strategy to synthesize azadipyrromethenes: Nitromethane adducts of chalcones are reacted at elevated temperatures to yield the one unsymmetrical product and two undesired symmetrical by-products.**

### 3.2 Position of the functional group:

Functionalization of the indicator with carboxyl group was tested on different positions of aza-dipyrromethene molecule. Functionalized carboxyl chalcones can be easily obtained via Michael-Claisen-condensation, giving the product in moderate yields (Fig. **44**).

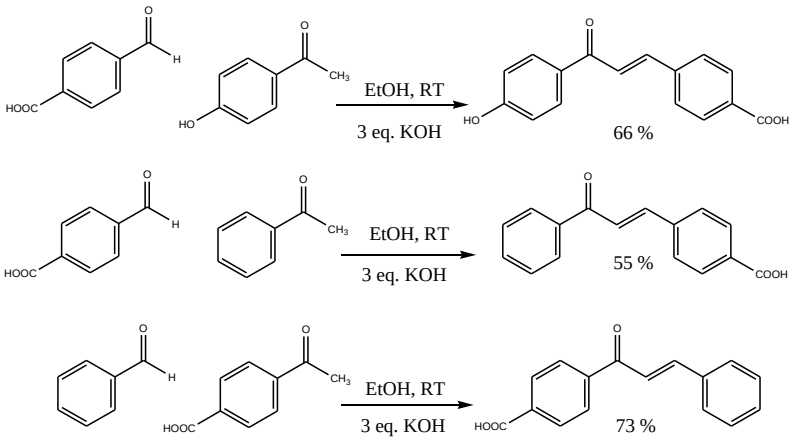


**Figure 44: Reaction scheme of functionalized chalcones via Micheal-Claisen condensation**

However, preliminary experiments indicated that no nitromethane adducts of the functionalized chalcones were sufficiently yielded according to procedure [30] (Figure **45a and b)**.

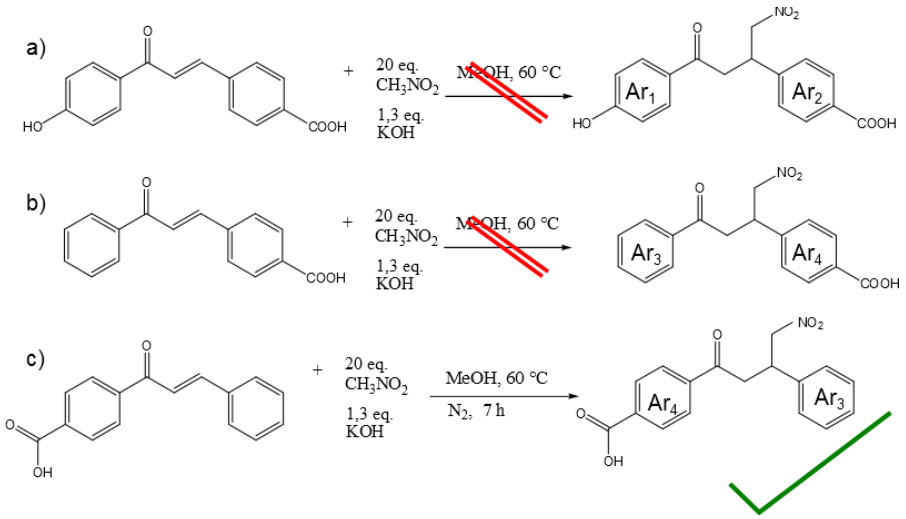


**Figure 45: Synthesis of the nitromethane adducts of the functionalized carboxyl chalcones. Preliminary experiments indicated that only reaction scheme 42.c could obtain the desired product in sufficient yield.**

The nucleophilic conjugate addition of nitromethane to a α,β-unsaturated carbonyl substrate of a chalcone was only successful when the functional carboxylate was introduced in the

phenyl residue which was located next to the ketone. Whereas, insertion of a carboxyl group in the phenyl ring which is adjacent to the double bond of the enone inhibits the synthesis of nitromethane adduct of a chalcone.

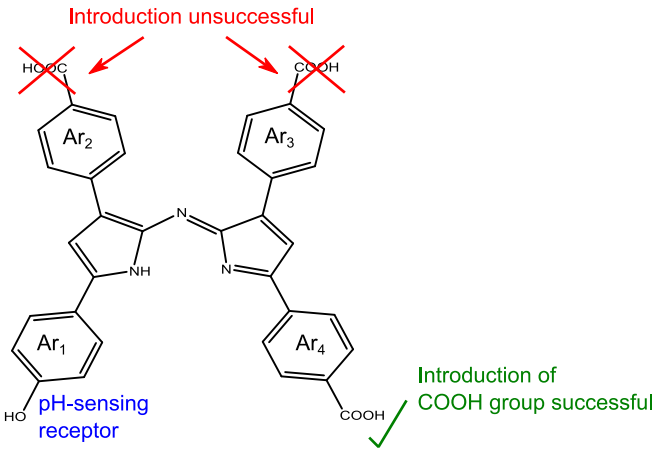


**Figure 46: Preliminary experiments indicated that introduction of the COOH group in the upper positions of the dye is unfavourable.**

### 3.3 Introduction of the polymerizable group:

In order to enable fluorescence emission, the indicator is chelated with boron trifluoride. Upon complexation the dye is forced into a planar molecule structure which facilitates fluorescence. The complexation reaction with boron trifluoride is usually performed in dichloromethane (Fig. **47**). Unfortunately, the indicator modified with a carboxylate group is not soluble in this solvent due to its increased hydrophilicity. However, many organic solvents (tetrahydrofuran, acetone, dimethylformamide, dimethylsulfoxide,) which are able to sufficiently dissolve the modified indicator have been tried for this complexation reaction. No complex could be obtained because boron trifluoride reacted with the solvent.

Diphenylether was the only solvent which enabled chelation of the dye with boron trifluoride. However, the dye was poorly soluble in this solvent and purification of the complexated dye could not be achieved.

Formation of ionic pairs with TBAH (tetrabutylammonium hydroxide) with the hydroxyl and carboxyl group of the dye could significantly increase its solubility. Unfortunately, subsequent complexation led to a variety of products which its isolation was not sufficient and the formed ionic pairs could not be removed.

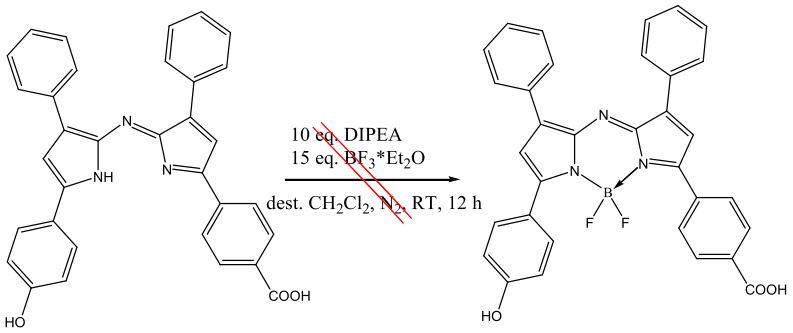


**Figure 47: Chelation of the dye with boron trifluoride is not possible due to its increased hydrophilicity. Preliminary experiments with other solvents were not successful because of the high reactivity of $BF_3$.**

In order to avoid solubility problem, attachment of a methacrylate group to the indicator molecule via amide bond formation is performed prior to complexation. Bioconjugate reagent EDC (1-Ethyl-3-(3-dimethylaminopropyl) carbodiimide) reacts with the carboxylate of the dye to form an amine-reactive intermediate which in turn can couple with the primary amine of the monomer (Fig. **48**). In this way hydrophilicity of the dye is decreased and therefore the modified dye can be chelated with boron trifluoride (Fig. **49**).

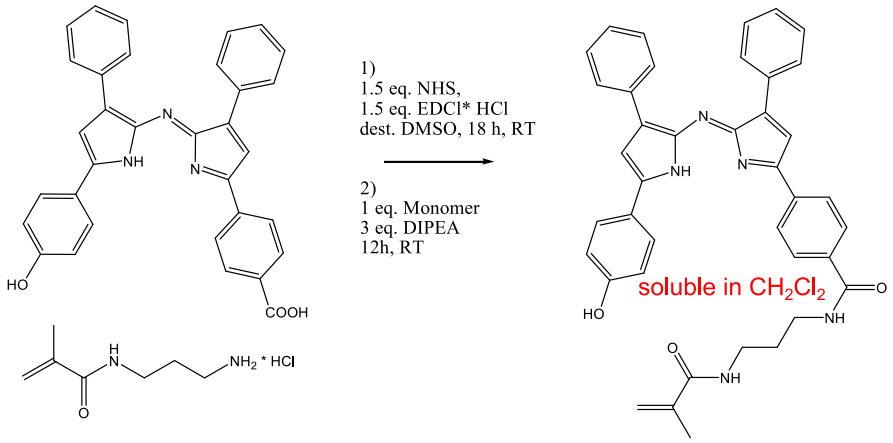


**Figure 48: Reaction scheme of EDC/NHS coupling. The dye is modified with a polymerizable methacrylate group via amide bond formation.**

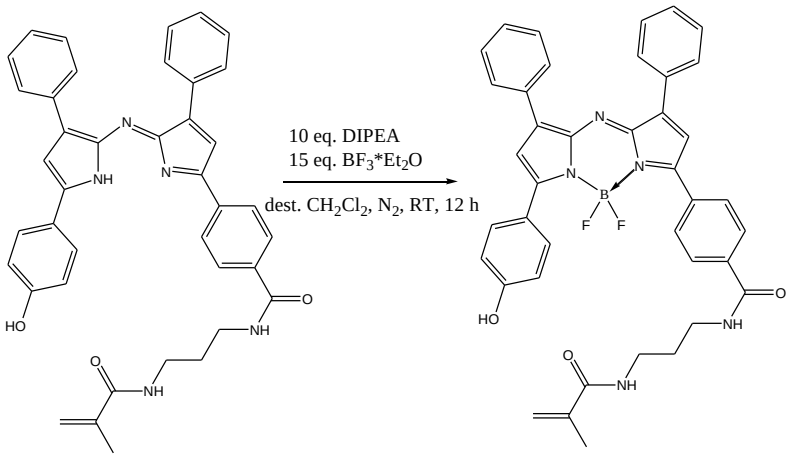


**Figure 49: Complexation of the modified dye is now possible due the increased hydrophobicity of the indicator molecule.**

### 3.4 Protection of the pH sensitive phenol group

The $BF_2$-chelated dye modified with a methacrylate group is ready for photo-co-polymerisation. However, subsequent photo-physical investigation of the pH sensor has indicated that the pH indicator is chemically altered during polymerisation (see section **3.7**). For this reason, the pH sensitive phenol group was protected via acetylisation. (Fig.**50**)

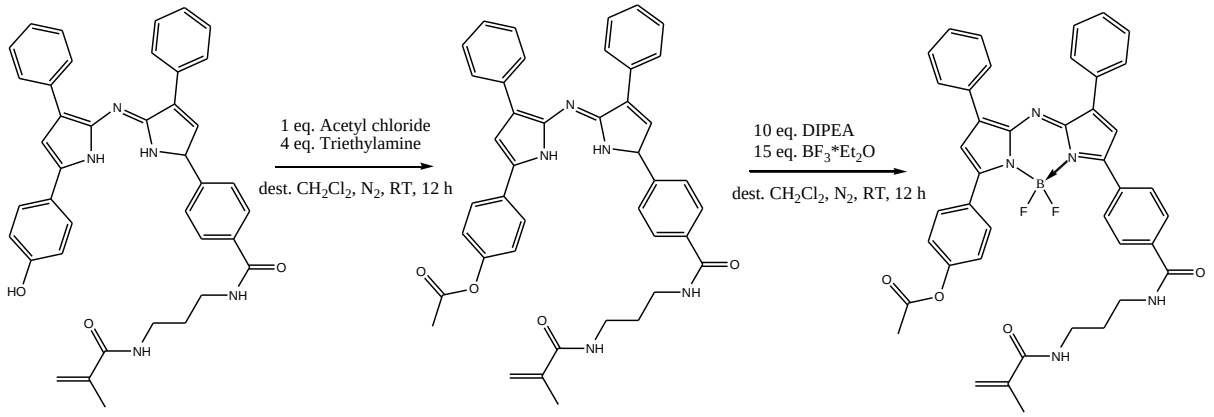


**Figure 50: Reaction scheme for the protection of the pH sensitive phenolate group of the indicator dye and subsequent complexation with boron trifluoride.**

The esterfication of the OH group with acetyl chloride is carried out before complexation. The introduction of an acetyl group increases hydrophobicity of the dye which provides better solubility in dichloromethane.

### 3.5 Photophysical properties of the indicator dye:

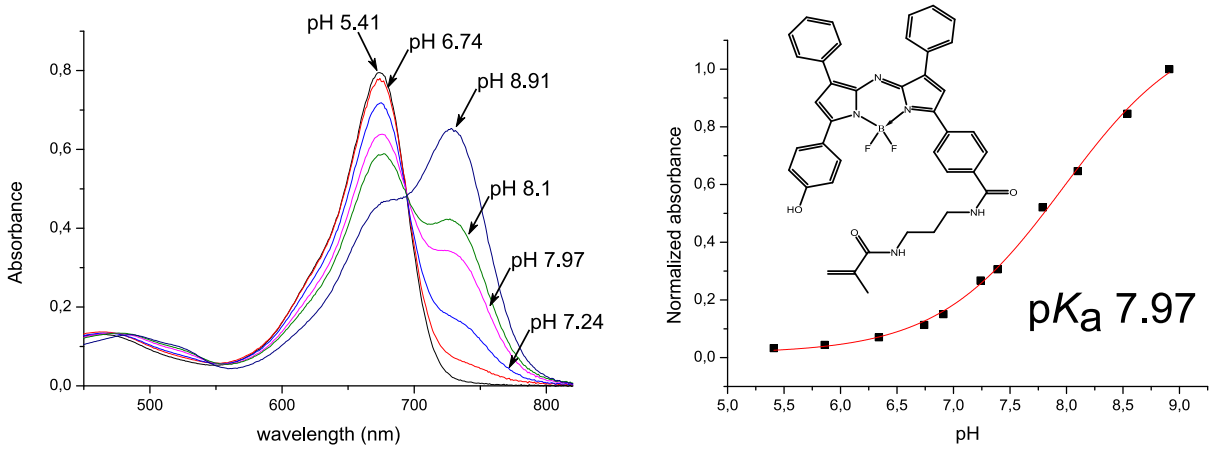


**Figure 51: Absorption spectra (left) and corresponding calibration curve (right) of pH indicator modified with methacrylate group (2) in EtOH/aqueous buffer solution (1:1, ionic strength IS 150mM), $\lambda_{max}$(protonated form) = 673nm), $\lambda_{max}$(deprotonated form) = 729nm). The isobestic point is located at 695nm.**

Introduction of amide bond in the *p*-position of the $Ar^4$ ring slightly decreases the p$K_a$ value (by about 0.4 units) in respect of the non-modified dye (p$K_a$ 8.36). This effect is in line with electron-withdrawing power of remote substituents.

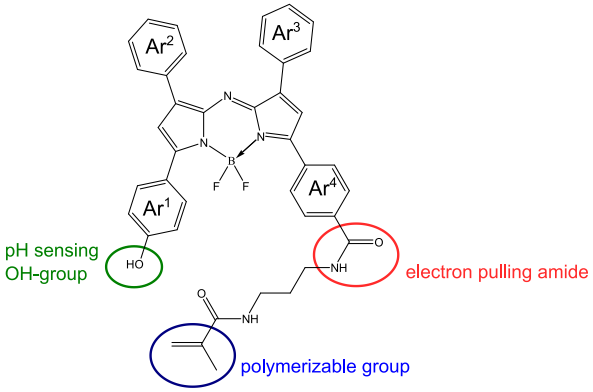


**Figure 52: Introduction of amide bond decreases electron density of the aromatic system which results in a lower p$K_a$ value of the indicator.**

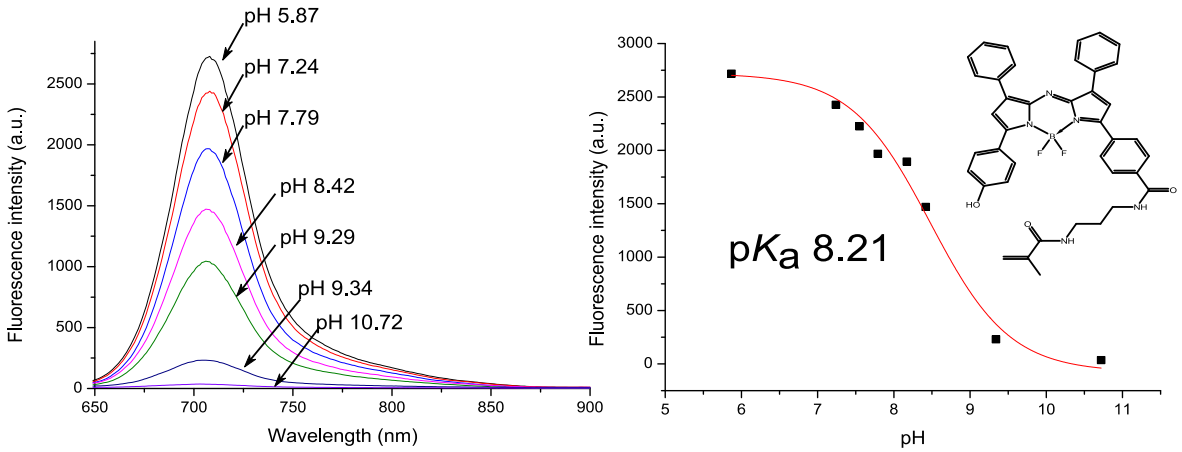


**Figure 53: pH dependence of fluorescence emission ($\lambda_{ex}$ = 630nm) for the indicator modified with methacrylate group (2) in ethanol/aqueous buffer mixture (1:1, IS 150mM) and the corresponding calibration curve ($\phi$= 0.22 in THF of acidic form).**

The spectral properties presented above are characteristic for a PET system. Fluorescence quenching of the deprotonated form is caused by photoinduced electron transfer from a hydroxyl group (receptor for $H^+$) to the aromatic backbone of the dye (Fig. **54**). Upon protonation of the phenolate transfer is blocked which results in fluorescence emission. The obtained 'apparent' p$K_a$ value is slightly higher than the one determined in absorption measurement ($\Delta$0.24). The determined quantum yield ($\phi$=0.22 in THF of acidic form) is not significantly altered compared with non-modified dye ($\phi$=0.15) which indicates that the introduced amide group has no influence on $\phi$.

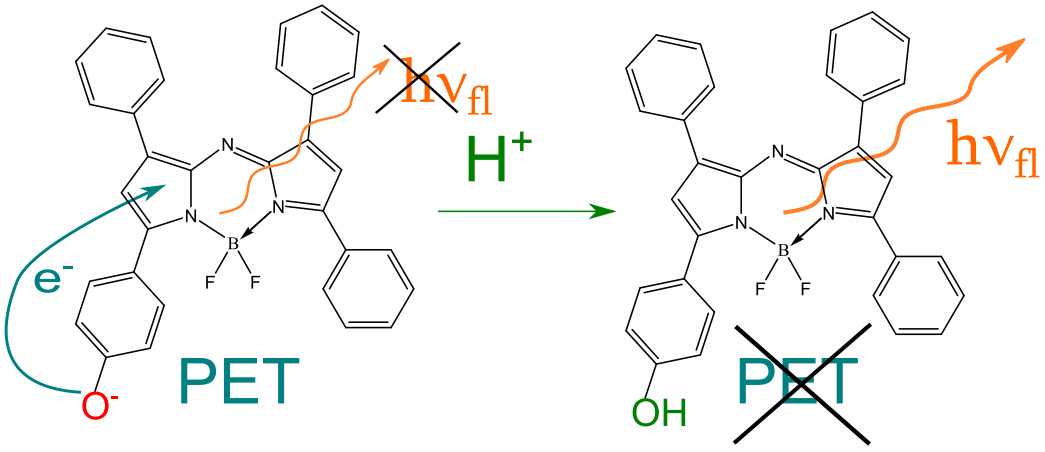


**Figure 54: Fluorescence quenching is caused by photoinduced electron transfer (PET)**

### 3.6 Photo-co-polymerisation:

Poly(acryloylmorpholine) was choosen as a bulk matrix because it provides high water-uptake (depending on the degree of cross-linking) which makes it proton-permeable. The polymer is chemically stable in acidic and basic conditions and the pH indicator is well soluble in the monomer. Ethylenebisacrylamide was used for crosslinking of the polymer due to its high stability against hydrolysis. The polymerization was initiated by 2-hydroxy-4'-(2-hydroxyethoxy)-2-methylpropiophenone by using UV light radiation. Figure **55** shows the emission spectrum of the used UV light source and the absorption spectrum of the pH indicator. The dye is rarely absorbing in the electromagnetic region of the UV light and thus there is no risk of photo-degradation.

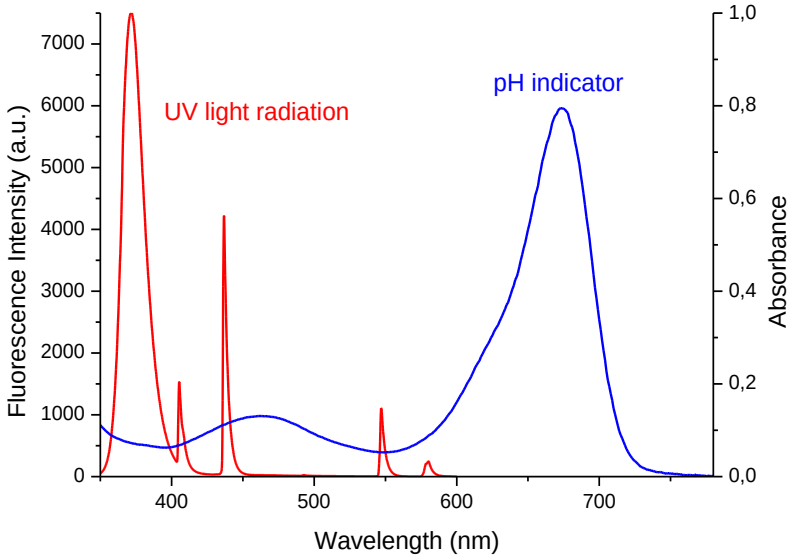


**Figure 55: Emission spectrum of the used UV light source and the absorption spectrum of the pH indicator are rarely overlapping and thus photo-degradation can be kept at a minimum.**

However, the dye is chemically altered during photo-co-polymerisation (Fig. **57).** It is a likely explanation that radicals formed during polymerization partly attack the phenol group of the dye which provides pH sensitivity. In order to prevent degradation of the indicator it is necessary to protect the pH sensitive group from radical attacks. This can be achieved by introducing an acetyl protection group to the phenol group. Upon photo-co-polymerisation, the attached protection group can be easily removed by treating the pH sensor with aqueous basic solution (0.1M NaOH).

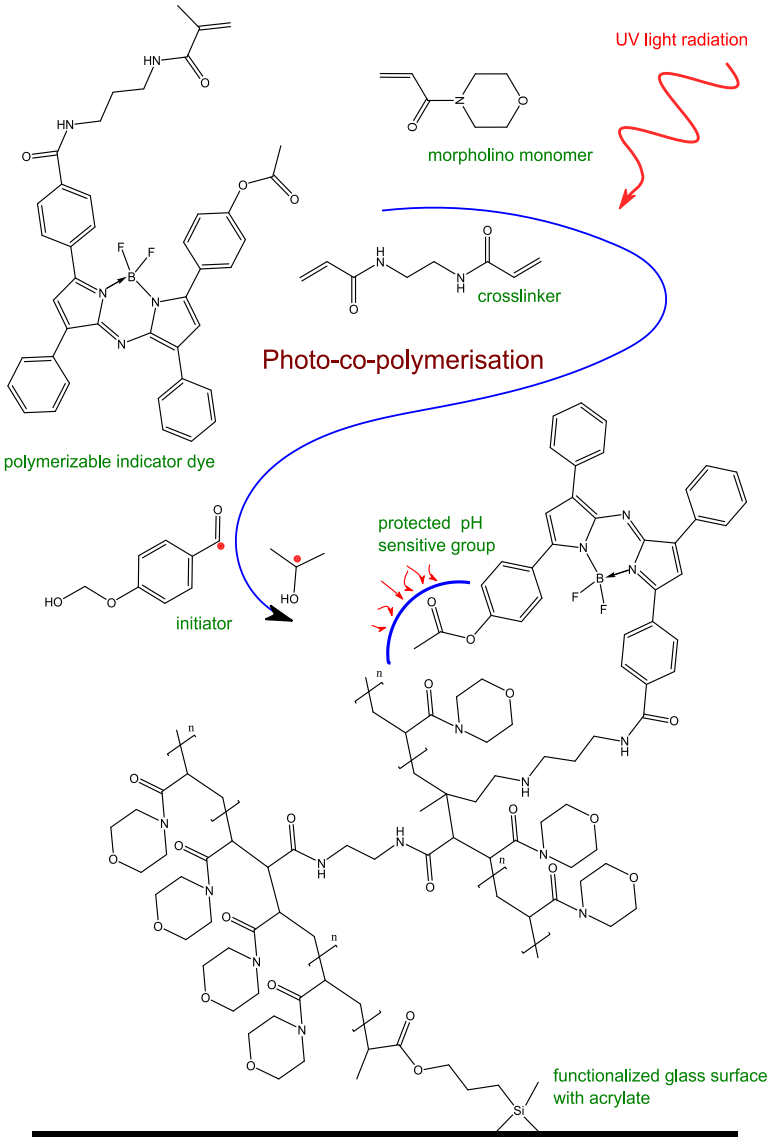


**Figure 56: The picture illustrates the polymerization scheme for preparation of the pH sensor. Poly(acryloylmorpholine) acts as bulk matrix and is cross-linked by ethylenebisacrylamide. In order to protect the pH sensitive phenolate from radical attacks acetyl protection group was introduced.**

### 3.6 Photophysical properties of pH sensors

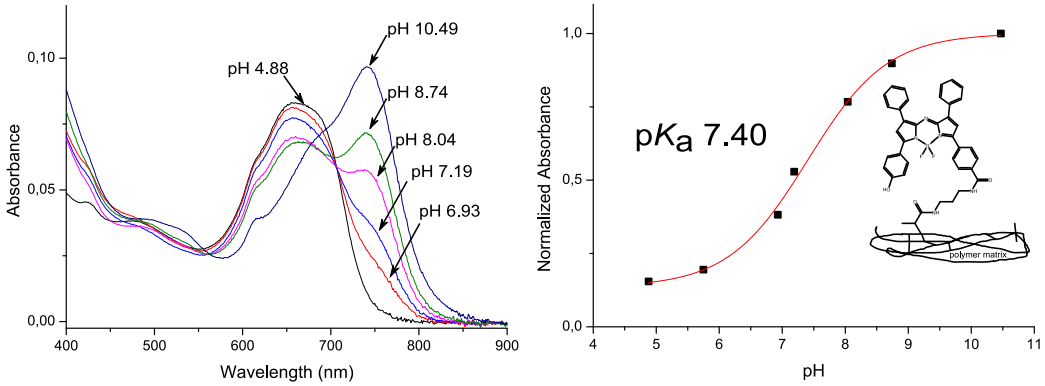


**Figure 57: Absorption spectra and corresponding calibration curve of unprotected dye covalently coupled to poly(acryloylmorpholine) (B) (IS 150mM, aqueous buffer).**

The absorption spectra above show an unprotected dye, covalently coupled to the bulk matrix. The acidic species located at 656 nm is very broad compared with the basic form (743 nm). Furthermore, high absorbance is observed at low wavelengths (550-450 nm) in respect to the dye monitored in solution.

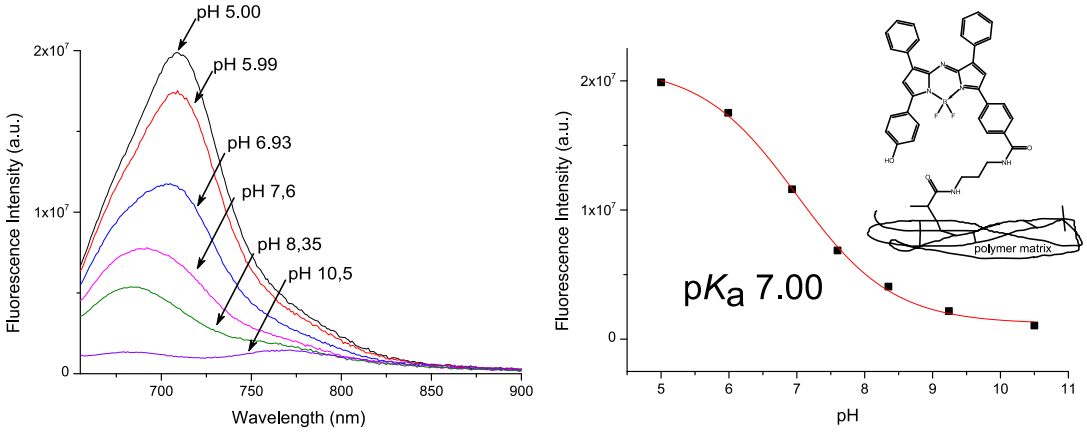


**Figure 58: pH dependence of fluorescence emission ($\lambda_{EXC}$ = 635nm) for unprotected dye, covalently linked to poly(acryloylmorpholine) (B) and the corresponding calibration curve (IS 150mM, aqueous buffer).**

The fluorescence spectrum above shows the emission of a covalently linked indicator dye which has not been protected by the ester before polymerization. Without protection of the pH-sensing hydroxyl group the radicals formed during polymerization can react with the phenolate. This reaction creates a new dye which is also fluorescent and pH-sensitive and causes a hypsochromic shift of the fluorescence emission from 709 nm to 680 nm.

Torgersen et al.[43] presented a photoinduced radical mechanism of diphenol crosslinking (Fig **59**).

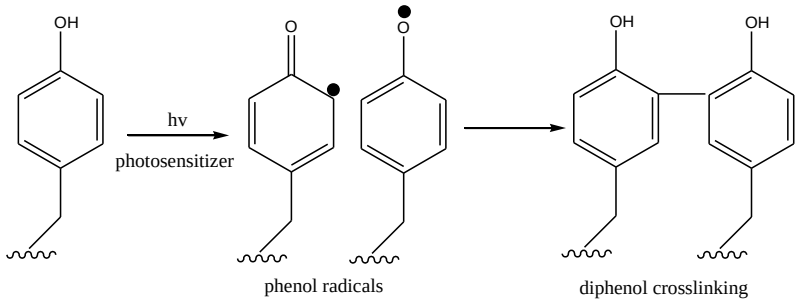


**Figure 59: Mechanism of photoinduced crosslinking of phenols**

It is very likely that this radical reaction is also taken place during the photo-co-polymerisation. However, protection of the hydroxyl group via acetylisation inhibits radical attacks during polymerisation.

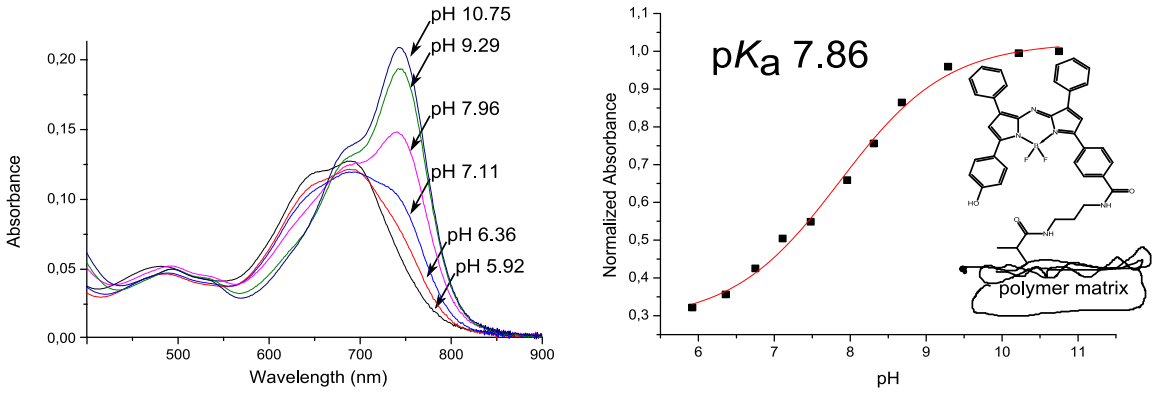


**Figure 60: Absorption spectra and corresponding calibration curve of ester-protected dye, covalently immobilized to a cross-linked poly(acryloylmorpholine) (A) (IS 150mM, aqueous buffer). The basic form ($\lambda_{MAX}$ = 743nm) is bathochromically shifted (Δ 50nm) with respect to the acidic species ($\lambda_{MAX}$ = 690nm). The isobestic point is located at 712 nm.**

The obtained p$K_a$ value (7.86) shows that the pH-sensitive properties of the dye are hardly influenced by covalent linking into a poly(acryloylmorpholine). It is only slightly decreased compared with the dye monitored in solution (Δ0.11). Unexpectedly, the acidic species ($\lambda_{MAX}$ = 690 nm) is very broad and has lower absorbance compared with the basic form ($\lambda_{MAX}$ = 743 nm). Additionally, the acidic species exhibits a shoulder located at 650 nm. Those phenomena can be explained with aggregation. Although dyes are covalently linked to the bulk matrix they are still able to partly move in its surroundings. In its protonated form

dyes are more hydrophobic and thus try to shield from the aqueous environment by aggregation. In basic solution, aggregation is less likely due to coulomb repulsion. Another reason for the broad peak of the acidic species can arise from formation of dimers during polymerisation. The protection of the phenol group during polymerization results in an increase of the p$K_a$ value (Δ0.46) compared to the one of the non-protected dye. The emission spectra presented above (Fig. **58**) gives proof that radical polymerization is partly altering the pH sensitivity of the dye. Thus, non-protected dye is modified to some extent which results in a lowered p$K_a$ value.

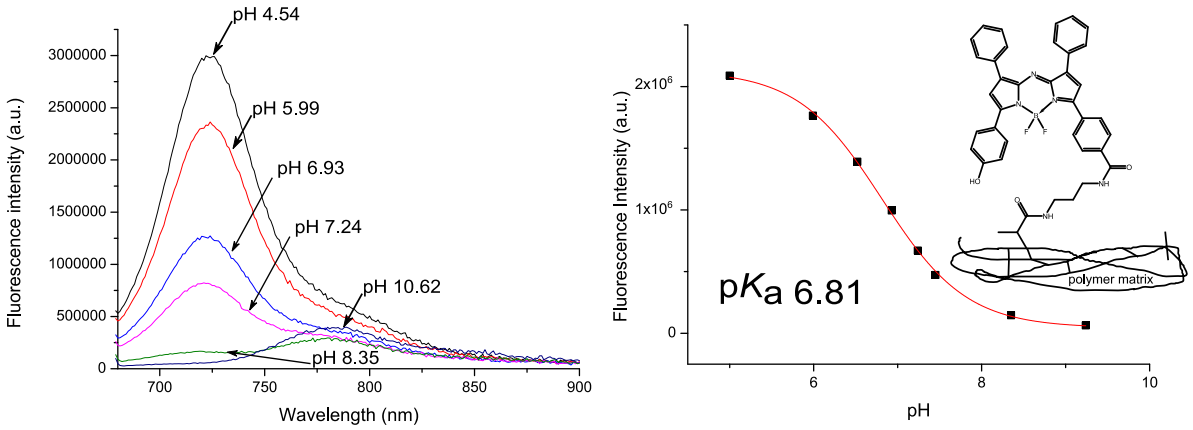


**Figure 61: pH dependence of fluorescence emission ($\lambda_{EXC}$ = 655nm) for ester-protected dye, covalently linked to polyacryloyl(morpholino) (A) and the corresponding calibration curve (IS 150mM, aqueous buffer).**

The fluorescence spectrum above shows the indicator which its phenolate was acetylated and hydrolyzed upon polymerization. The introduced protection group prevents from any side reactions during polymerization. No shift of the emission maximum is observed in the fluorescence spectrum compared to non- protected indicator.

Surprisingly, another fluorescent species is observed (780 nm, pH > 8) which is also pH-sensitive. The new species formed during polymerization can also be found in the emission spectrum of the unprotected dye but in less extent.

Acetylated dye which is more hydrophobic than unprotected dye might not be homogenously distributed in the hydrophilic monomer solution and thus, formation of a dimer during polymerization can occur. This phenomenon is less pronounced for unprotected dye due to its higher hydrophilicity.

The determined apparent p$K_a$ value (6.81) is about 1 pH unit lower than the one derived from absorption data (7.86). This decrease in the p$K_a$ value is less pronounced of non-acetylated indicator dye, covalently coupled to the polymeric support (Δ0.4). As already mentioned above the acetylated indicator is much more hydrophobic which may favour formation of domains with high concentration of indicator dye. Consequently, dye molecules are very close to one another and thus energy transfer from protonated to deprotonated form may occur. The extent of energy transfer correlates with the degree of spectral overlap (fig. **62**). Then some vibronic transitions in the donor and the corresponding transitions in the acceptor are practically of the same energy and can couple with each other (i.e. are in resonance). This phenomenon is called FRET effect (Förster resonance energy transfer).

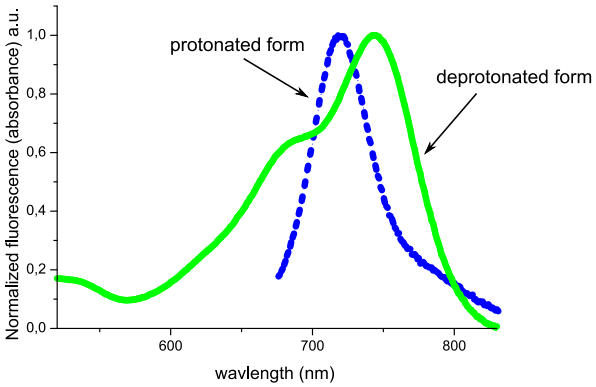


**Figure 62: Spectral overlap of absorbance and fluorescence (dashed lines, $\lambda_{EXC}$ = 655nm) of pH indicator covalently coupled into poly(acryloylmorpholine) matrix causing FRET.**

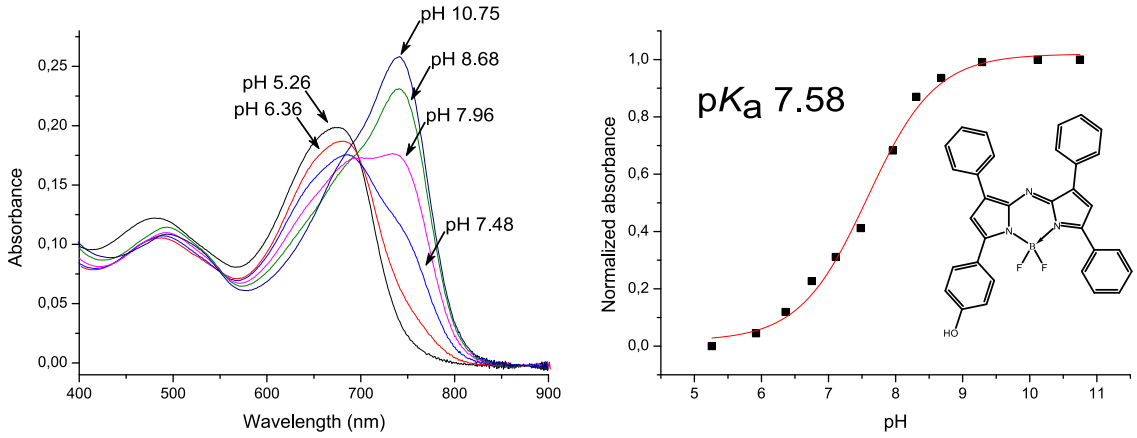


**Figure 63: Absorption spectra and corresponding calibration curve of ester-protected dye, physically entrapped in cross-linked poly(acryloylmorpholine) (C) (IS 150mM, aqueous buffer).**

The absorption spectra above show a dye (ester-protected during polymerization), which was only physically entrapped into the polymeric matrix. The p$K_a$ value is significantly decreased compared to the dye covalently linked into a polymer (7.97 →7.58, Δ0.39). The change in the p$K_a$ value can be explained by aggregation within the polymer matrix. The dye has only been physically entrapped and thus migration within the matrix is highly favoured.

### 3.7 Leaching properties

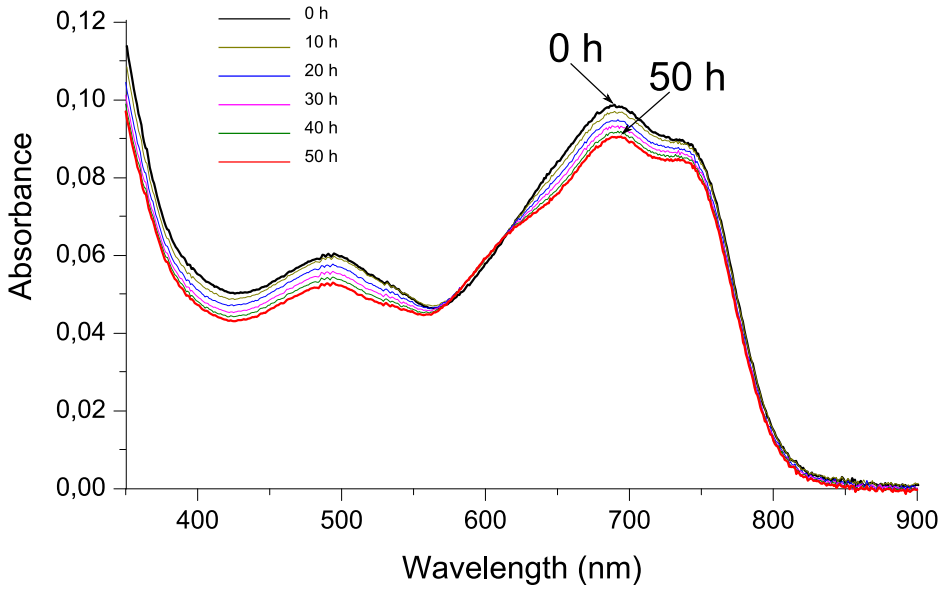


**Figure 64: Leaching of non-covalently linked pH indicator determined from the absorption measurement (C) (pH 7.9, IS 150mM).**

The dye (ester-protected during polymerization, compound **4**) has only been physically entrapped into a poly(acryloylmorpholine) matrix. The absorption spectra above show leaching into the aqueous solution to some extent.

Surprisingly, two isobestic points located at 580nm and 625 nm can be identified over time. Additionally, the decrease in absorption of the acidic and basic form is not of same extent. It should be mentioned that the used buffer solution which constantly flushes the pH sensor can slightly change pH value during this measurement. Another reason why no decrease in absorption between 580 nm and 652 nm is observed may arise from aggregation events of the dye over time.

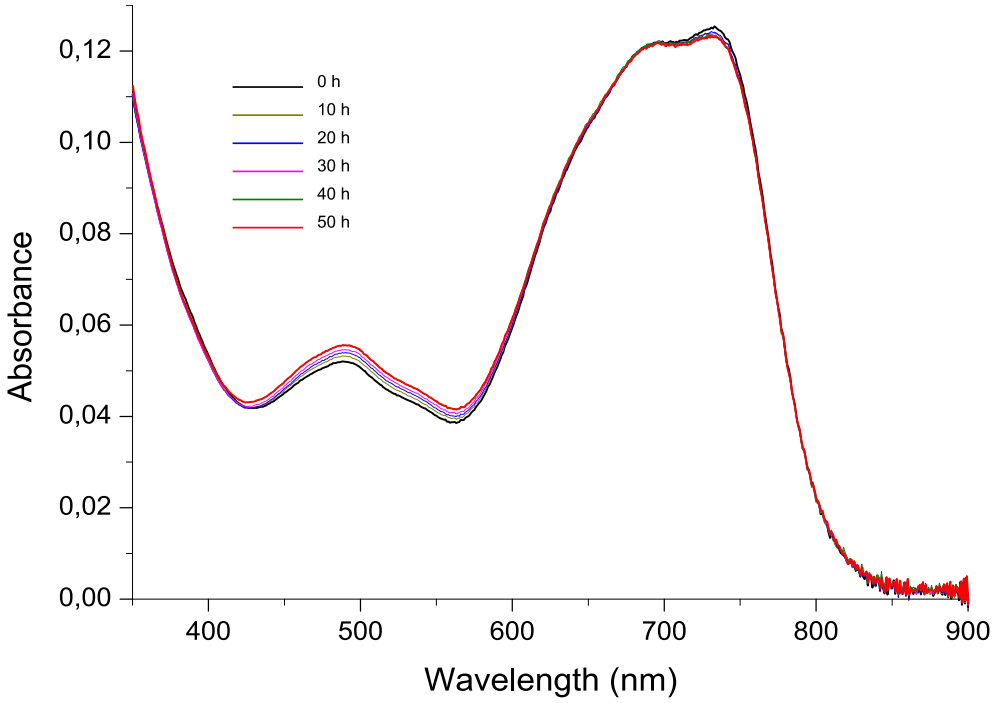


**Figure 65: Leaching of dye covalently crafted into poly(acryloylmorpholine) by monitoring the absorption (A) (pH 7.9, IS 150mM).**

The absorption spectra above show a pH sensor (compound **1**) covalently linked into poly(acryloylmorpholine). The decrease in the absorption was very low (less than 0.1%) which is within the experimental error. The slight change in absorption from 420 nm to 580 nm may arise from light scattering caused by some impurities released from the pH sensor. There is a slight decrease in absorption of the deprotonated at the beginning of the leaching experiment, but the sensor stabilizes over time (Fig. **65**).

### 3.8 Effect of the ionic strength:

Cross-sensitivity to ionic strength is usually a significant drawback in optical pH sensing. However, the covalently linked dye exhibits only a low charge in its deprotonated form (-1) and thus, influence of ionic strength is expected to be minimal.[30] Indeed, calibration curves monitored at different IS (20, 160 and 510mM) show that changes in ionic strength affect the $pK_a$ of the pH sensor only slightly, particularly at high ionic strength (Fig. **66**).

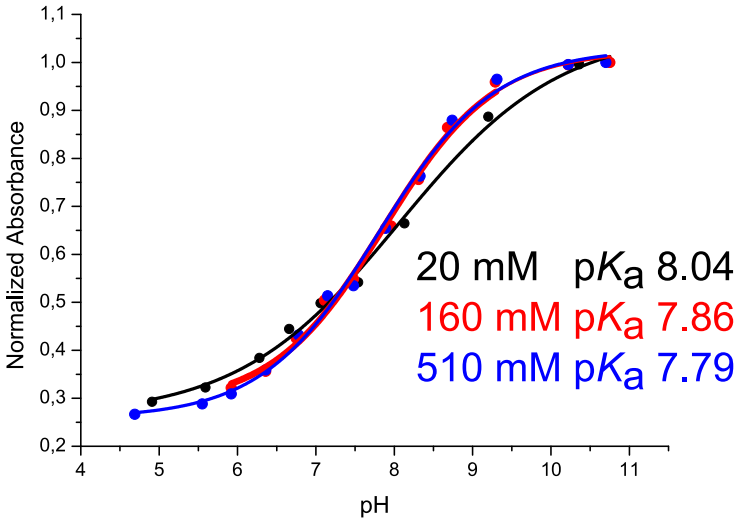


**Figure 66: Calibration curves of indicator dye, covalently linked into poly(acryloylmorpholine) at ionic strengths from 20 to 510mM**

Figure **66** shows that the lower the concentration of the ionic strength the higher is the obtained p$K_a$ value of the pH indicator.

### 3.9 Sensor response:

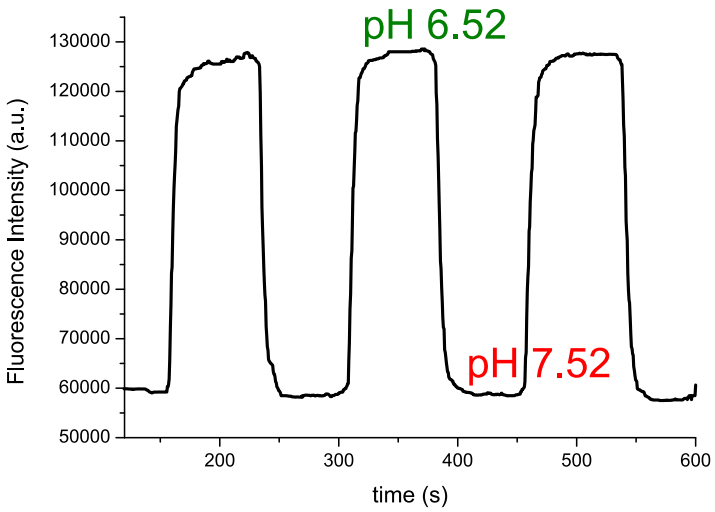


**Figure 67: Dynamic response of the pH sensor with covalently coupled indicator dye.**

The pH sensor shows a fast response to changes in pH values when switching from pH 6.52 to 7.52 and vice versa. The response time from basic to acidic buffer is 25s (95% of the signal change) and the response time from acidic to basic conditions is 22s.

## 4. Conclusion

In this work, a new pH sensor with covalently coupled aza-BODIPY based pH indicator was prepared and its potential application in optical pH measurements was assessed. The functional tetraarylazadipyrromethane derivative was synthesised via a relatively simple reaction route giving the product in moderate yield. The pH-sensitive hydroxyl group is protected via acetylisation in order to keep undesired side reactions during photo-co-polymerization at a minimum.

Due to covalent immobilization the pH indicator is prevented from leaching which results in enhancement of the performance of the pH sensor in respect to long-term use. However, aggregation of the dye could not be completely suppressed. Movements of the dye in its surroundings are still possible which can cause aggregation especially in acidic/aqueous conditions. Furthermore, pronounced hydrophobicity of the dye compared to the polymeric matrix may favour the formation of dimers.

The new pH sensor is suitable for biotechnological applications and measurements under physiological conditions. The 'apparent' $pK_a$ value (6.81) of the sensor and its sensitive range matches the pH region in fermentation processes. Ionic strength dependence measurement of the new synthesized pH sensor shows that its $pK_a$ value is only moderately influenced within a range of 20 to 510mM, a range which is mostly used in biotechnological applications and also marine science.

In this thesis, a new immobilization strategy has been developed and provides very promising possibilities regarding the design of optical pH sensors. Ongoing work will concern the prevention of aggregation and dimerisation of the dye in the polymeric network.

## 5. References


1. Valeur, B. *Molecular Fluorescence. Principles and Applications*. (Wiley-VCH, 2002 ) a) 3-4, b) 20-23, c) 35, d) 37-41 e) 43, f) 43, g) 46, h) 72-86, i) 90-97, j) 99-105, k) 110-112, l) 279-286 .
2. Lukas Hutter. On covalent immobilization of Indicators in Optical sensors. (2012).
3. Lakowicz, J. R. *Principles of Fluorescence Spectroscopy*. (Springer, 2010).
4. Zhang, W. *et al.* A highly sensitive acidic pH fluorescent probe and its application to HepG2 cells. *Analyst* **134,** 367–371 (2009).
5. Tang, B. *et al.* A near-infrared neutral pH fluorescent probe for monitoring minor pH changes: imaging in living HepG2 and HL-7702 cells. *J. Am. Chem. Soc.* **131,** 3016–3023 (2009).
6. Kühl, M. Optical microsensors for analysis of microbial communities. *Methods Enzymol.* **397,** 166–199 (2005).
7. Larsen, M., Borisov, S. M., Grunwald, B., Klimant, I. & Glud, R. N. A simple and inexpensive high resolution color ratiometric planar optode imaging approach: application to oxygen and pH sensing. *Limnol Ocean. Methods* **9,** 348–360 (2011).
8. Jeevarajan, A. S., Vani, S., Taylor, T. D. & Anderson, M. M. Continuous pH monitoring in a perfused bioreactor system using an optical pH sensor. *Biotechnol. Bioeng.* **78,** 467–472 (2002).
9. John, G. T., Goelling, D., Klimant, I., Schneider, H. & Heinzle, E. PH-sensing 96-well microtitre plates for the characterization of acid production by dairy starter cultures. *J. Dairy Res.* **70,** 327–333 (2003).
10. Arain, S. *et al.* Characterization of microtiterplates with integrated optical sensors for oxygen and pH, and their applications to enzyme activity screening, respirometry, and toxicological assays. *Sensors Actuators B Chem.* **113,** 639–648 (2006).
11. Schouest, K., Zitova, A., Spillane, C. & Papkovsky, D. Toxicological assessment of chemicals using Caenorhabditis elegans and optical oxygen respirometry. *Environ. Toxicol. Chem. Setac* **28,** 791–799 (2009).
12. Mills, A. Oxygen indicators and intelligent inks for packaging food. *Chem. Soc. Rev.* **34,** 1003–1011 (2005).
13. Gründler, P. *Chemische Sensoren: Eine Einführung für Naturwissenschaftler und Ingenieure*. (Springer, 2004).
14. Hamilton, N. Quantification and its applications in fluorescent microscopy imaging. *Traffic Cph. Den.* **10,** 951–961 (2009).
15. Acosta, M. A., Ymele-Leki, P., Kostov, Y. V. & Leach, J. B. Fluorescent microparticles for sensing cell microenvironment oxygen levels within 3D scaffolds. *Biomaterials* **30,** 3068–3074 (2009).

16. Roy, T. W. & Bhagwat, A. S. Kinetic studies of Escherichia coli AlkB using a new fluorescence-based assay for DNA demethylation. *Nucleic Acids Res.* **35,** e147–e147 (2007).

17. Weidgans, B. M., Krause, C., Klimant, I. & Wolfbeis, O. S. Fluorescent pH sensors with negligible sensitivity to ionic strength. *Analyst* **129,** 645–650 (2004).

18. Narayanaswamy, R. & Wolfbeis, O. S. *Optical Sensors: Industrial, Environmental and Diagnostic Applications*. (Springer, 2004).

19. Strömberg, N., Mattsson, E. & Hakonen, A. An imaging pH optode for cell studies based on covalent attachment of 8-hydroxypyrene-1,3,6-trisulfonate to amino cellulose acetate films. *Anal. Chim. Acta* **636,** 89–94 (2009).

20. Sergey M. Borisov, D. L. H. Fluorescent poly(styrene-block-vinylpyrrolidone) nanobeads for optical sensing of pH. *Sensors Actuators B Chem.* 52–58 doi:10.1016/j.snb.2008.08.028

21. Pastoriza-Munoz, E., Harrington, R. M. & Graber, M. L. Parathyroid hormone decreases HCO3 reabsorption in the rat proximal tubule by stimulating phosphatidylinositol metabolism and inhibiting base exit. *J. Clin. Invest.* **89,** 1485–1495 (1992).

22. Graber, M., Dixon, T., Coachman, D. & Devine, P. Acetazolamide inhibits acidification by the turtle bladder independent of cell pH. *Am. J. Physiol.* **256,** F923–931 (1989).

23. Bissell, R. A. *et al.* Luminescence and charge transfer. Part 2. Aminomethyl anthracene derivatives as fluorescent PET (photoinduced electron transfer) sensors for protons. *J. Chem. Soc. Perkin Trans. 2* 1559–1564 (1992). doi:10.1039/P29920001559

24. Daffy, L. M. *et al.* Arenedicarboximide Building Blocks for Fluorescent Photoinduced Electron Transfer pH Sensors Applicable with Different Media and Communication Wavelengths. *Chem. - Eur. J.* **4,** 1810–1815 (1998).

25. Borisov, S. M., Gatterer, K. & Klimant, I. Red light-excitable dual lifetime referenced optical pH sensors with intrinsic temperature compensation. *Analyst* **135,** 1711–1717 (2010).

26. Cooper, M. E., Gregory, S., Adie, E. & Kalinka, S. pH-Sensitive Cyanine Dyes for Biological Applications. *J. Fluoresc.* **12,** 425–429 (2002).

27. Ulrich, G., Ziessel, R. & Harriman, A. The Chemistry of Fluorescent Bodipy Dyes: Versatility Unsurpassed. *Angew. Chem. Int. Ed.* **47,** 1184–1201 (2008).

28. Hall, M. J., McDonnell, S. O., Killoran, J. & O'Shea, D. F. A Modular Synthesis of Unsymmetrical Tetraarylazadipyrromethenes. *J. Org. Chem.* **70,** 5571–5578 (2005).

29. Gorman, A. *et al.* In vitro demonstration of the heavy-atom effect for photodynamic therapy. *J. Am. Chem. Soc.* **126,** 10619–10631 (2004).

30. Jokic, T. *et al.* Highly Photostable Near-Infrared Fluorescent pH Indicators and Sensors Based on $BF_2$ -Chelated Tetraarylazadipyrromethene Dyes. *Anal. Chem.* **84,** 6723–6730 (2012).

31. Killoran, J., Allen, L., Gallagher, J. F., Gallagher, W. M. & O'Shea, D. F. Synthesis of BF2 chelates of tetraarylazadipyrromethenes and evidence for their photodynamic therapeutic behaviour. *Chem. Commun. Camb. Engl.* 1862–1863 (2002).

32. Murtagh, J., Frimannsson, D. O. & O'Shea, D. F. Azide conjugatable and pH responsive near-infrared fluorescent imaging probes. *Org. Lett.* **11,** 5386–5389 (2009).

33. McDonnell, S. O. & O'Shea, D. F. Near-infrared sensing properties of dimethlyamino-substituted BF2-azadipyrromethenes. *Org. Lett.* **8,** 3493–3496 (2006).

34. Killoran, J., McDonnell, S. O., Gallagher, J. F. & O'Shea, D. F. A substituted BF2-chelated tetraarylazadipyrromethene as an intrinsic dual chemosensor in the 650–850 nm spectral range. *New J. Chem.* **32,** 483–489 (2008).

35. Chen, J., Burghart, A., Derecskei-Kovacs, A. & Burgess, K. 4,4-Difluoro-4-bora-3a,4a-diaza-s-indacene (BODIPY) Dyes Modified for Extended Conjugation and Restricted Bond Rotations. *J. Org. Chem.* **65,** 2900–2906 (2000).

36. Callam, C. S. & Lowary, T. L. Suzuki Cross-Coupling Reactions: Synthesis of Unsymmetrical Biaryls in the Organic Laboratory. *J. Chem. Educ.* **78,** 947 (2001).

37. Miyaura, N. & Suzuki, A. Palladium-catalyzed cross-coupling reactions of organoboron compounds. *Chem. Rev.* **95,** 2457–2483 (1995).

38. Kolb, H. C., Finn, M. G. & Sharpless, K. B. Click Chemistry: Diverse Chemical Function from a Few Good Reactions. *Angew. Chem. Int. Ed.* **40,** 2004–2021 (2001).

39. Mansfeld, U., Pietsch, C., Hoogenboom, R., Becer, C. R. & Schubert, U. S. Clickable initiators, monomers and polymers in controlled radical polymerizations – a prospective combination in polymer science. *Polym. Chem.* **1,** 1560 (2010).

40. Hermanson, G. T. *Bioconjugate Techniques, Second Edition*. (Academic Press, 2008).

41. Crosby, G. A. & Demas, J. N. Measurement of photoluminescence quantum yields. Review. *J. Phys. Chem.* **75,** 991–1024 (1971).

42. Freyer, W., Mueller, S. & Teuchner, K. Photophysical properties of benzoannelated metal-free phthalocyanines. *J. Photochem. Photobiol. Chem.* **163,** 231–240 (2004).

43. Torgersen, J. *et al.* Hydrogels for Two-Photon Polymerization: A Toolbox for Mimicking the Extracellular Matrix. *Adv. Funct. Mater.* n/a–n/a (2013). doi:10.1002/adfm.201203880

# 6 Appendix

## 6.1 Chemicals Used

**Table 3: List of chemicals used**

| Substance | purchased from | CAS-Number |
|---|---|---|
| Dichloromethane | Roth | 75-09-2 |
| Tetrahydrofuran | Roth | 109-99-9 |
| Acetone | Roth | 67-64-1 |
| Ethanol | Roth | 64-17-5 |
| Methanol | Roth | 67-56-1 |
| Ethylacetate | Roth | 141-78-6 |
| 1-Butanol | abcr | 75-36-3 |
| abs. Dichloromethane | Sigma-Adrich | 75-09-2 |
| abs. Dimethyl sulfoxide | Sigma-Adrich | 67-68-5 |
| Tetramethylsilane | Euriso-top | 2956-58-3 |
| Chloroform D | VWR | 865-49-6 |
| DMSO D6 | Euriso-top | 67-68-5 |
| 4-Acryloylmorpholine | Sigma-Aldrich | 5117-12-4 |
| Acetyl chloride | Fluka | 75-36-5 |
| N-(3-Aminopropyl)methacrylamide hydrochloride | Polysciences, Inc. | 72607-53-5 |
| N,N'-Ethylenebisacrylamide | abcr | 2956-58-3 |
| N-Hydroxysucciinimide | Fluka | 6066-82-6 |
| Methacryloxypropylmethyldichlorosilane | abcr | 18301-56-9 |
| Nitromethane | abcr | 75-52-5 |
| Triethylamine | Sigma-Aldrich | 121-44-8 |
| 4-Acetylbenzoic Acid | TCI | 586-89-0 |
| Hydroxychalcone | abcr | 20426-12-4 |
| Benzaldehyde | abcr | 100-52-7 |
| Hydrochloric acid (0.1 M) | Roth | 7647-01-0 |
| Sodium hydroxide (0.1 M) | Roth | 1310-73-2 |
| Sodium hydroxide | Roth | 1310-73-2 |
| Sodium sulphate | VWR | 7757-82-6 |
| Magnesium sulphate | Roth | 7487-88-9 |
| Potassium hydroxide | Roth | 1310-58-3 |
| Sodium chloride | Fluka | 7647-14-5 |
| CHES | Roth | 103-47-9 |
| MOPS | Roth | 1132-61-2 |
| MES | Roth | 4432-31-9 |
| CAPS | Roth | 1135-40-6 |

## 6.2 $^{1}$H NMR and mass spectra of

## 4-(2-((5-(4- hydroxyphenyl)-3-phenyl-1H-pyrrol-2-yl)imino)-3-phenyl-2H-pyrrol-5-yl)benzoic acid

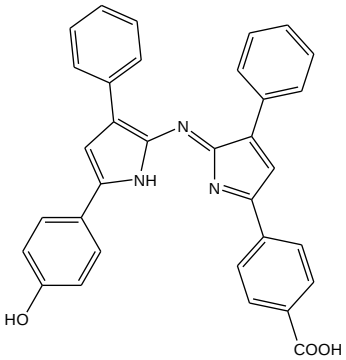


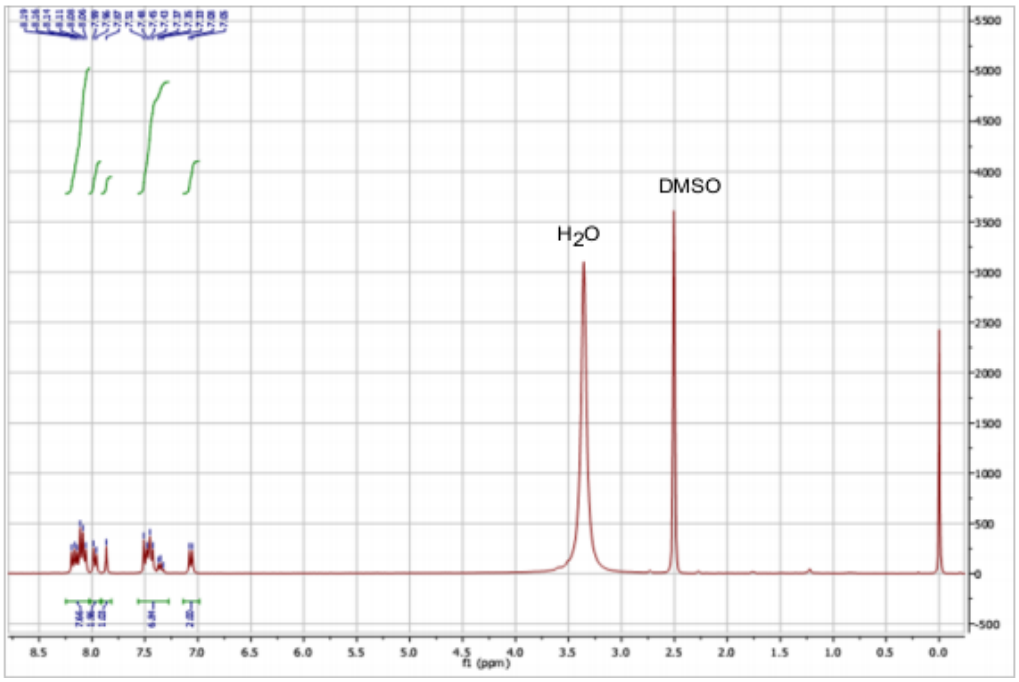


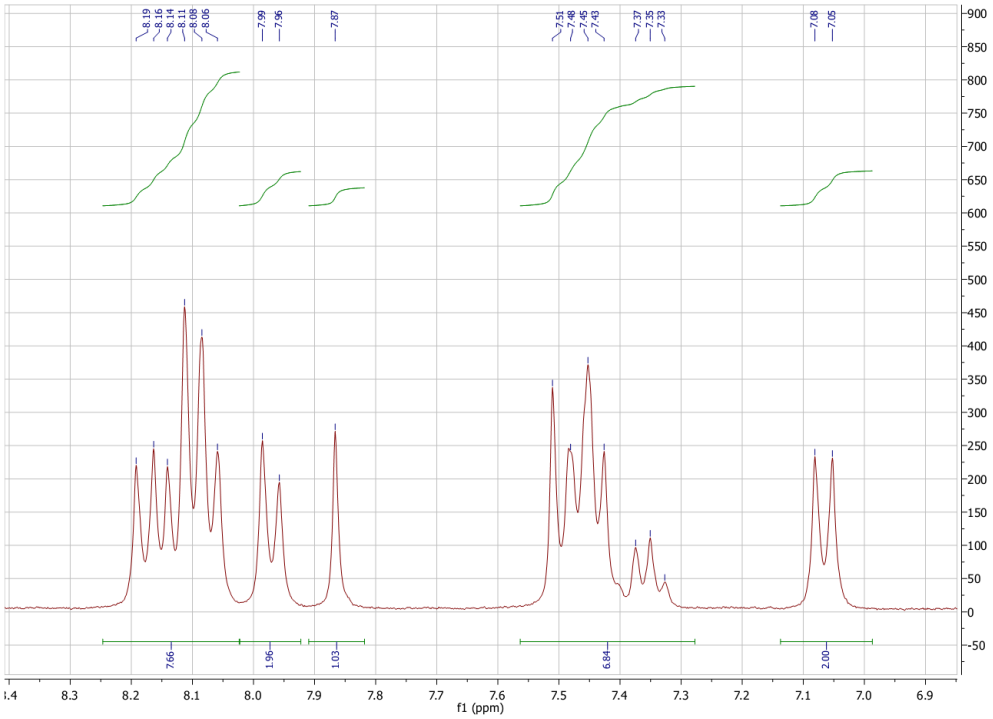

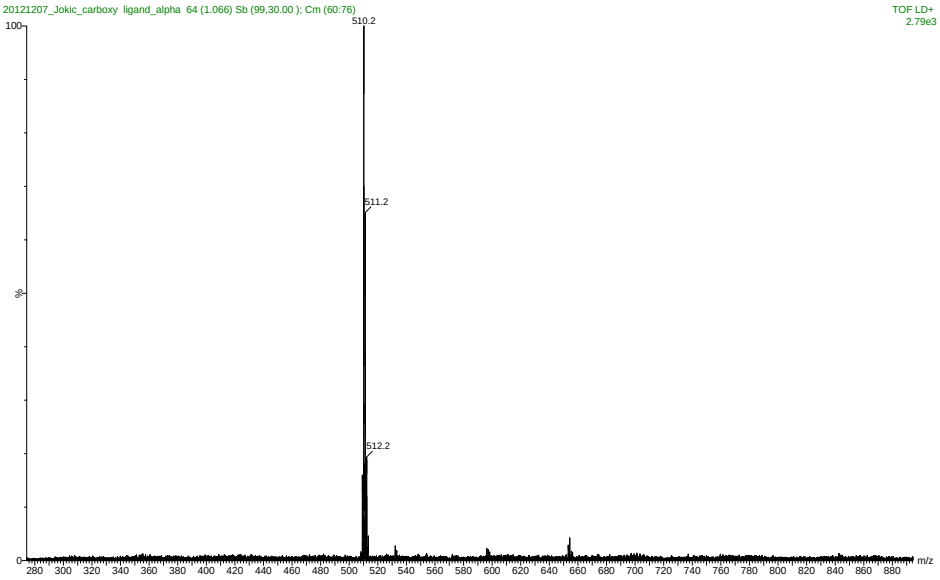
20121207_Jokic_carboxy ligand_alpha 64 (1.066) Sb (99,30.00 ); Cm (60:76)
TOF LD+
2.79e3
510.2
511.2
512.2
100
%
0
280 300 320 340 360 380 400 420 440 460 480 500 520 540 560 580 600 620 640 660 680 700 720 740 760 780 800 820 840 860 880
m/z

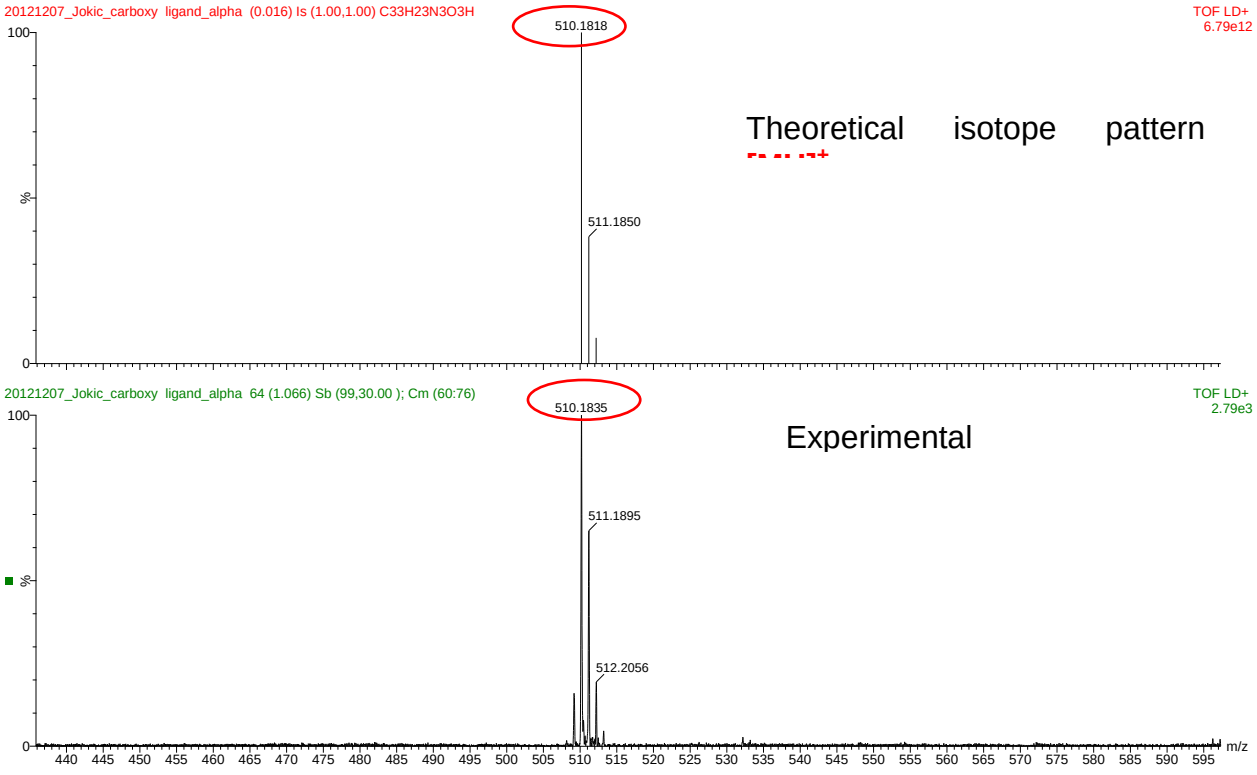
20121207_Jokic_carboxy ligand_alpha (0.016) Is (1.00,1.00) C33H23N3O3H
TOF LD+
6.79e12
510.1818
511.1850
100
%
0
Theoretical isotope pattern
20121207_Jokic_carboxy ligand_alpha 64 (1.066) Sb (99,30.00 ); Cm (60:76)
TOF LD+
2.79e3
510.1835
511.1895
512.2056
100
%
0
Experimental
440 445 450 455 460 465 470 475 480 485 490 495 500 505 510 515 520 525 530 535 540 545 550 555 560 565 570 575 580 585 590 595
m/z

## 6.3 $^{1}$H NMR and mass spectra of

**4-(2-((5-(4-hydroxyphenyl)-3-phenyl-1H-pyrrol-2-yl)imino)-3-phenyl-2H-pyrrol-5-yl)-N-(3-methacrylamidopropyl)benzamide**

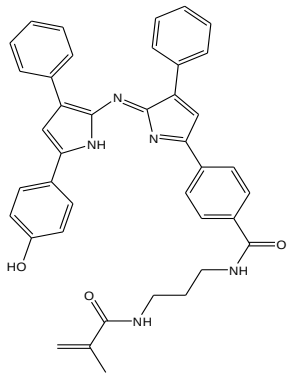


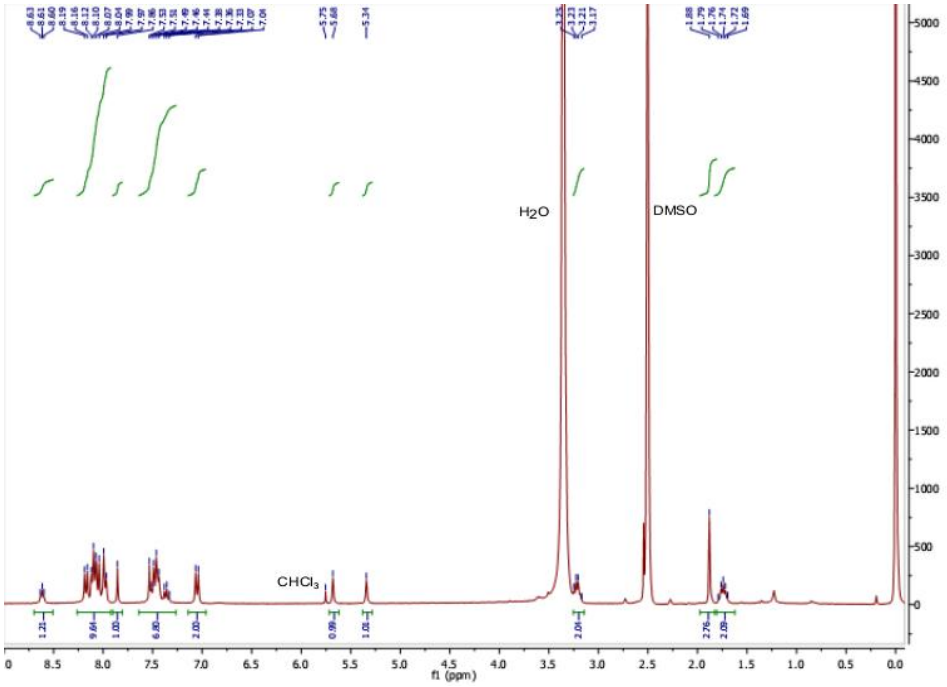


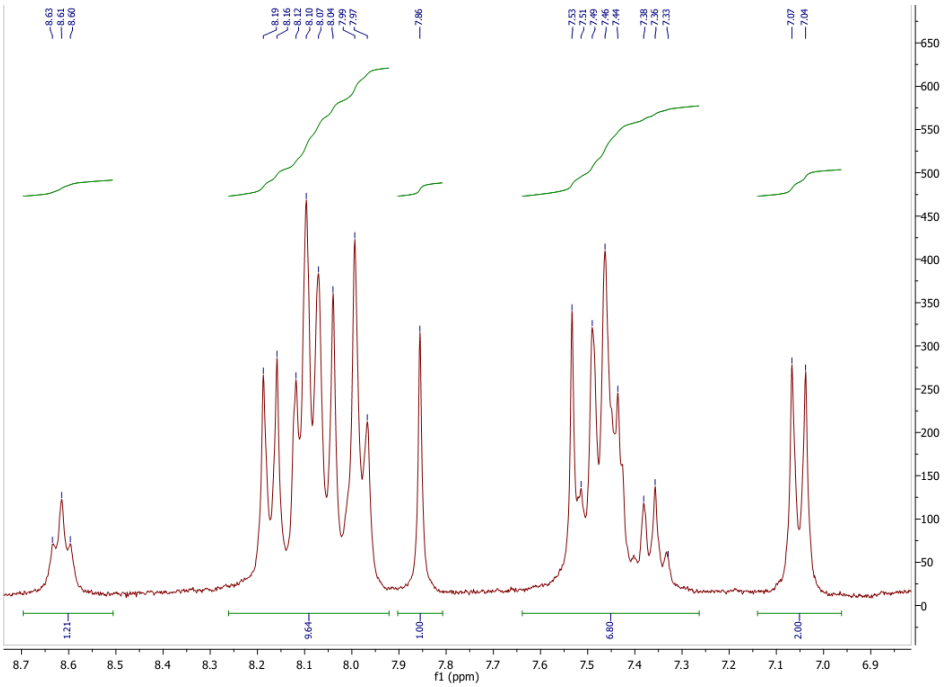

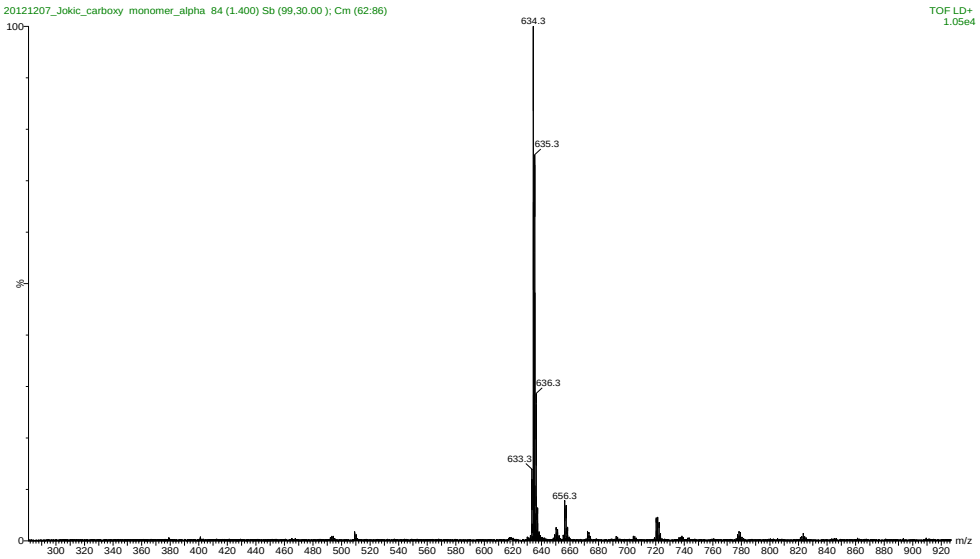
20121207_Jokic_carboxy monomer_alpha 84 (1.400) Sb (99,30.00 ); Cm (62:86)
TOF LD+
1.05e4
634.3
635.3
636.3
633.3
656.3
%
m/z

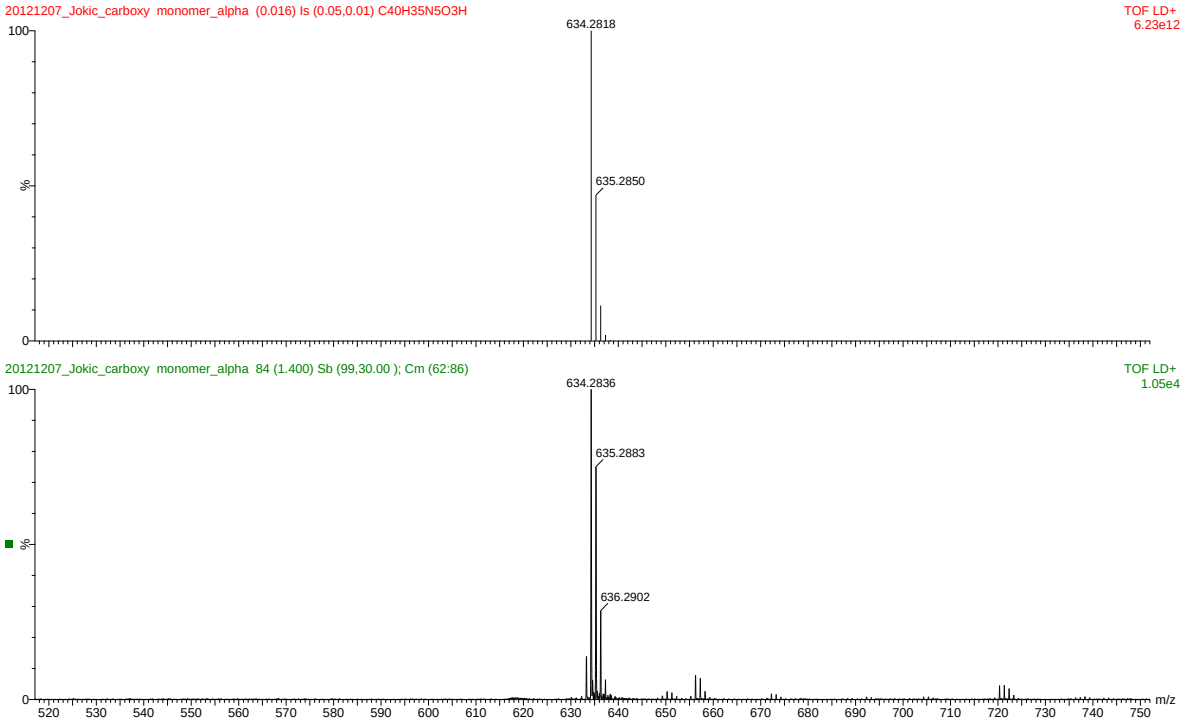
20121207_Jokic_carboxy monomer_alpha (0.016) Is (0.05,0.01) C40H35N5O3H
TOF LD+
6.23e12
634.2818
635.2850
20121207_Jokic_carboxy monomer_alpha 84 (1.400) Sb (99,30.00 ); Cm (62:86)
TOF LD+
1.05e4
634.2836
635.2883
636.2902
%
m/z

## 6.4 $^{1}$H NMR and mass spectra of

**(Z)-4-(5-((5-(4-((3-methacrylamidopropyl)carbamoyl)phenyl)-3-phenyl-2H-pyrrol-2-ylidene)amino)-4-phenyl-1H-pyrrol-2-yl)phenyl acetate**

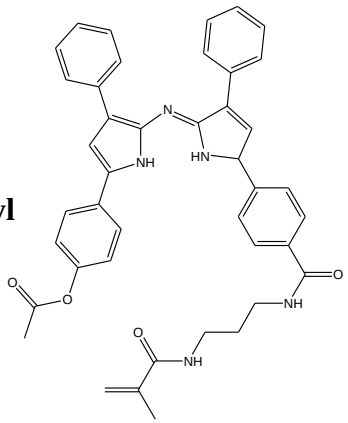


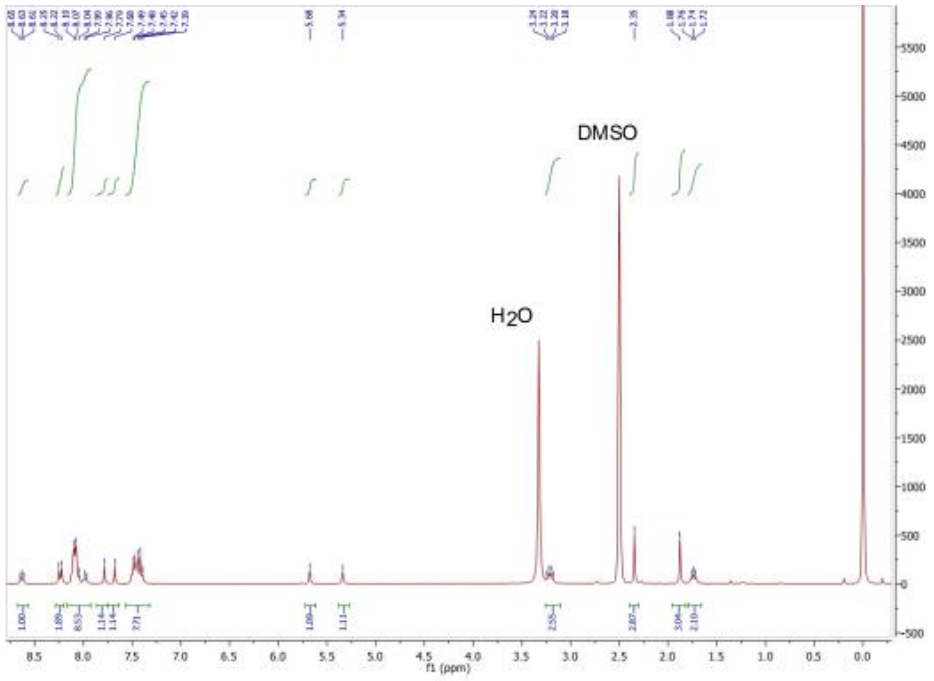


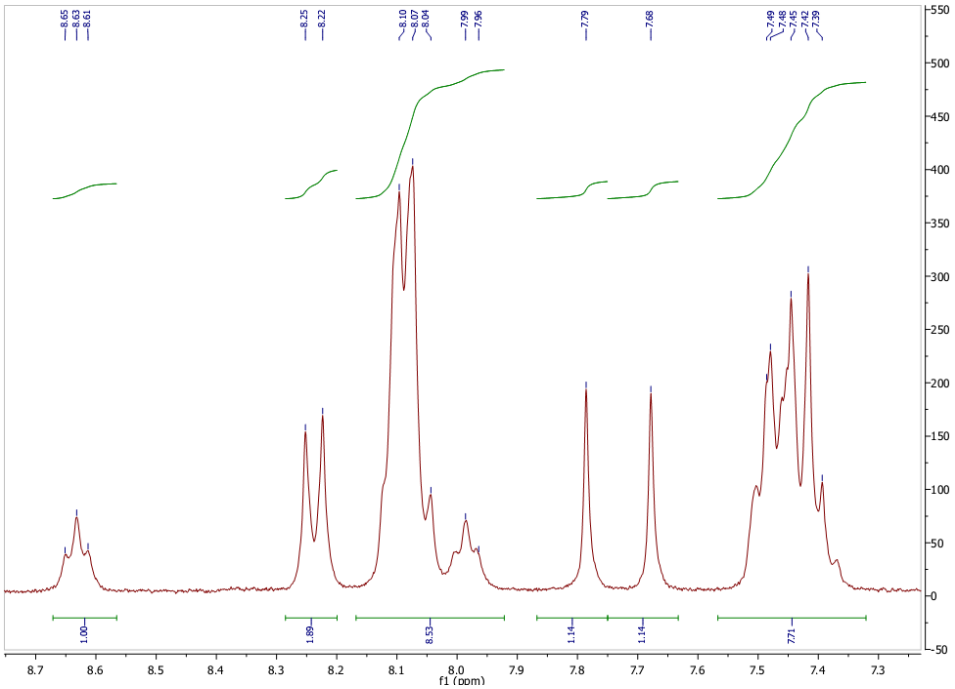

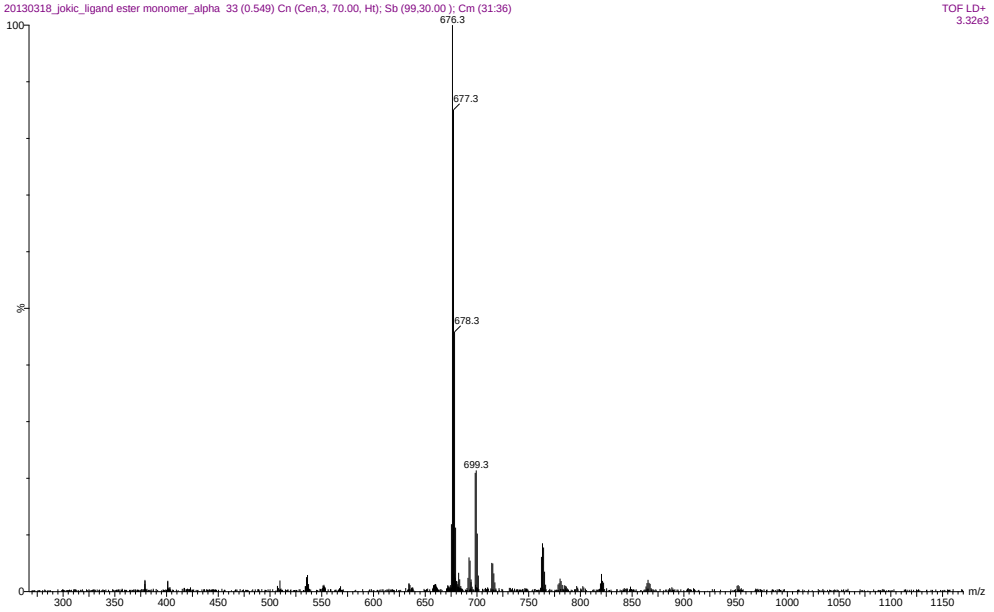
20130318_jokic_ligand ester monomer_alpha 33 (0.549) Cn (Cen,3, 70.00, Ht); Sb (99,30.00 ); Cm (31:36)
TOF LD+
3.32e3
676.3
677.3
678.3
699.3
%
m/z

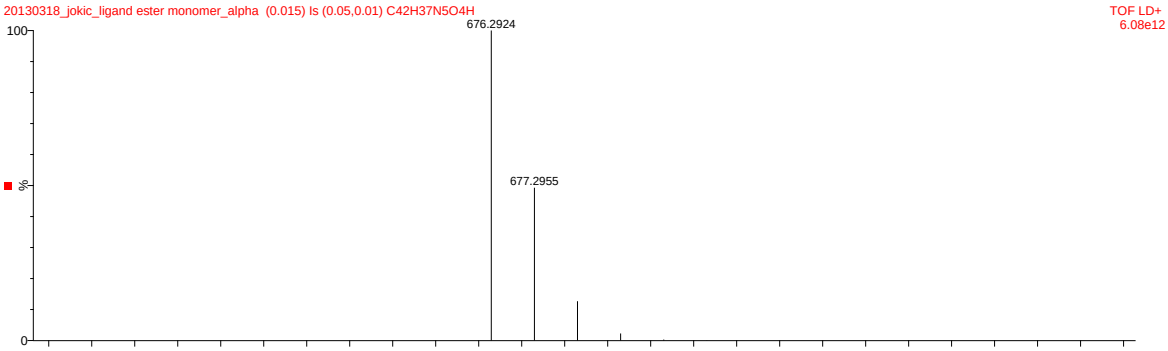
20130318_jokic_ligand ester monomer_alpha (0.015) Is (0.05,0.01) C42H37N5O4H
TOF LD+
6.08e12
676.2924
677.2955
%

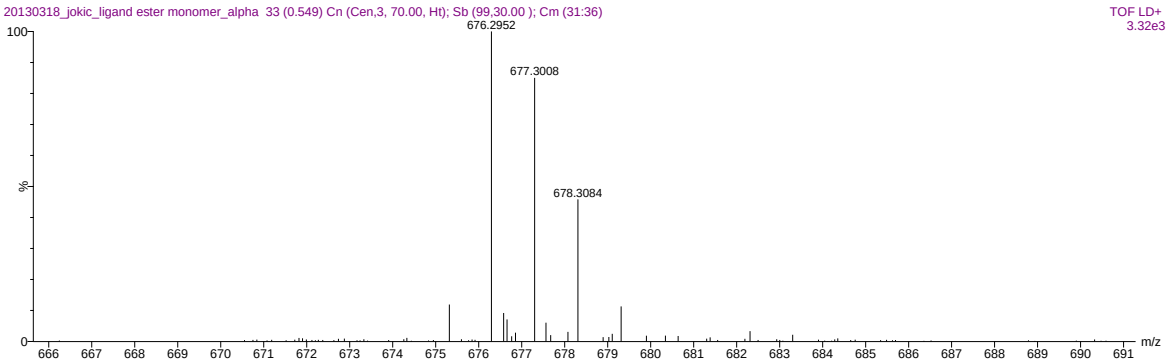
20130318_jokic_ligand ester monomer_alpha 33 (0.549) Cn (Cen,3, 70.00, Ht); Sb (99,30.00 ); Cm (31:36)
TOF LD+
3.32e3
676.2952
677.3008
678.3084
%
m/z

**6.5 $^{1}$H NMR and mass spectra of**

**$BF_2$ Chelate of (Z)-4-(5-((5-(4-((3-methacrylamidopropyl)carbamoyl)phenyl)-3-phenyl-2H-pyrrol-2-ylidene)amino)-4-phenyl-1H-pyrrol-2-yl)phenyl acetate**

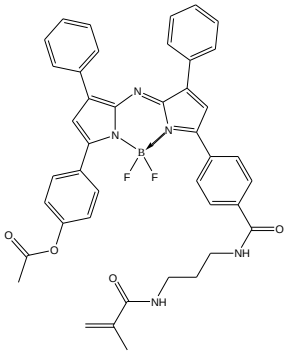

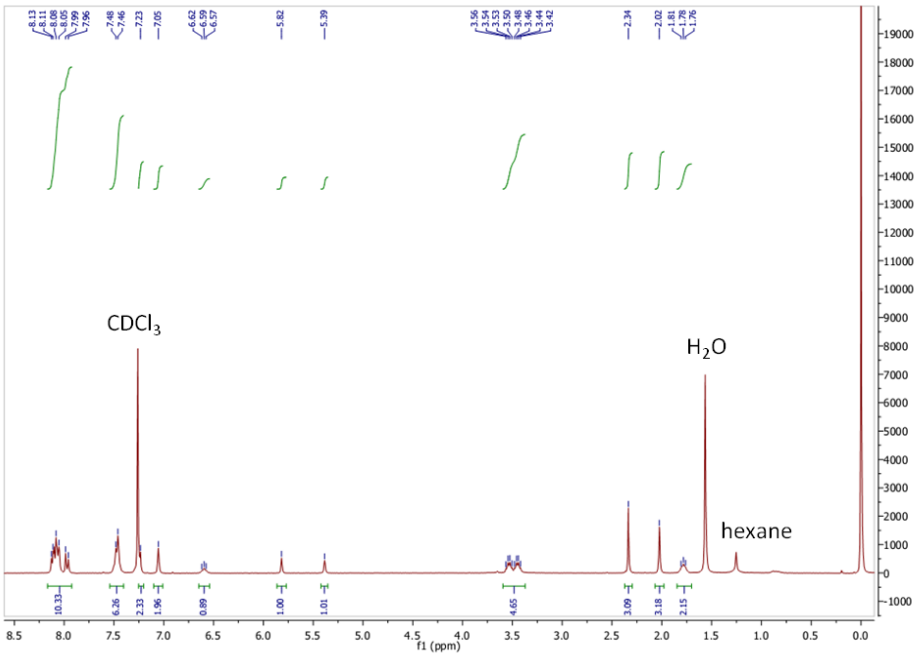


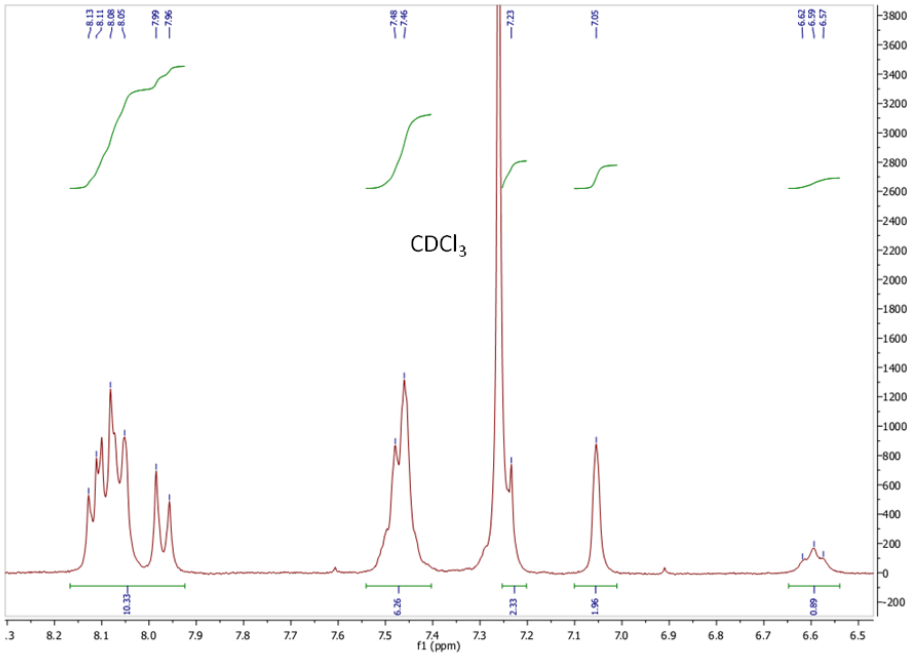

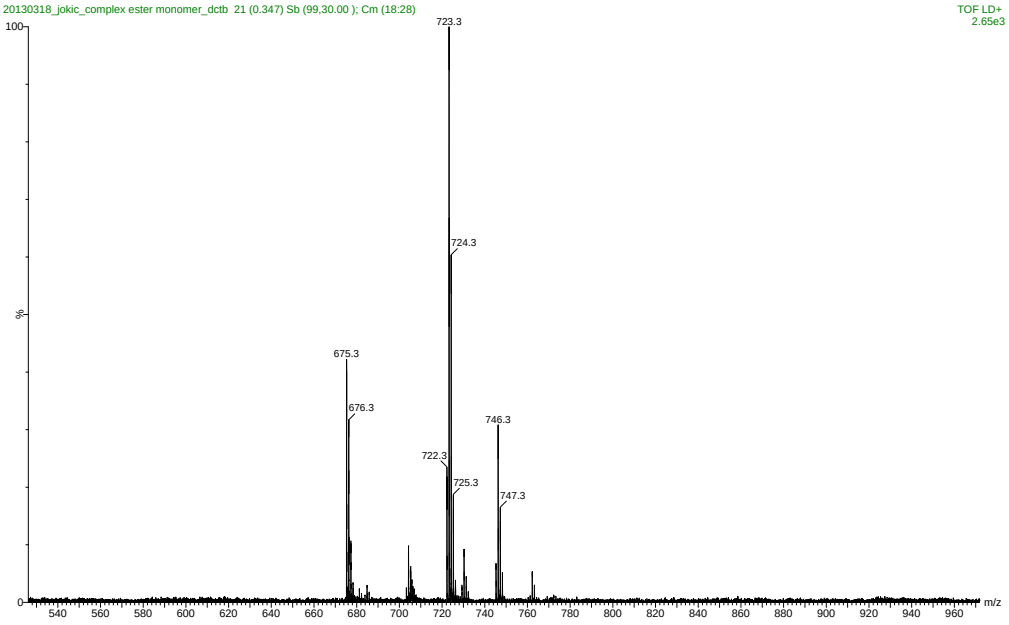


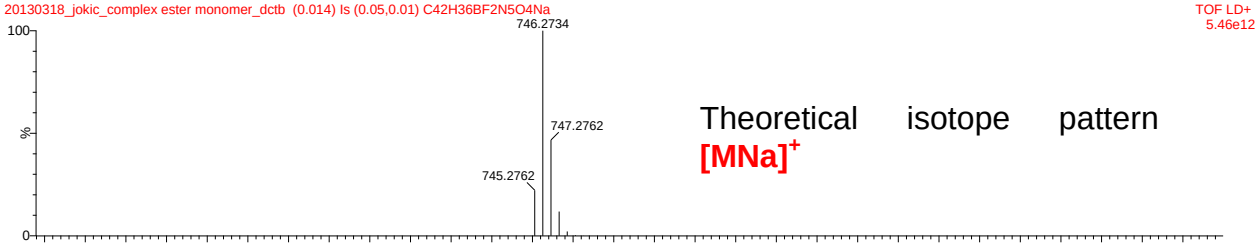


Theoretical isotope pattern **[MNa]$^+$**

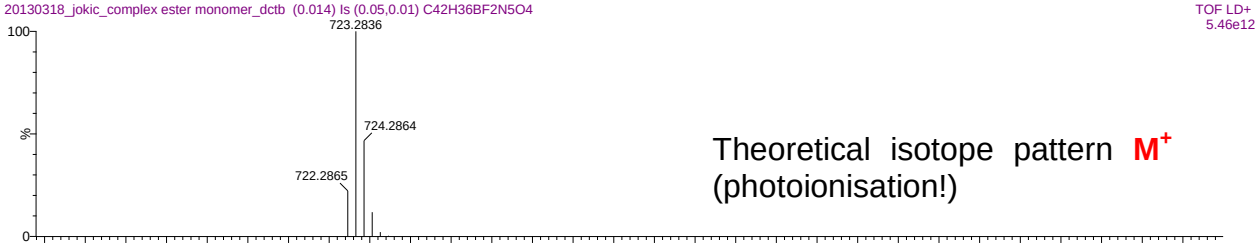


Theoretical isotope pattern **M$^+$** (photoionisation!)

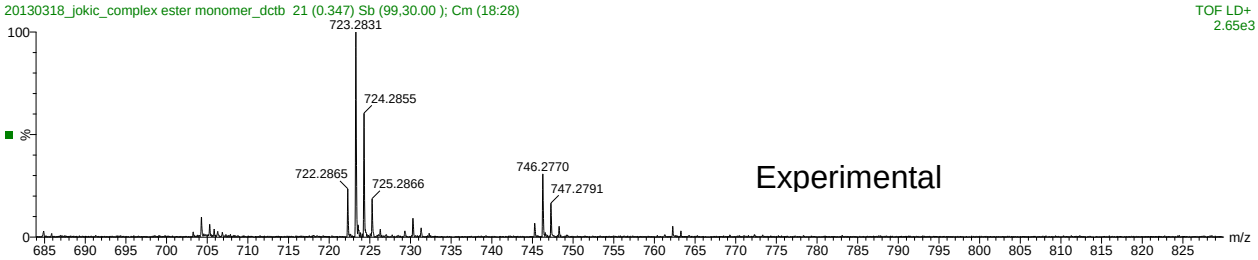


Experimental

**6.6 $^{1}$H NMR and mass spectra of**

**$BF_2$ Chelate of 4-((5Z)-5-(3,5-diphenyl-2H-pyrrol-2-ylideneamino)-4-phenyl-1H-pyrrol-2-yl)phenyl acetate**

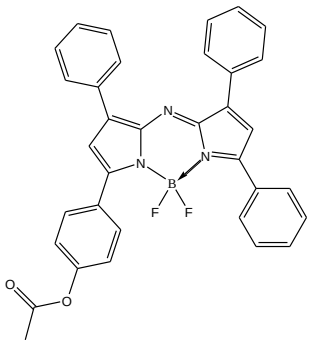


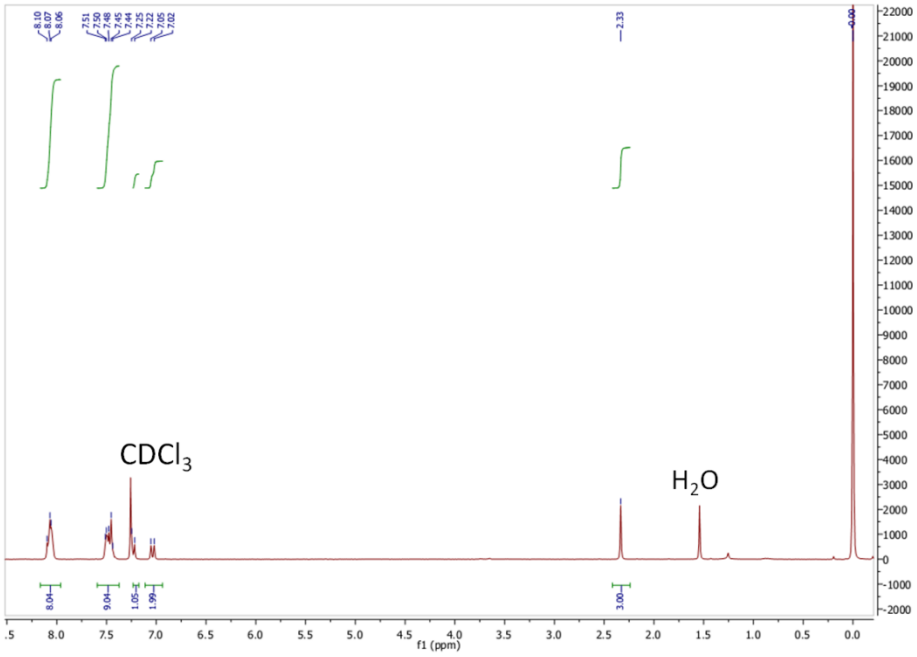


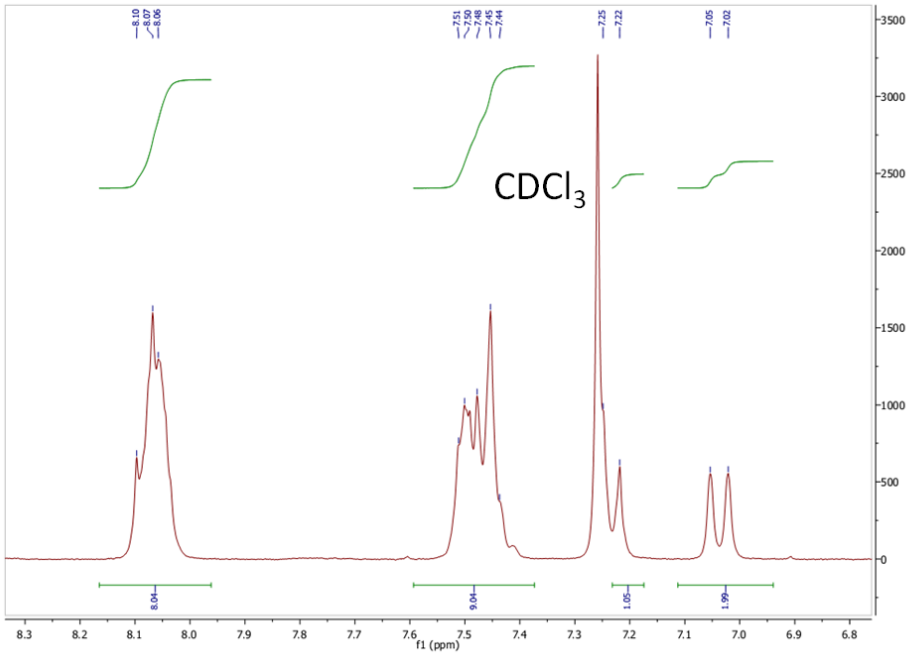

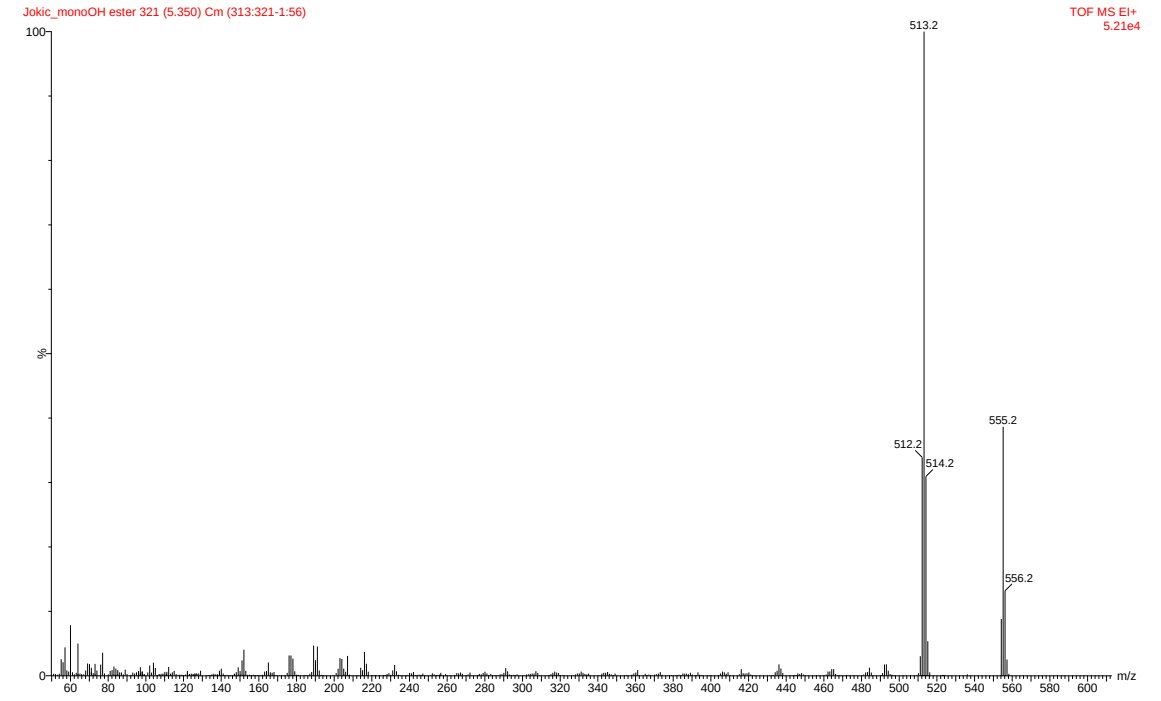
Jokic_monoOH ester 321 (5.350) Cm (313:321-1:56)
TOF MS EI+
5.21e4
100
%
0
513.2
555.2
512.2
514.2
556.2
m/z
60 80 100 120 140 160 180 200 220 240 260 280 300 320 340 360 380 400 420 440 460 480 500 520 540 560 580 600

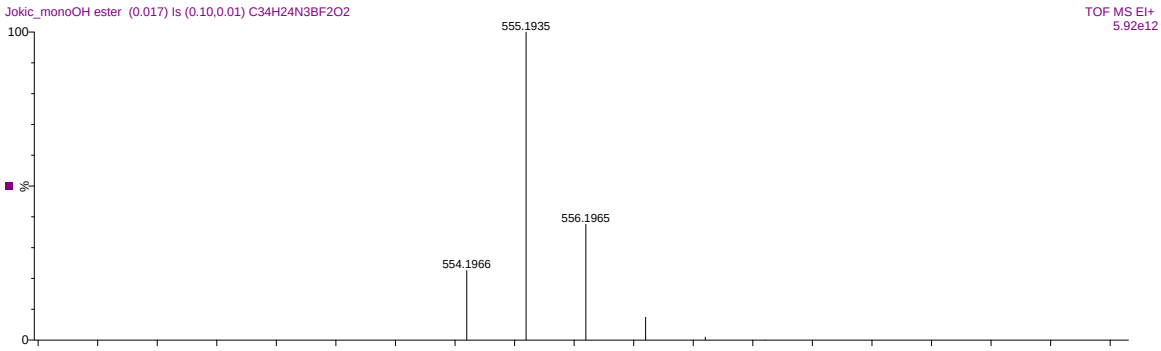
Jokic_monoOH ester (0.017) Is (0.10,0.01) C34H24N3BF2O2
TOF MS EI+
5.92e12
100
%
0
555.1935
556.1965
554.1966

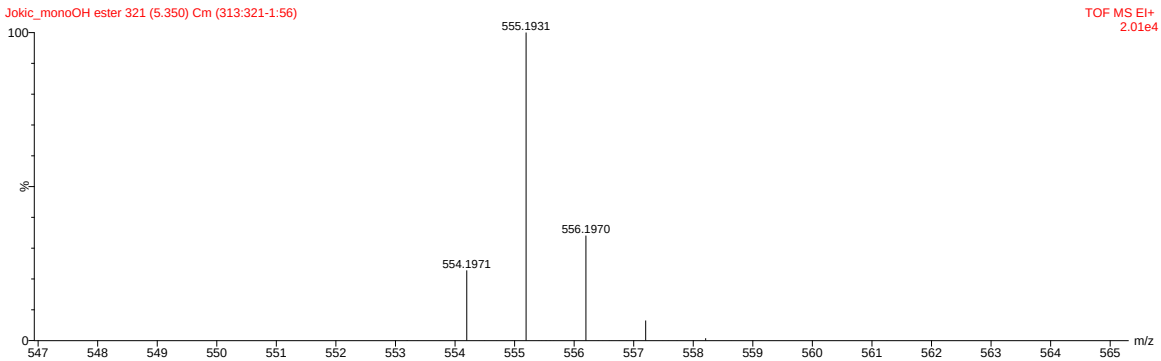
Jokic_monoOH ester 321 (5.350) Cm (313:321-1:56)
TOF MS EI+
2.01e4
100
%
0
555.1931
556.1970
554.1971
m/z
547 548 549 550 551 552 553 554 555 556 557 558 559 560 561 562 563 564 565

**6.7 $^{1}$H NMR and mass spectra of**

**$BF_2$ Chelate of 4-(2-((5-(4-hydroxyphenyl)-3-phenyl-1H-pyrrol-2-yl)imino)-3-phenyl-2H-pyrrol-5-yl)-N-(3-methacrylamidopropyl)benzamide**

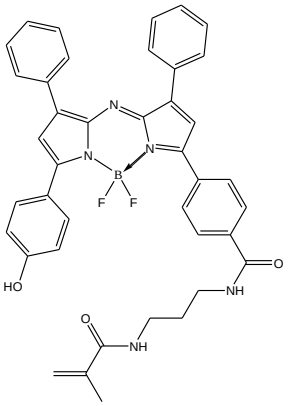


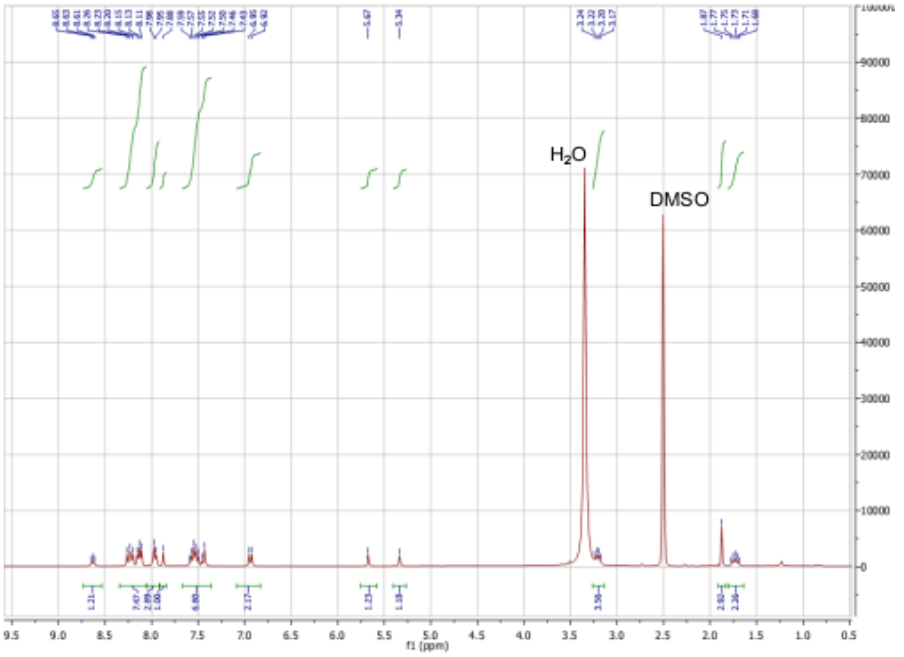


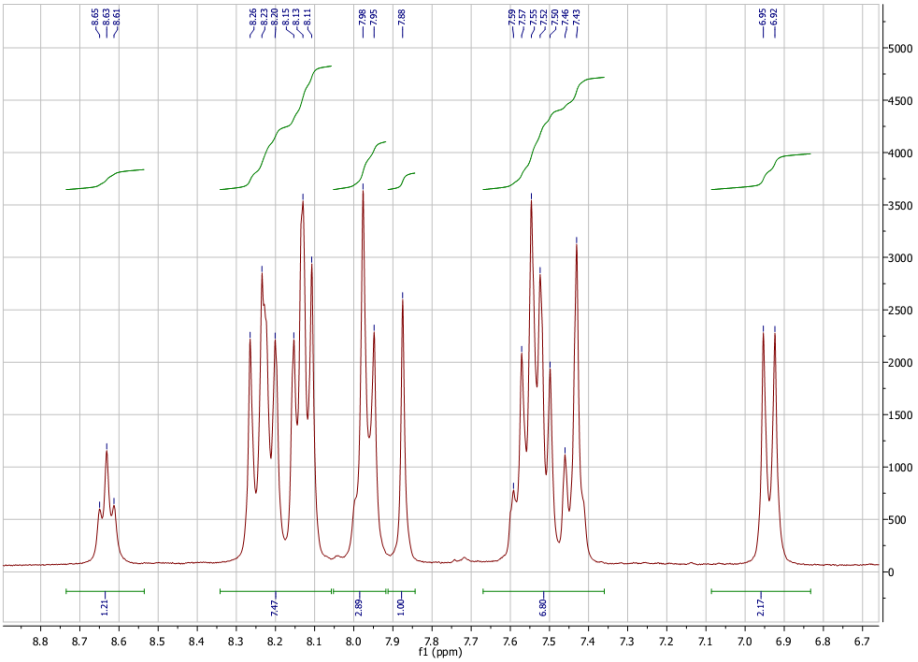

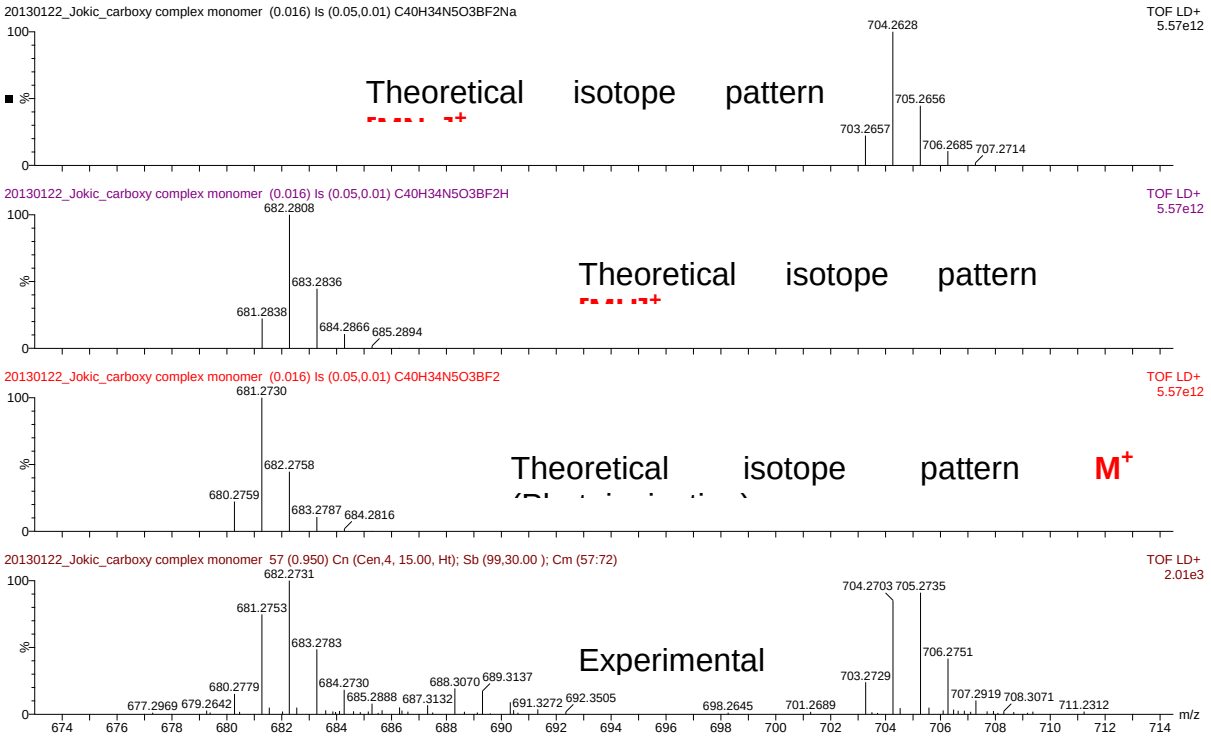
20130122_Jokic_carboxy complex monomer (0.016) Is (0.05,0.01) C40H34N5O3BF2Na
TOF LD+
5.57e12
Theoretical isotope pattern
20130122_Jokic_carboxy complex monomer (0.016) Is (0.05,0.01) C40H34N5O3BF2H
TOF LD+
5.57e12
Theoretical isotope pattern
20130122_Jokic_carboxy complex monomer (0.016) Is (0.05,0.01) C40H34N5O3BF2
TOF LD+
5.57e12
Theoretical isotope pattern M+
20130122_Jokic_carboxy complex monomer 57 (0.950) Cn (Cen,4, 15.00, Ht); Sb (99,30.00 ); Cm (57:72)
TOF LD+
2.01e3
Experimental
m/z

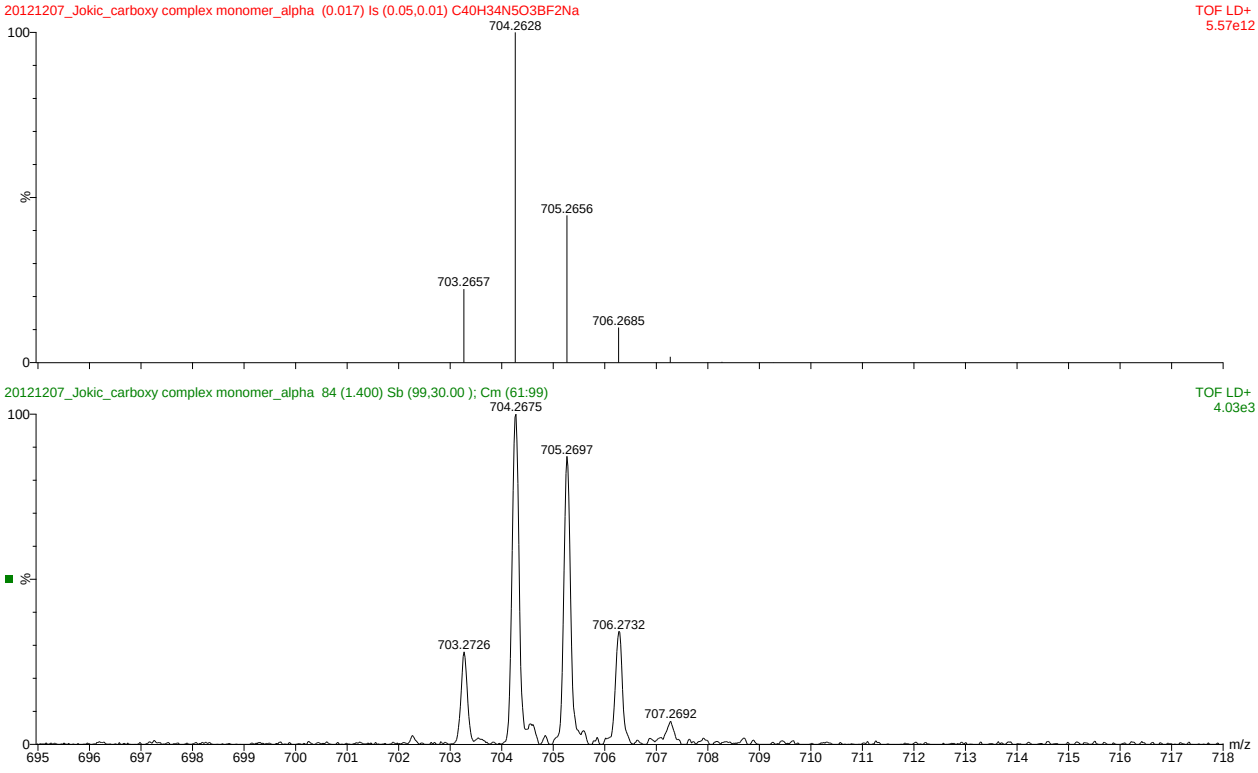
20121207_Jokic_carboxy complex monomer_alpha (0.017) Is (0.05,0.01) C40H34N5O3BF2Na
TOF LD+
5.57e12
20121207_Jokic_carboxy complex monomer_alpha 84 (1.400) Sb (99,30.00 ); Cm (61:99)
TOF LD+
4.03e3
m/z

## 6.8 List of Figures

### 6.9 List of Tables